N O T I C E

THIS DOCUMENT HAS BEEN REPRODUCED FROM
MICROFICHE. ALTHOUGH IT IS RECOGNIZED THAT
CERTAIN PORTIONS ARE ILLEGIBLE, IT IS BEING RELEASED
IN THE INTEREST OF MAKING AVAILABLE AS MUCH
INFORMATION AS POSSIBLE

DEPARTMENT OF MECHANICAL ENGINEERING

School of Engineering and Architecture

UNIVERSITY OF MIAMI

Coral Gables, Florida 33124

DEPARTMENT OF MECHANICAL ENGINEERING

School of Engineering and Architecture

UNIVERSITY OF MIAMI

Coral Gables, Florida 33124

*Volume I: Review of Mathematical
Formulations*

Three Dimensional Thermal
Pollution Models

NASA

THREE DIMENSIONAL THERMAL
POLLUTION MODELS
VOLUME 1 - REVIEW OF MATHEMATICAL FORMULATIONS

by
Samuel S. Lee and Subrata Sengupta

Department of Mechanical Engineering
School of Engineering and Environmental Design
University of Miami
Coral Gables, Florida

May, 1978

STANDARD TITLE PAGE

1. Report No. CR-154624	2 Government Accession No.	3. Recipient's Catalog No.

4. Title and Subtitle	5. Report Date
Three Dimensional Thermal Pollution Models Volume I - Review of Mathematical Formulations	May 1978
	6. Performing Organization Code

7. Author(s) Samuel S. Lee and Subrata Sengupta	8. Performing Organization Report No. KSC TR 43-2

9. Performing Organization Name and Address School of Engineering and Architecture University of Miami Coral Gables, Fla.	10. Work Unit No.
	11. Contract or Grant No. NAS10-8926

12. Sponsoring Agency Name and Address National Aeronautics and Space Administration John F. Kennedy Space Center, Fla.	13. Type of Report and Period Covered Final
	14. Sponsoring Agency Code

15. Abstract

This volume is the first of a three volume set presenting the description and program documentation of a mathematical model package for thermal pollution analyses and prediction.

These models, intended as User's manuals, are three-dimensional and time-dependent using the primitive equation approach.

Although they have sufficient generality for application at sites with diverse topographical features; they also present specific instructions regarding data preparation for program execution and sample problems.

Volume I presents the mathematical formulation of these models including: assumptions, approximations, governing equations, boundary and initial conditions, numerical method of solution, and same results.

Supplementary Note: Prepared under the sponsorship of the Research and Technology Projects Branch (Roy Bland) John F. Kennedy Space Center, Florida.

16. Key Words
Thermal Pollution
Models
Remote Sensing

17. Bibliographic Control STAR Category 43	18. Distribution Unlimited Distribution

19. Security Classif.(of this report) Unclassified	20. Security Classif.(of this page) Unclassified	21. No. of Pages 191	22. Price

PREFACE

.This volume is the first of a three volume set presenting
the description and program documentation of a mathematical model
package for thermal pollution analyses and prediction. This vol-
ume presents the mathematical formulation of these models, including
assumptions, approximations, governing equations, boundary and in-
itial conditions, numerical method of solution and sample results.
The two model formulations are the rigid-lid and free-surface, re-
spectively. These programs were developed by the Thermal Pollution
Group at the University of Miami, and were funded by the National
Aeronautics and Space Administration (NASA), thus the program
names NASUM I, NASUM II and NASUM III were given to reflect this
joint effort.

These models are three-dimensional and time-dependent using
the primitive equation approach. They have sufficient generality
in programming procedure to allow application at sites with diverse
topographica. features. NASUM I is a rigid-lid formulation and is
presented in detail in Volume II. NASUM I consists of both near
and far field versions. The near field simulates thermal plume
areas, and the far field version simulates larger receiving aquatic
ecosystems. The models in NASUM I simulate the velocity and tem-
perature fields for given meteorological and plant intake and dis-
charge conditions. Three versions of the rigid-lid formulation are
presented in Volume II comprising NASUM I; one for near field
simulation, the second for far field unstratified situations, and
the third is for stratified basins, far field simulation.

i

NASUM II and NASUM III are free-surface formulations
and are presented in detail in Volume III. Both programs
present surface height variations, velocity field and tem-
perature field for the "complete field". NASUM II is a
far field formulation and is used without including the plant
thermal discharge. NASUM III used horizontal stretching in
order to provide higher resolution at thermal discharge point,
as well as including far field influences such as varying tide
and ambient currents at points far from the point of discharge.
It also includes far field influences such as varying tide
and ambient currents at points far from the point of discharge.

The three volumes are intended as User's manuals and,
accordingly, they present specific instructions regarding data
preparation for program execution and specific sample problems.

ACKNOWLEDGEMENTS

Various members contributed in different areas of expertise during the course of the study. Special gratitude is expressed to Mr. Harvey Miller for contribution to Volume I and III. Dr. Josyula Venkata was a prime contributor to Volume II.

TABLE OF CONTENTS - VOLUME 1

LIST OF SYMBOLS FOR RIGID-LID MODEL

A_H Horizontal kinematic eddy viscosity

A_v Vertical kinematic eddy viscosity

A_z Vertical eddy viscosity

A_{ref} Reference kinematic eddy viscosity

A_v^* A_v/A_{ref}

B_H Horizontal eddy thermal diffusivity

B_v Vertical eddy thermal diffusivity

B_{ref} Reference eddy thermal diffusivity

B_v^* B_v/B_{ref}

B_z Vertical conductivity, $\rho C_p B_v$

C_p Specific heat at constant pressure

E_u Euler number

f Coriolis parameter

g Acceleration due to gravity

h Depth relative to rigid lid

H Reference depth, or vertical length scale

I Grid index in x-direction or i-direction

J Grid index in y-direction or j-direction

K Grid index in z-direction or k-direction

K_s Surface heat transfer coefficient

L Horizontal length scale

P Pressure

P_s Surface or lid pressure

P_r Turbulent Prandtl number, A_{ref}/B_{ref}

1

Pe	Peclet number
R_b	Rossby number
Re	Reynolds number (turbulent)
R_i	Richardson number
T	Temperature
T_{ref}	Reference temperature
T_e	Equilibrium temperature
T_s	Surface temperature
t	Time
t_{ref}	Reference time
u	velocity in x-direction
v	velocity in y-direction
w	velocity in z-direction
x	horizontal coordinate
y	horizontal coordinate
z	vertical coordinate

Greek Symbols

ξ	Horizontal coordinate in stretched system, $=x$
η	Horizontal coordinate in stretched system, $=y$
ζ	Vertical coordinate in stretched system
δ	H/L
ω	Transformed vertical velocity
ρ	Density
τ_{yx}	Surface shear stress in x-direction
τ_{yz}	Surface shear stress in y-direction

2

Superscripts

(‾) Dimensional quantity

(˙) Dimensional mean quantity

(') Dimensional fluctuating quantity

( ) Dimensional quantity

( )$_{ref}$ Reference quantity

3

LIST OF SYMBOLS FOR FREE-SURFACE MODEL

A_1	First term in $\eta_o(t)$, which is defined below
A_2	Coefficient of second term in $\eta_o(t)$.
B_H	Horizontal eddy thermal diffusivity
B_v	Vertical eddy thermal diffusivity
C_o	Phase velocity or celerity of surface gravity waves, $\sqrt{gH}$
C_p	Specific heat at constant pressure
f	Coriolis parameter
g	Acceleration due to gravity
h	Depth relative to the mean water level
H	Depth contour relative to the free-surface, $h + \eta$
I	Grid index in x-direction or α---direction
J	Grid index in y-direction or β---direction
K	Grid index in z-direction or σ -direction
K_H	Horizontal kinematic eddy viscosity
K_v	Vertical kinematic eddy viscosity
K_s	Surface heat transfer coefficient
L	Width of bay at ocean-bay interface
P	Pressure
P_s	Surface pressure (atmospheric)
T	Temperature
T_{air}	Air temperature
T_{amb}	Water ambient temperature
T_e	Equilibrium temperature
T_s	Surface temperature
t	Time

4

$t_{\flat}$ time lag in $\eta_o(t)$, which is defined below

u   Velocity in x-direction (dimensional)

v   Velocity in y-direction (dimensional)

v_o Amplitude of inlet tidal velocity $v_o(t)$, $v_o = \dfrac{2A_2C_o}{h} \dfrac{2\Pi l}{\lambda}$

$v_o(t)$ Inlet tidal velocity $= v_o \cos \omega(t+\Phi)$

w   Velocity in z-direction (dimensional)

$\dot{x}$ Horizontal coordinate

y   Horizontal coordinate

z   Vertical position relative to the mean water level

Z   Vertical position relative to the free surface, $z + \eta$

<div align="center">

Horizontal Stretching Parameters
</div>

X   Horizontal stretching coordinate in x-direction

Y   Horizontal stretching coordinate in y-direction

X' $\dfrac{dX}{d\alpha}$

X'' $\dfrac{d^2Y}{d\alpha^2}$

Y' $\dfrac{dY}{d\beta}$

Y'' $\dfrac{d^2Y}{d\beta^2}$

a   The distance at which minimum step size is desired in x-direction (see transformation relation below)

b   The distance at which minimum step size is desired in y-direction (see transformation relation below)

     $a, b, c_1, c_2, c_3, c_4, d$ and e are related as

     $\alpha = a + c_1 \operatorname{Sinh}\{c_2(X-d)\}$

     $\beta = b + c_3 \operatorname{Sinh}\{c_4(Y-e)\}$

<div align="center">5</div>

Greek Symbols

α	Horizontal coordinate in stretched system, x
β	Horizontal coordinate in stretched system, y
σ	Vertical coordinate in stretched system, Z/H
ω	Transformed vertical velocity
ρ	Density
η	Free-Surface elevation above mean water level
$\eta_o(t)$	Inlet tide level $= A_1 + A_2 \cos \omega (t+t_o)$
λ	Wave length of progressive wave at inlet
τ_{xz}	Surface shear stress in x-direction
τ_{yz}	Surface shear stress in y-direction
ω	Angular frequency of progressive wave at inlet, $\omega = C_o(2\pi/\lambda)$
ϕ	Phase angle in expression for variable tidal current velocity

Subscripts and Superscripts

H	Horizontal quantity
i	Initial quantity
interior	Quantity at interior point one grid step from inlet
n	One time level back
n+1	Current time level
n-1	Two time levels back
o	Quantity at inlet
s	Surface quantity
v	Vertical quantity
w	Lateral boundary
w+1	Quantity at interior point one grid step from lateral boundary, for energy equation

6

List of Figures

7

Background

The management of waste heat from power plants is a
dominant consideration in making power production compatible
with ecological concerns. For every unit of energy converted
to electricity approximately two units are discharged into the
environment. The ultimate heat sink is space. However, the
intermediate heat transfer links. namely, the hydrosphere and
the atmosphere may undergo changes harmful to life supporting
ecosystems.

Some quantitative estimates of efficiency, operating
temperature and waste heat have been made by Harleman and
Stolzenbach (1972) and are presented in Table I. Typical
condenser water flow rate is about 1500 ft^3/sec (675,000 gal/min)
or $3.4 \times 10^8 16$/hr. This results in about $12^{\circ}F$ increase in
cooling water temperature for fossil fuel and $20^{\circ}F$ for nuclear
plants. An idea of the magnitude of these discharges can be
formed by observing the estimates given by Krenkel and Parker
(1970). According to their estimate the cooling water flow in
the United States (based on a $15^{\circ}F$ rise in temperature) is
approximately 40 trillion gallons per year which is approx-
imately 10% of the total yearly flow of waters in the rivers
and streams in the U.S. The problems are real.

While the effects of thermal pollution have not been sys-
tematically quantified, it is accepted that there are effects
of significant nature in the biology and chemistry of the eco-
system disturbed. Thermal discharges may result in anomalous

12

stratification of lakes, lowering of capacity to hold oxygen, increased reaction and increased metabolism. The lethal effects of thermal pollution are sometimes obvious, whereas the sub-lethal effects on food chains and waste assimilation capacities are not easy to foresee unless careful, fluid mechanical, chemical and biological interactive studies are conducted in an integrated fashion.

In the past, waste heat was primarily discharged directly by open cycle systems to aquatic ecosystems, eg. lakes, rivers, cooling ponds, etc. Recently, the shortage of land, particularly in Europe has resulted in closed systems, eg. cooling towers that discharge waste heat directly to the atmosphere. The incremental change in ecological impact implied by going from open to closed systems is still in the realm of investigation. Comparative statements are difficult to make especially when considering such non-ecological factors as economics. The present effort is directed solely towards hydrothermal analysis and predictions for open cycle cooling systems.

Need for Models

Accurate understanding of the behavior of thermal discharges is important for the following reasons.

I.   To analyse the receiving body of water such that recirculation between intake and discharge from the condensor and consequent decrease in cooling efficiency can be minimized.

II.   To assess the thermal impact on the aquatic life forms existing in the receiving ecosystem.

III. To provide a priori information about the nature and extent of thermal impact for site selection.

13

It is therefore, apparent that not only environmental but design interests also are at stake.

The above mentioned objectives can only be met by having large data sets over the entire discharge flowfield. Measurements for temperature and velocity made over the affected domain could be used to develop maps for velocity and temperature distribution. However, there are some major drawbacks to this procedure.

1. Unless the flowfield is adequately covered with fixed measuring installations which record temperature and velocity continuously, synoptic data is near impossible to obtain. In-situ measurements have been conventionally obtained from moving boats with towed measuring devices; the data consequently is non-synoptic giving distorted plume shapes except in rare situations where a steady state plume exists.

2. The information obtained is usually site and time specific and is quite difficult to use either for diagnostic or predictive purposes even at the same site under different meteorological and plant conditions or at other sites. Thus, the data obtained merely serves as a monitoring tool providing little information regarding the behavior of heated discharges that would be useful in analysis of existing discharges or design of outfall location for future power plants.

3. Regulatory agencies often require data for worst meteorology situations which can only be obtained by simulation.

4. For comparative studies of prospective sites and discharge geometry prior information regarding plume behavior is essential.

14

In-situ measurements are of no help in such site selection decisions.

While in-situ measurements can serve for diagnostic and monitoring purposes under limited circumstances for meeting objective I and II they are not relevant for objective III. Models for simulating behavior of thermal discharges are therefore imperative.

Basic Considerations in Model Development

In order to establish the rationale of model formulation the physical mechanisms underlying the heat dispersion from a heated discharge need to be outlined. Thermal discharges can either be in the form of surface jets or in the form of submerged jets. The surface jet is usually from a canal discharge whereas submerged jets are from either single-port or multiport diffusers which release the thermal discharge at some finite depth below the air-water interface. Both for submerged jets and surface jets the following mechanisms govern the heat dispersal.

1.   Entrainment of ambient fluid into the thermal discharge.

2.   Buoyant spreading of discharged heated effluent.

3.   Diffusion by ambient turbulence.

4.   Interaction with ambient currents.

5.   Heat loss to the atmosphere through the air-water interface.

The first four mechanisms redistribute heat and momentum in the domain. The last mechanism transfers heat to the atmosphere.

15

Two factors which affect plume behavior are:

1. Discharge geometry and location with respect to ambient stratification.

2. Interaction of discharge with bottom topography.

The mechanisms mentioned play roles of varying importance as the heated effluent travels away from the mouth of the discharge. It has been customary therefore, to divide the flow into the following regions:

1. Near-Field

In this region the initial properties of the discharges are important. The flow field is dominated by the jet like structure of the discharge. Discharge geometry, bottom topography, initial velocity, temperature, etc. are dominating variables. Thus, non-dimensional qualities such as jet Reynolds No., densimetric Froude No., aspect ratio, bottom slope, and jet depth to domain depth ratio are important. Redistribution of heat from the discharge to the ambient is primarily by entrainment of ambient fluid. Non-significant amounts of heat is transferred to the atmosphere.

2. Far-Field

Here the ambient conditions are dominant in heat dispersal. Ambient turbulent diffusion and surface heat loss are significant.

The boundary between near and far field is quite qualitative with no easily definable separation line.

Owing to the relative importance of different heat and mass transfer processes in the two regimes and consequent

16

different approximations it has been customary to develop
different models for each of the domains. Models that con-
sider the complete domain are termed complete-field models.
It is important to note that almost all models to date do net
simulate the ambient conditions but input them as boundary
conditions obtained by measurement.

The approach in the models developed in the present effort
has been to develop complete field models, which not only
simulate the thermal anomaly region, but also the total
ambient condition. Therefore, the models are comprehensive
and the following definitions of near and far fields are
stipulated.

1. Near-Field - The complete region where effects of thermal
discharges show measureable and distinct thermal perturba-
tion to ambient conditions. Thus, this definition includes
near, and far fields of traditional definition.

2. Far-Field - This is the total domain whose thermodynamic and
hydrodynamic characteristics affects the discharge, but is large
enough not to be significantly affected by the discharge.

Thus the far-field solution affects the near field boun-
dary conditions. whereas the far-field is significantly un-
affected by the near field characteristics. Throughout the
three volume report these definitions of near and far field are
used.

The first step for model development is to mathematically
represent the conservation of mass, momentum and heat in terms
of a set of equations. A relationship between the temperature

17

and velocity field in the form of an equation of state completes the set of equations. The second step involves assumptions and approximations for different flow regions in order to make the equation mathematically tractable. The final step is to develop a solution procedure which obtains solutions with appropria e boundary conditions.

Review of Other Modeling Efforts

An excellent review and evaluation of 40 surfaces plume models have been presented by Dunn et al (1975). Salient features of past modeling efforts will be highlighted in this section.

Models can be classified in the following groups:

1. Phenomenological Models

These models are basically empirical correlations of numerous data bases. Measured plume characteristics such as centerline temperature decay, jet width, isotherm areas are correlated with jet and domain variables such as initial densimetric Froude No., Reynolds No., bottom slope, outfall geometric parameters, etc. These models are relatively easy to use. However, information regarding detailed distributions are not available from such models. Another major disadvantage is that these models are only applicable to specific physical situations for which correlations were obtained. The models developed by Carter and Regier (1974) and Pritchard (1973) are representative examples of such models. While these models give gross parametric descriptions of plume behavior they are not useful in analysis of recirculation, interaction with

18

ambient currents,winds, tides, etc., or in understanding the
time dependent dispersion of heat in the receiving water body
under varying boundary conditions.

Integral Models

In these models only regions arbritarily defined as the
plume are considered. Forms of velocity and temperature pro-
files normal to the axis of the jet are assumed to provide
closure for integrated conservation equations. Numerous
models of this type are in existence with varying degrees of
simulation success depending on discharge and domain geometry.
There are some basic deficiences in these Models.

1. Domain boundaries are not considered.

a) Domains are considered to have sufficient depths to
eliminate bottom boundary flow effects.

b) Effects of lateral boundaries are completely neglected.

2. Ambient stratification is ignored thus resulting in serious
errors in incorporating bouyancy effects. This is a major
limiting feature. While integral models may sometimes be ade-
quate for non-bouyant jets, their applicability for bouyant
jets is almost universally questionable.

3. Changing ambient currents can not be incorporated.

4. Wind effects are ignored.

5. These are steady state models, and verification is near
impossible in field situations owing to near impossibility of
encountering steady state plumes.

6. Entrainment coefficients are a function of numerous jet and
ambient parameters making generally acceptable coefficients
difficult to compute.

19

This class of models has been widely used since they have some predictive capability and are computationally economical compared to numerical models. Table II shows a list of representative integral models. Sharazi and Davis (1974) have developed workbooks using Prych (1973) integral type model. They present numerous nomograms facilitating use of this model.

Numerical Models

The state at a point in a flow field is described by the solution of a system of equations that describe the local conservation laws for total mass, species mass, momentum and energy. For thermal pollution modeling the conservation laws for mass, momentum and energy are relevant. The constitutive equations complete the set. Since most environmental flows are turbulent a closure condition for the turbulence model is required. This system of equations together with appropriate boundary conditions constitute a mathematical model. The equations are coupled, non-linear, second order, three dimensional partial differential equations. Analytical solutions are not possible for most practical situations. Various assumptions regarding dimensions and relative importance of physical mechanisms are required to make the equations mathematically tractable. The differential numerical approach attempts to find solutions to this system using numerical techniques. With the advent of high speed computers and appropriate numerical techniques this approach in thermal pollution modeling has become increasingly popular. The main advantage of this procedure compared to the others described in previous sections is in the promise of adequate simulation of all important physical mechanisms without

20

the need for damaging assumptions regarding the nature of the
flow. However, assumptions and approximations can still be
made for specific situations. More importantly the three-di-
mensional nature of bouyant plumes can be accurately simulated
by this approach. These models also have the capability of
simulating time dependent behavior with time varying boundary
conditions.

A number of models of this class are in existence. Table
III shows a representative group of these models. It can be
seen that though there are a number of three-dimensional models
available all have some limiting assumptions. The purpose of
the present modeling effort was to develop a model package that
could be applied to a large variety of discharge, domain and
meteorological conditions with relative ease. The existing models
mainly suffer for inadequate ability to include bottom topography ·
effects, and ambient meterological conditions. They also lack
adequa ^ verification.

Rationale for Present Models

A report by Lee and Sengupta (1976) presents the details of
model development. The present section presents the summary
of this effort.

The Thermal Pollution research team at the University of
Miami, under the sponsorship of NASA-KSC, has been for the last
few years developing a package of mathematical models which can
have general application to problems of power plant heated
discharge to the aquatic ecosystem. The effort is closely in-
tegrated with simultaneous remote sensing and ground-truth
data acquisition support. The concept being the development of

21

adequately calibrated and verified models for direct application
by the user community. The user community being the utilities
and the regulatory agencies like the Environmental Protection
Agency and the Nuclear Regulatory Commission.

Critical evaluation of mathematical models in use for
thermal pollution analysis, indicated that though some models
may perform well under certain conditions, a generalized three
dimensional model which accounts for wind, current, tide, bot-
tom topography and diverse meteorological conditions was not
in existence. The NASA-KSC-University of Miami project has
specifically proceeded to develop a model package which satis-
fies these requirements with emphasis on remote sensing data
input and verification during the model development. The com-
plete effort in flow chart form is shown in Fig.1-1 to indicate
the relationship between data acquisition and model development.

The Model Package

Critical evaluation of mathematical models used for thermal
pollution analysis has been made by Dunn et al (1975). They
compared the performance of various models in predicting a stan-
dard data base. A general conclusion that can be made from their
analysis is that though some models may perform well under cer-
tain conditions a generalized model which accounts for wind,
current, tide, bottom topography and diverse meteorological
conditions is yet to be developed. The models in existence can
be classified into three categories: integral models which
make similarity assumptions, phenomenological models which rely
heavily on data and numerical models which solve boundary value
formulations directly using numerical tehcniques. Finite
difference methods are widely used though some finite-element

22

algorithms have been tried. The integral models of Motz and Benedict (1972), Prych (1972), Shirazi and Davis (1974), and Stolzenbach and Harleman (1972), are the ones that have been applied to a number of situations with mixed success. The two phenomenological models that have been widely used are by Pritchard (1971, 1974). The numerical models can be classified in terms of spatial dimensions used and physical assumptions made. There are a number of two dimensional models that have been developed by Trent (1974, 1975). The formulations even for the three dimensional methods vary widely from primitive variable to velocity-vorticity and velocity-corrector potential methods. One of the first three dimensional models was by Waldrop and Farmer (1973, 1974, a,b). This model was essentially a free surface formulation. One of the first three-dimensional models which adequately accounted for bottom topography and comprehensive meteorological conditions was a rigid-lid model developed by Sengupta and Lick (1974a, 1976b). They used a vertical stretching to convert a variable depth basin to constant depth. Irregular shorelines could be easily included without modification of the program. Modified versions of this model has been used at a number of sites with satisfactory results, e.g., Sengupta and Lee (1976a), as part of the University of Miami model development effort.

Most mathematical models for environmental flows require detailed verification. The nature of the governing equations and the state of the art in solution techniques demand restrictive assumptions and approximations. Often boundary conditions and initial conditions are not adequate. Thus a careful calibration

23

procedure is an integral part of a model development effort. It is not sufficient to verify the model after it has been developed. Simultaneous calibration as the model is developed leads to modifications which check whether assumptions are valid and may even help to simplify models. A detailed discussion of the need and methodology for calibration and verification of numerical models is presented by Sengupta et al (1975). The present study incaporates a program of airborne radiometer data and in-situ measurements to enhance the model development effort. Figure 2-1 shows the interrelationship of the data gathering and model development efforts. The details of the mathematical package and formulation are presented in a number of reports by Vezirogli et al (1974, 1975), and a summary presentation is given by Sengupta and Lee (1976a). A brief discussion will be given here.

The primary motivation behind the effort was to develop a series of models which make minimal site restrictive assumptions enabling application to diverse basin and discharge configurations. Two separate formulations were made one with the rigid-lid approximation and the other with the free-surface included.

The rigid-lid formulation was essentially an extension of the effort by Sengupta (1976b), to facilitate application to thermal pollution studies. The free-surface formulation is similar to that of Freeman et al (1972), used in a study of Lake Huron. The models are further modified to have specific application to near field and far field. The near field being that region affected by the plume and the far-field being the encompassing domain. The far field affects the near field. The near

24

field has minor effects on the far field. The near field models
are especially capable of modeling open-boundary conditions.
Thus there are four separate versions of the program, near and
far field versions of rigid-lid and free-surface models. All
the models include a vertical normalization with respect to
local height to convert variable depth domains to constant
depth. The programs have a horizontal grid-point marking
system which allows application to different shore line geometry
without any modification to the program. One version of the
free-surface model has a hyperbolic sine stretching similar to
Waldrop and Farmer's (1974a), tangent stretching to allow finer
resolution at discharge points. Figure 1-2 shows the component
programs of the mathematical package and present application sites.

The governing equations for the rigid-lid model are the
incompressible Navier-Stokes Equation, conservation of mass,
energy and an equation of state. A predictive equation for lid
pressure is derived from the vertically integrated horizontal
momentum equations. The hydrostatic, Boussinesq and rigid-lid
approximations are made. The turbulent closure condition is made
by using eddy transport coefficients. The boundary conditions
at solid boundaries are no-slip, no normal velocity and adiabatic
conditions. At the air-water interface wind stress and heat
transfer coefficients are specified (a conduction formulation).
At open boundaries conditions are specified for temperature and
velocities where available. Otherwise normal derivatives are
equal to zero. Complete conditions in space and time are
specified at discharge locations. Explicit numerical schemes
with Dufort-Frankel differencing of the diffusion terms are used.

The pressure equation is solved by the SOR technique.

The free surface model also uses the same equations except the predictive equation for pressure is the hydrostatic equation. The surface pressure is atmospheric. One extra equation for surface height obtained by vertically integrating the continuity equation is used. The other approximations are the same as that for the rigid lid formulation. The boundary conditions are also the same except that at open boundaries conditions for surface height are required especially for tidal situations. Lateral walls have slip conditions.

The mathematical model package therefore consists of:

1. Rigid-Lid Model

    a) Far field version

    b) Near field version

2. Free surface model

    a) Far field version

    b) Near field version with horizontal stretching

The features of the models can be detailed as follows:

Features of rigid-lid model

        Three-dimensional
        Non-linear
        Baroclinic
        Time-dependent
        Irregular topography
        Driving forces: wind, heat and mass flux

        Predicts three-dimensional fields for velocity and temperature

        Surface pressure is defined as the pressure on a rigid-lid

26

Features of the free-surface model

Three-dimensional
Non-linear
Baroclinic
Time-dependent
Irregular topography
Driving forces: wind, tide, heat, and mass flux
Predicts three-dimensional fields for velocity and temperature.
Predicts surface height.

Application Sites

The application sites were chosen to represent as diverse a group of topographical situations as possible. The sites were Biscayne Bay in South Florida, Hutchinson Island in mid-Florida along the Atlantic coast and Lake Belews in North Carolina. Biscayne Bay shown in Fig. 1-3 is a shallow estuarine basin with tidal exchange with the Atlantic Ocean through a safety valve region and a number of creeks. There are two power plants on the Bay, operated by the Florida Power and Light Company. The Cutler Ridge Plant shown in Fig. 1-4 has a canal surface discharge into the Bay. The Turkey Point Plant has a closed canal cooling system. Florida Power and Light Company has a newly built plant at Hutchinson Island. This is an open ocean, coastal discharge approximately 1200 feet offshore. The discharge mouth is Y-shaped pipe with one leg 60° to the other. This is a submerged discharge. Fig. I-5 shows the site. Lake Belews of Duke Power Company in North Carolina has a mixing pond for the heated discharge. Connected by a canal to a larger cooling lake where plant intake is situated. This is a typical man-made lake for the Southeastern United States. Fig. 1-6 shows the lake configuration. The

mixing pond is thermally well mixed whereas the main lake displays a seasonal thermocline. This is a surface discharge situation.

Detailed results for each application site are presented in reports by Lee et al (1974, 1975, 1976) and in dissertations by Venkata (1977), Mathavan (1977) and Tsai (1977). Applications to each site was verified with a number of data bases collected during field experiments using boats and fixed stations for ground truth and in-situ measurements and airborne radiometer for remote measurements of surface temperature. Calibration and verification was conducted by specifying detailed initial conditions and comparing simulated results for given time intervals with subsequent data bases. Thus, the capability of the models to include varying boundary conditions in simulating time dependent behavior was severely tested.

Conclusions

The salient conclusions of the project, to date, are as follows:

1. The importance and need for airborne remote sensing data has been demonstrated for thermal pollution studies.

2. The unique role of synoptic data bases obtained by remote sensing, has been clearly established as imperative for complex model development efforts.

3. A mathematical model package has been developed with adequate inclusion of complex transport processes to serve as a predictive tool for thermal discharge studies and site selection.

4. The component programs of the package have been applied to diverse discharge and topographical conditions. The models have performed satisfactorily for different meteorological inputs.

28

5. It can be concluded that a reasonably general model package
    has been developed for application by the user community.
    Minimal programming effort is required by the prospective
    users of the model package.

Recommendations

While the models have been verified for a number of sites,

in order to inspire greater user confidence it is imperative

that applications to at least two other sites be made. One

site should be such that the rigid-lid model is appropriate.

The other site should have the features which test the cap-

abilities of the free-surface model. Careful verification of

velocity prediction should also be emphasized.

TABLE I
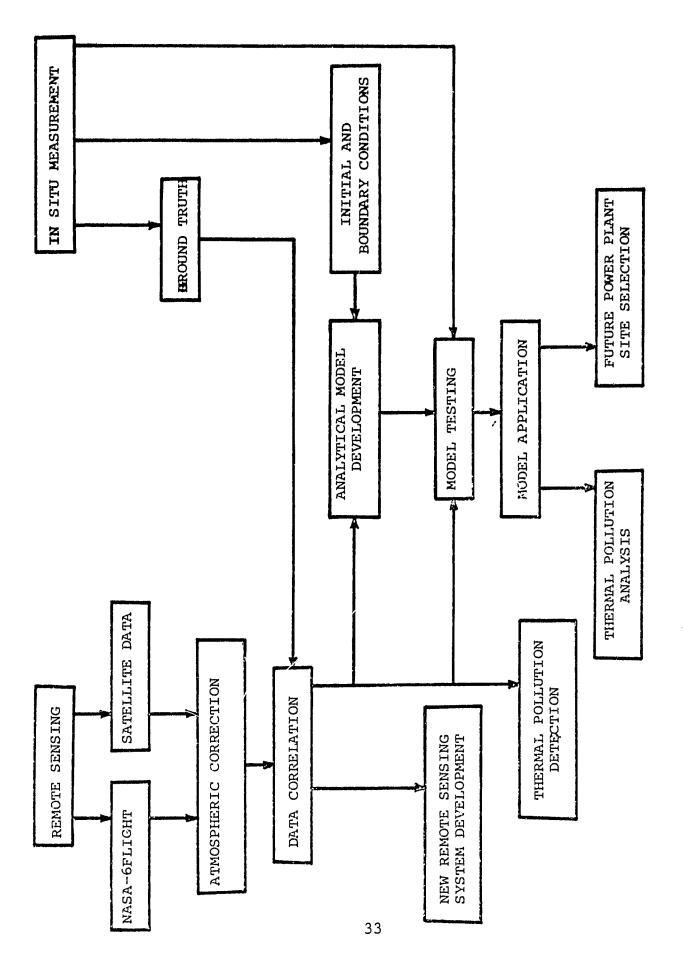
Type of Plant	Max Temp.	Ideal Efficiency	Working Efficiency	Waste heat per 1000 MW
Fossil	$1200^{\circ}F$	68%	40%	4.2×10^9 B.T.U/Hr.
Nuclear	$650^{\circ}F$	53%	32%	6.6×10^9 B.T.U/Hr.

TABLE NO III

LIST OF THE NUMERICAL MODELS DEVELOPED

S.NO	INVESTIGATORS	DIMENSIONALITY	BUOYANCY	BOTTOM SLOPE	SURFACE HEAT TRANSFER	AMBIENT CROSS FLOW	WIND STRESS	VERIFICATION
1	Brady & Gayer	3	Yes	Yes	Yes	Yes	No	None
2	Barry & Hoffman	3	Yes	Yes	Yes	Yes	No	With field data
3	Till J	3	Yes	Yes	Yes	Yes	No	With field data
4	McLay, Hondal Martirer & Henson	2	No	No	Yes	Yes	Yes	None
5	Pritchett, England & Taft	3	Yes	Yes	Yes	Yes	No	Field data
6	Sengupta & Lick	3	Yes	Yes	Yes	Yes	Yes	Field data
7	Markham	3	Yes	No	No	No	No	Field data
8	Waldrop & Farmer	3	Yes	Yes	Yes	Yes	No	Field data
9	Present Investigation	3	Yes	Yes	Yes	Yes	Yes	IR data & Field data

31

TABLE NO: II   LIST OF THE INTEGRAL MODELS DEVELOPED

S.NO	INVESTIGATORS	DIMENSIONALITY	BUOYANCY	BOTTOM SLOPE	SURFACE HEAT TRANSFER	AMBIENT CROSS FLOW	WIND STRESS	VERIFICATION
1	Carter	2	No	No	No	Yes	No	With tank data
2	Cavana & Folli	2	No	No	No	Yes	No	With Field data
3	Engelund & Pederson	3	Yes	No	No	No	No	With tank data
4	Hoopes, Zeller & Rohlich	2	No	No	Yes	Yes	Yes	Field data
5	Motz & Benedict	2	No	No	Yes	Yes	Yes	Reld data
6	Wada	3	Yes	Yes	Yes	No	No	Unknown
7	Stefan & Vaidyaraman	3	Yes	No	Yes	Yes	Yes	With tank data
8	Koh & Fan	2	Yes	No	Yes	No	No	None
9	Stolzeback & Harleman	3	Yes	Yes	Yes	Yes	No	With tank data

Figure 1-1 Relationships between various phases of the program

33

MATHEMATICAL   MODEL   PACKAGE

RIGID LID MODEL   FREE-SURFACE MODEL

i.   Far Field Version   i.   Far Field Version
     Biscayne Bay   Biscayne Bay

ii. Near Field Version   ii. Near Field Version
     Cutler Ridge Plume   With Horizontal
                                    Streching
                                    Hutchinson Island

iii. Verification Site
     Belews Lake

ALL MODELS INCORPORATED A NORMALIZATION WITH RESPECT TO LOCAL DEPTH

Figure 1-2

34
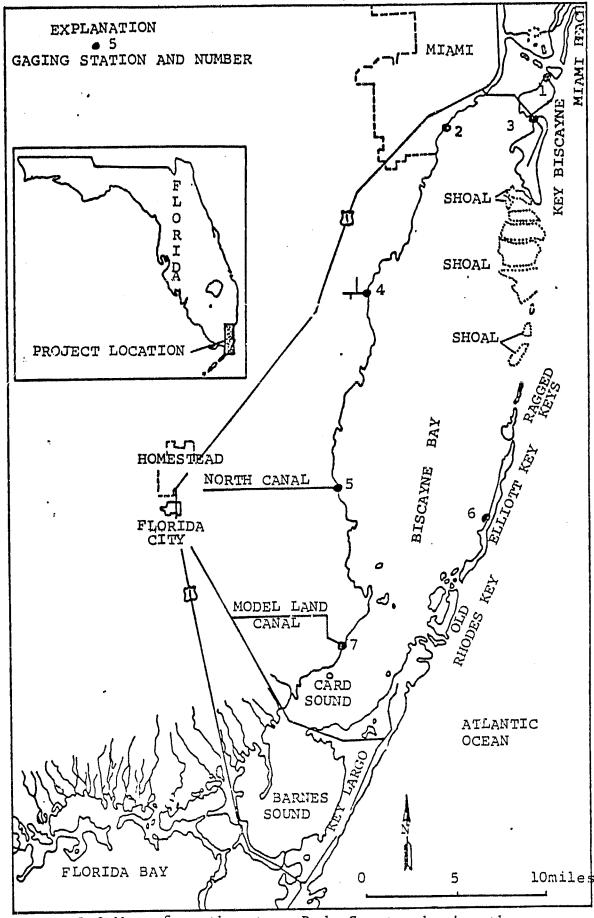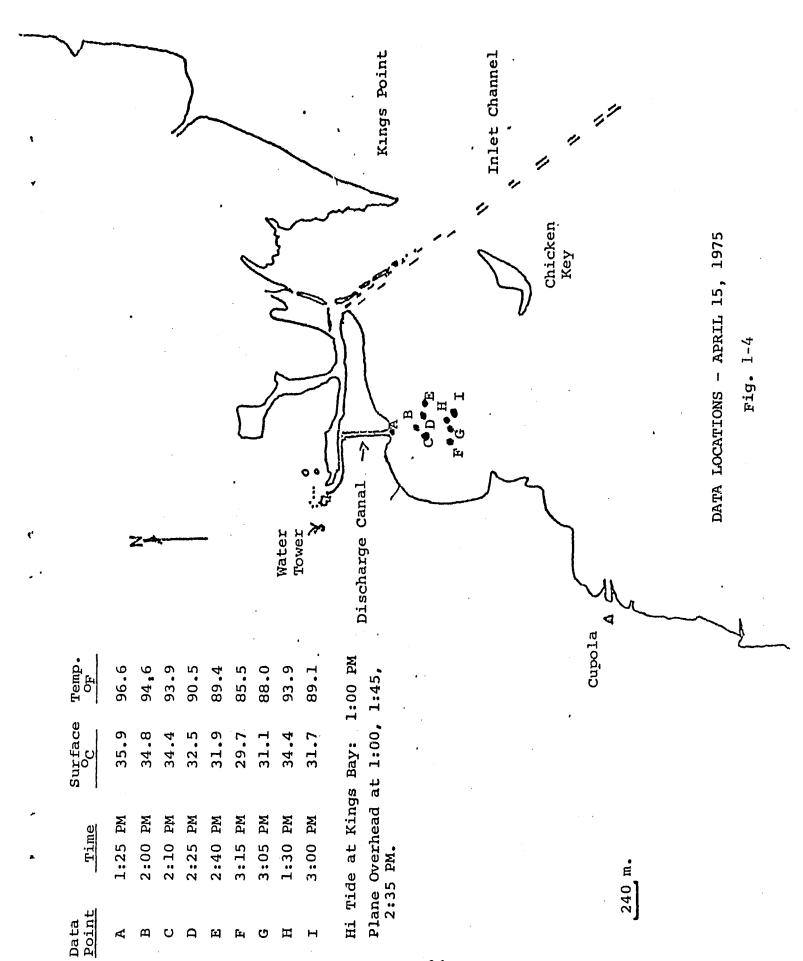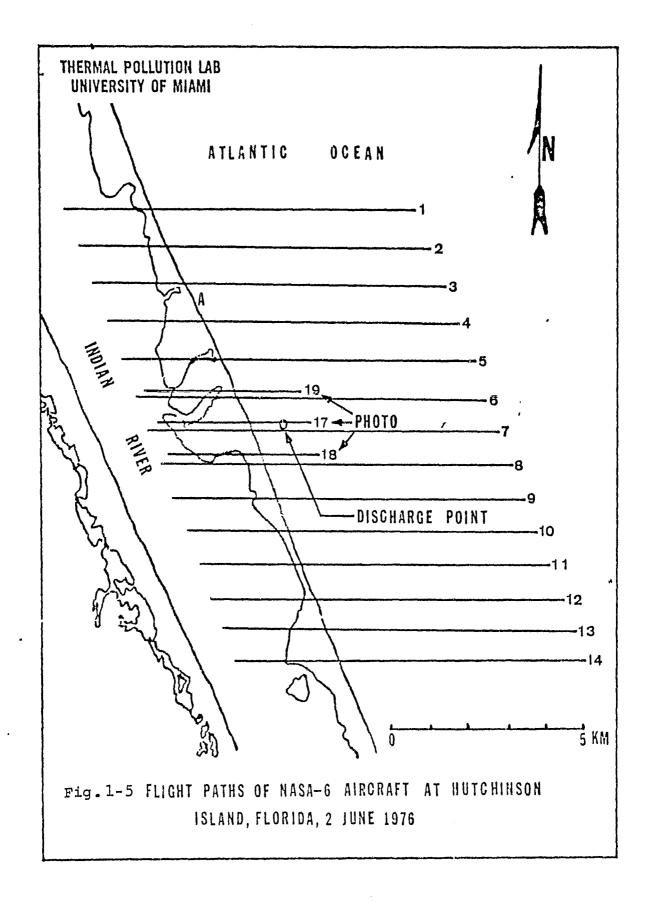
Fig. 1-3 Map of southeastern Dade County showing the area
of investigation and location of gaging stations.   35

Data Point	Time	Surface °C	Temp. °F
A	1:25 PM	35.9	96.6
B	2:00 PM	34.8	94.6
C	2:10 PM	34.4	93.9
D	2:25 PM	32.5	90.5
E	2:40 PM	31.9	89.4
F	3:15 PM	29.7	85.5
G	3:05 PM	31.1	88.0
H	1:30 PM	34.4	93.9
I	3:00 PM	31.7	89.1

Hi Tide at Kings Bay: 1:00 PM

Plane Overhead at 1:00, 1:45, 2:35 PM.

240 m.

Kings Point

Inlet Channel

Chicken Key

Water Tower

Discharge Canal

Cupola

N

DATA LOCATIONS – APRIL 15, 1975

Fig. 1-4

36

Fig. 1-5 FLIGHT PATHS OF NASA-6 AIRCRAFT AT HUTCHINSON ISLAND, FLORIDA, 2 JUNE 1976

THERMAL POLLUTION LAB
UNIVERSITY OF MIAMI

MAIN LAKE

INTAKE

POWER PLANT

DISCHARGE

MIXING POND

CANAL

o   320   640   960m

Fig.1-6   The Belews Lake Site.

38

II. The Rigid-Lid Model

2.1 Brief Description of Past Experience with Rigid-Lid Formulations; Relevant Advantages and Disadvantages

One of the first three-dimensional models which adequately accounted for bottom topography and comprehensive meteorological conditions was a rigid-lid model developed by Sengupta and Lick (1974, 1976). They used a vertical stretching to convert a variable depth basin to constant depth, thereby permitting a constant vertical grid size to be applied everywhere in the domain. Irregular shorelines could be easily included without modification of the computer program. Modified versions of the rigid-lid model have been used, by the Thermal Pollution Research team at the University of Miami, at a number of sites with satisfactory results; Lee and Sengupta (1976).

The major advantage associated with the rigid-lid model is the elimination of surface gravity waves with a consequent larger integration time steps. For sites where gravity waves do not determine the maximum allowable time step (for example, in the case for which vertical diffusion determines the maximum allowable time step. This could be the case for a shallow water basin), no time step advantage is gained by the rigid-lid model.

The major disadvantage associated with the rigid-lid model is its inability to predict surface heights.

Thus, for example, real tidal conditions cannot be accounted for, since the surface is not permitted to move.

2.2. Assumptions and Approximations

The system of governing equations (see next section, 2.3) for the fluid flow invoke several simplifying assumptions and approximations in the interest of saving computational time without losing significant accuracy. The following assumptions and approximations have been employed:

39

2.2.1 The Boussinesq Approximation

The effect of density variation on the inertial and diffusion terms in the governing conservation equations is neglected. Density variation is retained in the bouyancy terms in the equations of motion. The effect of bouyancy is thereby accounted for by allowing density variations which produce horizontal pressure gradients which influence the fluid motion through the horizontal momentum equations.

2.2.2 The Hydrostatic Approximation

The hydrostatic approximation involves neglecting the vertical convection and diffusion terms in the vertical momentum equation. This approximation implies that the vertical fluid acceleration, $\frac{Dw}{Dt}$, is negligible.

2.2.3 Constant Eddy Transport Coefficients

Turbulence modeling is very complex and has an extensive body of literature of its own. Turbulent closure has been obtained in this model by using constant eddy transport co-efficients, except for the case (Lake Belews site) for thermal stratification. For this case a Richardson number dependent variable vertical eddy transport coefficient was used. Due to the horizontal scale length, L, being much larger than the vertical scale length H, the horizontal eddy transport co-efficient is orders of magnitude larger than the vertical eddy transport coefficient.

2.2.4 Variation of Surface Wind Stresses

The variation of the wind produced surface shear stresses with respect to x and y, $\frac{\partial \tau_{xz}}{\partial x}$ and $\frac{\partial \tau_{yz}}{\partial y}$, are considered negligible for the horizontal length scales of the water bodies studied. However, if the physical dimensions of the water body are so large as to require including variation of the wind stresses with respect to x and y, then the computer programs can be quite easily modified by replacing τ_{xz} and τ_{yz} with matrices $\tau_{xz}(I,J)$ and $\tau_{yz}(I,J)$. Where the indices I and J refer to the location of a grid point with respect to the x,y plane

2.2.5 The Rigid-Lid Approximation

This approximation effectively eliminates surface gravity waves by imposing a zero vertical velocity at the surface. This means that the surface allows slip conditions without any normal velocity. In other words, a rigid, frictionless lid has been placed at the undisturbed free surface of the water body. The surface pressure is no longer atmospheric, but represents a "lid-pressure", which under some special steady state conditions can be related to the free surface elevation that would occur if no lid were present.

2.3 Governing Equations

The set of equations governing the behavior of the fluid flow are those expressing the conservation of mass, momentum and energy in turbulent flow, and an equation of state.

2.3.1 Cartesian Coordinate Representation (x,y,z)

The Cartesian coordinate system is used with the z-coordinate in the downward vertical direction as shown in Fig. 2.1, i.e. a so-called "left-handed" coordinate system. In order to keep the generalized nature of the model, all the significant terms in the respective conservation equations are retained. Included are the effects of bouyancy, inertia, coriolis, density and turbulent mixing. Wind shear and heat flux at the surface are also considered.

The following system of non-linear partial differential equations, written in cartesian coordinates, describes the three-dimensional; unsteady fluid flow where the variables are in non-dimensional form.

Continuity Equation

$$\frac{\partial u}{\partial x} + \frac{\partial v}{\partial y} + \frac{\partial w}{\partial z} = 0 \qquad\qquad (2.1)$$

41

Horizontal Momentum Equations

$$\frac{\partial u}{\partial t} + u\frac{\partial u}{\partial x} + v\frac{\partial u}{\partial y} + w\frac{\partial u}{\partial z} - \frac{1}{R_b} v = -\frac{\partial P}{\partial x}$$
$$+ \frac{1}{R_e} \{\frac{\partial}{\partial x} (A_H^* \frac{\partial u}{\partial x}) + \frac{\partial}{\partial y} (A_H^* \frac{\partial u}{\partial y})\} + \frac{1}{R_e \varepsilon^2} \frac{\partial}{\partial z} (A_v^* \frac{\partial u}{\partial z})$$

$$(2.2)$$

$$\frac{\partial v}{\partial t} + u\frac{\partial v}{\partial x} + v\frac{\partial v}{\partial y} + w\frac{\partial v}{\partial z} + \frac{1}{R_b} u = -\frac{\partial P}{\partial y}$$

$$+ \frac{1}{R_e} \{\frac{\partial}{\partial x} (A_H^* \frac{\partial v}{\partial x}) + \frac{\partial}{\partial y} (A_H^* \frac{\partial v}{\partial y})\} + \frac{1}{R_e \varepsilon^2} \frac{\partial}{\partial z} (A_v^* \frac{\partial v}{\partial z})$$

$$(2.3)$$

Hydrostatic Pressure Equation

$$\frac{\partial P}{\partial z} = E_u(1 + \rho)$$

$$(2.4)$$

Energy Equation

$$\frac{\partial T}{\partial t} + u\frac{\partial T}{\partial x} + v\frac{\partial T}{\partial y} + w\frac{\partial T}{\partial z} = \frac{1}{P_e} \{\frac{\partial}{\partial x} (B_H^* \frac{\partial T}{\partial x}) + \frac{\partial}{\partial y} (B_H^* \frac{\partial T}{\partial y})\}$$

$$+ \frac{1}{P_e \varepsilon^2} \frac{\partial}{\partial z} (B_v^* \frac{\partial T}{\partial z})$$

$$(2.5)$$

Equation of State

$$\rho = \rho(T)$$

$$(2.6)$$

Where the set of non-dimensional quantities are defined as:

$$u = \frac{\tilde{u}}{U_{ref}} \;;\quad v = \frac{\tilde{v}}{U_{ref}} \;;\quad w = \frac{L}{H} \frac{\tilde{w}}{U_{ref}}$$

$$x = \frac{\tilde{x}}{L} \;;\quad y = \frac{\tilde{y}}{L} \;;\quad z = \tilde{z}/H \;;\quad \varepsilon = H/L$$

$$t = \frac{\tilde{t}}{t_{ref}} \quad ; \quad P = \tilde{P}/\rho_{ref} U^2_{ref} \quad , \quad T = \frac{\tilde{T} - T_{ref}}{T_{ref}} \quad , \quad \rho = \frac{\tilde{\rho} - \rho_{ref}}{\rho_{ref}}$$

$$A^*_H = A_H/A_{ref} \quad ; \quad A^*_v = A_v/A_{ref} \quad ; \quad B^*_H = B_H/B_{ref} : \quad B^*_v = B_v/B_{ref}$$

where quantities with the subscript 'ref' are reference quantities for the respective variables. The tilda denotes dimensional quantities. The quantities with an asterisk superscript are non-dimensional quantities.

L is the horizontal length scale.

H is the vertical length scale.

The other symbols in equations (2.1) - (2.6) are defined in the list of symbols for the rigid-lid model.

2.3.2 <u>Vertical Stretched Coordinate Representation</u>(α, β, γ)

The programming difficulties for a three-dimensional basin suggest a stretching of the vertical coordinate of the form

$$\gamma = \frac{\hat{z}}{\hat{h}(x,y)} \tag{2.70}$$

This coordinate transformation converts the basin to a constant depth one, so that a constant vertical grid size, $\Delta \gamma$, can be used throughout the domain. The horizontal coordinates (x,y) are transformed by letting

$$\alpha = \hat{x}$$
$$\beta = \hat{y} \tag{2.8}$$

Fig. 2.2 shows the α, β, γ coordinate system for 100 grid points.(sample) Once again although the symbols used in this section are defined in the list of symbols for the rigid-lid model, it is worthwhile to explain here the meaning of the subscripts and wavy lines

(tildas) used in the following vertically stretched equations.
Quantities with subscript 'ref' are reference quantities, H
and L are vertical and horizontal length scales, respectively.
The variables with wavy lines on top are dimensional quantities.
The quantities with an asterisk superscript are non-dimensional.

By converting the basin to constant depth, the same number
of grid points, and of constant grid size, can be used in the
vertical direction in shallow as well as in deep regions. The
details of transforming the equations in the (x,y,z) coordinate
system into the α, β, δ coordinate system is given in Sengupta
and Lick (1974)

The non-dimensional governing equations in the α, β, δ
coordinate system are expressed as follows:

Continuity Equation

$$\frac{\partial(hu)}{\partial \alpha} + \frac{\partial(hv)}{\partial \beta} + h\frac{\partial \Omega}{\partial \delta} = 0 \qquad (2.9)$$

Horizontal Momentum Equations

$$\frac{\partial(hu)}{\partial t} + \frac{\partial(huu)}{\partial \alpha} + \frac{\partial(huv)}{\partial \beta} + h\frac{\partial(\Omega u)}{\partial \delta} - \frac{h}{R_B} v$$

$$= -h \frac{\partial Ps}{\partial \alpha} - h B_x + \frac{1}{R_e} \frac{\partial}{\partial \alpha} (h\frac{\partial u}{\partial \alpha}) + \frac{1}{R_e} \frac{\partial}{\partial \beta} (h\frac{\partial u}{\partial \beta})$$

$$+ \frac{1}{\varepsilon^2 R_e} \frac{1}{h} \frac{\partial}{\partial \delta} (A_v^* \frac{\partial u}{\partial \delta}) \qquad (2.10)$$

44

$$\frac{\partial(hv)}{\partial t} + \frac{\partial(huv)}{\partial x} + \frac{\partial(hvv)}{\partial \beta} + h \frac{\partial(\ldots v)}{\partial \delta} + \frac{h}{R_b} u$$

$$= -h \frac{\partial Ps}{\partial \beta} - h By + \frac{1}{R_e} \frac{\partial}{\partial x} (h \frac{\partial v}{\partial x}) + \frac{1}{R_e} \frac{\partial}{\partial \beta} (h \frac{\partial v}{\partial \beta})$$

$$+ \frac{1}{\epsilon^2 R_e} \frac{1}{h} \frac{\partial}{\partial \delta} (A_v^{\star} \frac{\partial v}{\partial \delta})$$

$$(2.11)$$

where

$$\frac{\partial P}{\partial x} = B_x + \frac{\partial Ps}{\partial x}$$

$$\frac{\partial P}{\partial y} = B_y + \frac{\partial Ps}{\partial y}$$

and

$$B_x = E_u \frac{\partial}{\partial x} \int_0^{\pi} \rho dz$$

$$B_y = E_u \frac{\partial}{\partial y} \int_0^z \rho dz$$

and

P_s = Surface Pressure

Hydrostatic Equation

$$\frac{\partial P}{\partial \delta} = E_u (1+\rho)h \qquad (2.12)$$

Energy Equation

$$\frac{\partial(hT)}{\partial t} + \frac{\partial(huT)}{\partial \alpha} + \frac{\partial(hvT)}{\partial \beta} + h\frac{\partial(\omega T)}{\partial \delta}$$

$$= \frac{1}{P_e}\frac{\partial}{\partial \alpha}(h\frac{\partial T}{\partial \alpha}) + \frac{1}{P_e}\frac{\partial}{\partial \beta}(h\frac{\partial T}{\partial \beta}) + \frac{1}{P_e \epsilon^2}\frac{1}{h}\frac{\partial}{\partial \delta}(B_v^*\frac{\partial T}{\partial \delta})$$

$$(2.13)$$

Equation of State

$\tilde{\rho} = \tilde{\rho}\ (\tilde{T})$ is given for fresh and salt water as follows:

Salt Water: $\tilde{\rho}\ (\tilde{T}) = 1.029431 - .0000020\hat{T} - .0000048\hat{T}^2$ (2.14)
(for salinity of 38 parts per thousand)

Fresh Water: $\tilde{\rho}\ (\tilde{T}) = 0.000428 - .000019\hat{T} - .0000046\hat{T}^2$ (2.15)

where again the wavy line denotes dimensional quantities. Note,
$\hat{T}$ is in degrees celsius.

<u>Actual Vertical Velocity</u> in $(\tilde{x},\tilde{y},\tilde{z})$ coordinate system

$$\tilde{w} = \gamma(\tilde{u}\frac{\partial \tilde{h}}{\partial \tilde{x}} + \tilde{v}\frac{\partial \tilde{h}}{\partial \tilde{y}}) + \tilde{h}\,\tilde{\Omega} \qquad (2.16)$$

$$\tilde{\Omega} = \frac{\partial \gamma}{\partial \tilde{t}}$$

(note, by virtue of the rigid-lid approximation, $\tilde{w}\ (\tilde{z}=0)=0$)

46

Due to the rigid-lid approximation the surface pressure, P_s, is not atmospheric as in the case for a free surface model. To obtain a predictive equation for surface pressure, P_s, the horizontal momentum equations (2.10) and (2.11) are integrated from z=o to z=h, where h is the non-dimensional depth $\overset{\smile}{h}/H$. The integrated equations are then differentiated once with respect to α and β and then summed. This derivation yields the Poisson equation for surface pressure, P_s. Sengupta and Lick (1974).

Surface Pressure Equation

$$\frac{\partial^2 Ps}{\partial \alpha 2} + \frac{\partial^2 Ps}{\partial \beta 2} = \frac{1}{h} \frac{\partial}{\partial \alpha} (-A_{x1} + A_{x2} + C_x - X_p)$$

$$+ \frac{1}{h} \frac{\partial}{\partial \beta} (-A_{y1} - A_{y2} + C_y - Y_p)$$

$$- \frac{1}{h} (\frac{\partial h}{\partial \alpha} \frac{\partial Ps}{\partial \alpha} + \frac{\partial h}{\partial \beta} \frac{\partial Ps}{\partial \beta}) - \frac{\partial \Omega}{\partial t}\Bigg|_{z=0} = \Pi(\alpha \ \beta)$$

$$(2.17)$$

The last term is the Hirt and Harlow (1964) correction term which accounts for non-zero vertical velocities at the rigid-lid. The variables $(B_x, B_y,$ and $A_{x1}, A_{x2},$ etc) are given below:

$$A_{x1} = \int_0^1 \left[\frac{\partial}{\partial \alpha}(huu) + \frac{\partial}{\partial \beta} (huv) + h\frac{\partial}{\partial \gamma} (\Omega u) \right] d\gamma$$

$$A_{x2} = \frac{h}{R_b} \int_0^1 v d\gamma$$

$$C_x = \left[\frac{1}{Re} \int_0^1 \frac{\partial}{\partial \alpha} (h\frac{\partial u}{\partial \alpha}) + \frac{\partial}{\partial \beta} (h\frac{\partial u}{\partial \beta}) + \frac{1}{\epsilon^2} \frac{1}{H} \frac{\partial}{\partial \gamma} (A_v^* \frac{\partial u}{\partial \gamma}) \right] d\gamma$$

47

$$A_{X_1} = \int_0^1 \left\{ \frac{\partial}{\partial\alpha}(huu) + \frac{\partial}{\partial\beta}(huv) + h\frac{\partial}{\partial\gamma}(\Omega u) \right\} d\gamma$$

$$A_{X_2} = \frac{h}{R_B} \int_0^1 v\, d\gamma$$

$$C_X = -\frac{1}{R_e} \int_0^1 \left\{ \frac{\partial}{\partial\alpha}(h\frac{\partial u}{\partial\alpha}) + \frac{\partial}{\partial\beta}(h\frac{\partial u}{\partial\beta}) + \frac{1}{\epsilon^2} \frac{1}{h} \frac{\partial}{\partial\gamma}(A_V^* \frac{\partial u}{\partial\gamma}) \right\} d\gamma$$

$$X_p = E_u \int_0^1 h\left\{ \frac{\partial h}{\partial X} \int_0^\gamma \rho\, d\gamma + h\frac{\partial}{\partial\alpha} \int_0^\gamma \rho\, d\gamma - \gamma\frac{\partial h}{\partial\alpha}\rho \right\} d\gamma$$

$$A_{Y_1} = \int_0^1 \left\{ \frac{\partial}{\partial\alpha}(huv) + \frac{\partial}{\partial\beta}(huv) + h\frac{\partial(\Omega v)}{\partial\gamma} \right\} d\gamma$$

$$A_{Y_2} = \frac{h}{R_B} \int_0^1 u\, d\gamma$$

$$C_y = \frac{1}{R_e} \int_0^1 \left\{ \frac{\partial}{\partial\alpha}(h\frac{\partial u}{\partial\alpha}) + \frac{\partial}{\partial\beta}(h\frac{\partial u}{\partial\beta}) + \frac{1}{\epsilon^2} \frac{1}{h} \frac{\partial}{\partial\gamma}(A_V^* \frac{\partial u}{\partial\gamma}) \right\} d\gamma$$

$$Y_p = E_u \int_0^1 h\left\{ \frac{\partial h}{\partial\beta} \int_0^\gamma \rho\, d\gamma + h\frac{\partial}{\partial\beta} \int_0^\gamma \rho\, d\gamma - \gamma\frac{\partial h}{\partial\beta}\rho \right\} d\gamma$$

$$B_x = E_u\frac{\partial h}{\partial\alpha} \int_0^\gamma \rho\, d\gamma + E_u h\frac{\partial}{\partial\alpha} \int_0^\gamma \rho\, d\gamma - E_u\gamma\frac{\partial h}{\partial\alpha}\rho$$

$$B_y = E_u\frac{\partial h}{\partial\beta} \int_0^\gamma \rho\, d\gamma + E_u h\frac{\partial}{\partial\beta} \int_0^\gamma \rho\, d\gamma - E_u\gamma\frac{\partial h}{\partial\beta}\rho$$

2.4 Boundary Conditions (closed basins and open basins)

The nature of the system of governing equations requires initial and boundary conditions to be specified. The boundary conditions for both near-field (open basin) and far-field (closed basin) versions of the rigid-lid model are presented in this section. The initial conditions will be presented in the next section.

2.4.1 Near-Field (open basin)

The rigid-lid model, near-field has been applied to an open boundary domain with thermal discharge along the lateral solid boundary, Venkata (1977). This model has also been applied by Mathavan (1977) to a mixing pond which has an opening at one boundary and a thermal discharge at another boundary. The set of boundary conditions for the domain having open boundaries will be given in this section, since these open boundary conditions are most difficult to specify.

At solid boundaries no-slip and zero normal velocity conditions are specified. All solid boundaries are considered adiabatic. At the air-water interface $\frac{\partial u}{\partial z}$ and $\frac{\partial v}{\partial z}$ are set proportional to the wind shear stress components in the x and y directions, respectively. The rigid-lid approximation sets the vertical velocity w to be zero at the air-water interface. Also at the surface $\frac{\partial T}{\partial z}$ is set proportional to the heat flux from the surface. The heat flux from the surface is in turn proportional to $(T_s - T_e)$, where T_e is the so-called equilibrium temperature. The equilibrium temperature is the surface temperature at which the heat entering the water body at the air-water interface is equal to heat leaving the water surface. At the open boundaries the first order derivatives of temperature and velocity are set equal to zero. Thus, the boundary conditions are in summary:

At the surface, $\gamma = 0$

$$\Omega = 0$$

$$(1) \quad \frac{\partial u}{\partial \sigma} = -\left(\frac{hH}{U_{ref}\rho A_v}\right)\tau_{zx}$$

$$\frac{\partial v}{\partial \gamma} = -\left(\frac{hH}{U_{ref}\rho A_v}\right)\tau_{zy}$$

$$\frac{\partial T}{\partial \gamma} = -\left(\frac{hHK_s}{\rho \, \varphi_p B_v}\right)(T_e - T_s)$$

At lateral solid boundaries on x-boundaries:

$$\Omega = 0$$

$$u = 0$$

$$v = 0$$

$$\frac{\partial T}{\partial x} = \frac{\partial T}{\partial \alpha} - \frac{\gamma}{h}\frac{\partial h}{\partial \alpha}\frac{\partial T}{\partial \gamma} = 0$$

[1] Note: H is vertical scale length for rigid-lid model.

49

At the bottom, $\gamma = 1$

$\Omega = 0$

$u = 0$

$v = 0$

$\dfrac{\partial T}{\partial \gamma} = 0$

At lateral open boundaries

on x-boundaries

$\Omega = 0$

(2) $\dfrac{\partial u}{\partial \alpha} = 0$

$v = 0$

$\dfrac{\partial T}{\partial x} = \dfrac{\partial T}{\partial \alpha} - \dfrac{\gamma}{h}\dfrac{\partial h}{\partial \alpha}\dfrac{\partial T}{\partial \gamma} = 0$

At Discharge

Velocity
Density   } Specified
Temperature

on y-boundaries

$\Omega = 0$

$u = 0$

$v = 0$

$\dfrac{\partial T}{\partial y} = \dfrac{\partial T}{\partial \beta} - \dfrac{\gamma}{h}\dfrac{\partial h}{\partial \beta}\dfrac{\partial T}{\partial \gamma} = 0$

on y-boundaries

$\Omega = 0$

$u = 0$

(2) $\dfrac{\partial v}{\partial \beta} = 0$

$\dfrac{\partial T}{\partial y} = \dfrac{\partial T}{\partial \beta} - \dfrac{\gamma}{h}\dfrac{\partial h}{\partial \beta}\dfrac{\partial T}{\partial \gamma} = 0$

2.4.2 Far-Field (closed basin)

The rigid-lid model, far-field has been applied to the Biscayne Bay, Sengupta (1975), and to Lake Belews, Mathavan (1977). For both applications there is no direct thermal discharge modeled, but open boundaries are treated in much the same manner as was outlined for the near-field studies. The boundary conditions are in summary:

At the surface, $\gamma = 0$

$\Omega = 0$

$\dfrac{\partial u}{\partial \gamma} = -\left(\dfrac{hH}{U_{ref}\rho A_v}\right)\tau zx$

$\dfrac{\partial v}{\partial \gamma} = -\left(\dfrac{hH}{U_{ref}\rho A_v}\right)\tau zy$

$\dfrac{\partial T}{\partial \gamma} = -\left(\dfrac{hHKs}{\rho c_p B_v}\right)(T_e - T_s)$

At lateral solid boundaries

on x-boundaries

$\Omega = 0$

$u = 0$

$v = 0$

$\dfrac{\partial T}{\partial x} = \dfrac{\partial T}{\partial \alpha} - \dfrac{\gamma}{h}\dfrac{\partial h}{\partial \alpha}\dfrac{\partial T}{\partial \gamma} = 0$

(2) Note: If u is into domain then u=u far field value. If u points out of domain then $u_{boundary}$ = u adjacent interior point. Similarly for v specification.

50

At the bottom, $\gamma = 1$

$\Omega = 0$

$u = 0$

$v = 0$

$\dfrac{\partial T}{\partial \gamma} = 0$

on y-boundaries

$\Omega = 0$

$u = 0$

$v = 0$

$\dfrac{\partial T}{\partial y} = \dfrac{\partial T}{\partial \beta} - \dfrac{\gamma}{h}\dfrac{\partial h}{\partial \beta}\dfrac{\partial T}{\partial \gamma} = 0$

At lateral open boundaries (inlets or outlets)

on x-boundaries

$\Omega = 0$

(3) $u = u(t)$ or $\dfrac{\partial u}{\partial \alpha} = 0$

$\dfrac{\partial T}{\partial x} = \dfrac{\partial T}{\partial \alpha} - \dfrac{\gamma}{h}\dfrac{\partial h}{\partial \alpha}\dfrac{\partial T}{\partial \gamma} = 0$

on y-boundaries

$\Omega = 0$

$v = v(t)$ or $\dfrac{\partial v}{\partial \beta} = 0$

$u = 0$

$\dfrac{\partial T}{\partial y} = \dfrac{\partial T}{\partial \beta} - \dfrac{\gamma}{h}\dfrac{\partial h}{\partial \beta}\dfrac{\partial T}{\partial \gamma} = 0$

2.5 Initial Conditions

The initial conditions are specified by using the corrected IR data base for temperature; as will be illustrated in the sample problems in Volume II and zero velocity everywhere in the domain ($u=v=\Omega=0$), since it is quite difficult to obtain ground truth current measurements for the entire domain for the kind of grid size resolution that would be required.

2.6 Method of Solution

2.6.1 General

It is obvious that closed-form analytical solution of the system of governing aquations (2.9) - (2.17) is impossible to get. The set of equations consists of coupled, unsteady, three-dimensional, nonlinear partial differential equations. Therefore, the finite difference method is used to obtain numerical solutions.

A three-dimensional grid system is established with respect to the (α, β, γ) coordinate system for the rigid-lid model. The governing equations are then solved over finite time steps which are carefully selected to obey numerical stability criteria. This will be discussed in detail in a following subsection on stability criteria (2.6.5).

[3] Note: At an inlet either $u(t)$ or $v(t)$ must specified, and at an outlet $\dfrac{\partial u}{\partial \alpha}$ or $\dfrac{\partial v}{\partial \beta}$ may be specified.

51

In general, several methods are available for integrating over time the governing equations for incompressible fluid flow as discussed by Roache (1972). The two most common techniques for integrating time-dependent partial differential equations are the implicit and explicit finite difference methods. The implicit method involves the solution of a set of simultaneous equations which are obtained by writing the spatial derivatives in terms of the respective unknown quantities at the current time level, n+1, knowing the values of the remaining quantities of the set (u,v,Ω,P,ρ,T) at the two previous time levels n and $n-1$. For the one-dimensional case, implicit methods are convenient because the set of simultaneous equations is tri-diagonal, Richtmyer and Morton (1967), and, hence, a direct matrix inversion method of solution is used. However, in the case of a three-dimensional model, the implicit method becomes too time consuming; since the simultaneous equations must be solved at each time step by an iterative technique. Thus, although the advantage of implicit methods is that they allow larger time steps, for the three dimensional case the iteration time for each time step more than offsets the inherently larger time step. Furthermore, alternating direction-implicit (ADI) methods may be used to obtain tri-diagonal matrices even for multidimensional equations, however, for irregular boundaries the ADI methods are impractical.

Therefore, the explicit finite difference method is used for numerical solution of the rigid-lid model. The solution to a particular partial differential equation is propagated from point to point on the numerical grid system. The current time level value $n + 1$, of a particular system variable (u,v,Ω,P,ρ,T) is computed in general from known values of the corresponding system variables at the two previous time levels n and n-1. Thus, this is an explicit scheme. However, as will be seen later, the governing

52

equations for surface (or lid) pressure for the rigid-lid model is elliptic; Sengupta and Lick (1974), and, therefore, values of P_s for the entire domain are computed at each time step, iteratively.

The mathematical model is an initial-value, boundary value problem and, hence, requires specification of both initial conditions and boundary conditions (see sections 2.4 and 2.5).

2.6.2 Computational Grid System

A schematic of the computational grid system for the rigid-lid model is illustrated in Fig. 2.3. A half-grid (dashed-line grid) is superimposed on a full grid (solid line grid) in the $\alpha\beta$ plane. The horizontal velocity components u and v are defined at the nodes of the full grid at (I,J,K); and Ω, P,ρ, T are defined at the nodes of the half-grid ($I+\frac{1}{2}$, $J+\frac{1}{2}$, K). This arrangement allows better meshing of the system variables at all the nodes of this staggered mesh system. Constant grid spacing is used in the γ direction. Constant grid spacing may or may not be used in the α and β directions, respectively.

During computation; values of the system variables u and v in the full grid system (I,J,K) are averaged, as follows , for computation of the system variables Ω,P,ρ and T in the half-grid system ($I+\frac{1}{2}$, $J+\frac{1}{2}$, K):

$$(u,v)_{I+\frac{1}{2},\ J+\frac{1}{2}} = \left[(u,v)_{I,J,K} + (u,v)_{I+1,\ J+1,K} + (u,v)_{I,J+1,K} \right.$$

$$\left. + (u,v)_{I+1,\ J,K} \right] / 4 \tag{2.18}$$

2.6.3 MAR and MRH Numbering System

The computational full grid system is divided into separate regions depending on the type of spatial finite difference used. That is, a two-dimensional matrix call MAR (I,J) is used in the model which distinguishes between interior points, points on the boundary; and points out-side the domain of solution. Similarly, for the half-grid

system a two-dimensional matrix call MRH ($I + \frac{1}{2}$, $J + \frac{1}{2}$)
is used to distinguish between spatial finite differencing
in the interior, on the boundary, and outside the domain of
solution; Sengupta and Lick (1974). The MAR numbering system
and the MRH numbering system will be clearly specified in
the sample problems in Volume II.

   2.6.4 Finite Difference Schemes

   2.6.4.1 Approximation of Spatial and Temporal Partial
          Derivatives; Conservative Form

The spatial derivatives are central differenced in the
interior; for example in the full grid system;

$$\frac{\partial u}{\partial \alpha} \simeq \frac{u(I+1, J, K) - U(I-1, J, K)}{2\Delta\alpha} \tag{2.19}$$

and,

$$\frac{\partial^2 u}{\partial \alpha^2} \simeq \frac{u(I+1,J,K) + u(I-1,J,K) - 2u(I,J,K)}{(\Delta\alpha)^2} \tag{2.20}$$

and in the half-grid system:

$$\frac{\partial T}{\partial \alpha} \simeq \frac{T(I+3/2,J,K) - T(I-\frac{1}{2},J,K)}{2\Delta\alpha} \tag{2.21}$$

and,

$$\frac{\partial^2 T}{\partial \alpha 2} \simeq \frac{T(I+3/2,J,K) + T(I-\frac{1}{2},J,K) - 2T(I+\frac{1}{2},J,K)}{(\Delta\alpha)^2} \tag{2.22}$$

At the boundaries, however, three-point single sided schemes
are used by fitting a parabola through three points (the
boundary point and the next two coincident interior points).
Thus, for example, at the left α- boundary:

$$\frac{\partial u}{\partial \alpha} \simeq \frac{4u(I+1,J,K) - 3u(I,J,K) - u(I+2,J,K)}{2\Delta\alpha} \tag{2.23}$$

and,

$$\frac{\partial^2 u}{\partial \alpha^2} \simeq \frac{u(I,J,K) + u(I+2,J,K) - 2u(I+1,J,K)}{(\Delta\alpha)^2} \tag{2.24}$$

and, at the right α -boundary:

$$\frac{\partial u}{\partial \alpha} \simeq \frac{3u(I,J,K) + u(I-2,J,K) - 4u(I-1,J,K)}{2\Delta\alpha} \tag{2.25}$$

and,

$$\frac{\partial^2 u}{\partial \alpha^2} \cong \frac{u(I,J,K) + u(I-2,J,K) - 2u(I-1,J,K)}{(\Delta\alpha)^2} \tag{2.26}$$

Similar expression to equations (2.23) - (2.26) may be
obtained for system variables in the half-grid system by
simply replacing (I+1,J,K) with (I+3/2,J,K), (I-1,J,K)
with (I-½,J,K), (I, J, K) with (I+½,J,K), (I+2,J, K)
with (I+5/2,J,K), and (I-2, J, K) with (I-3/2,J,K).

Note, that the spatial finite difference approximations
(2.19) -(2.26) are on order of accuracy of ($\Delta\alpha$)^2. Crandall (1965).

The <u>temporal derivatives</u> can be expressed in two forms, first

$$\frac{\partial u}{\partial t} \cong \frac{u(I,J,K)^{n+1} - u(I,J,K)^{n}}{\Delta t} \tag{2.27}$$

for forward differencing in time; which is on the order of
accuracy of Δt; and

$$\frac{\partial u}{\partial t} \cong \frac{u(I,J,K)^{n+1} - u(I,J,K)^{n-1}}{2\Delta t} \tag{2.28}$$

for central differencing in time; which is on the order of
accuracy of(Δt)^2.

The finite differences in both space and time in the
model are expressed in the full <u>conservation</u> forms following
Arakawa (1966), for example:

$$\frac{\partial(Hu)}{\partial\alpha} \cong \frac{(Hu)_{I+1,J,K} - (Hu)_{I-1,J,K}}{2\Delta\alpha} \tag{2.29}$$

This is done to avoid possible "leaking" of mass, momentum,
and energy for long term integration with respect to time
of the governing time-dependent equations.

2.6.4.2 <u>Finite Difference Equations</u>

The far-field and near-field versions of the rigid-lid
model use the same set of finite difference equations; although
the initial conditions and boundary conditions are quite

different. Equations (2.9)-(2 13) for continuity, hori-
zontal momentum conservation, and conservation of energy are
approximated by finite difference equations by using a for-
ward time, central space scheme (so-called FTCS), with DuFort-
Frankel (1953) differencing performed on the diffusion terms.
The finite difference equation for u-momentum may be written
as for example

$$\frac{u^{n+1} - u^n}{\Delta t} = (\text{Inertia})^n + (\text{Coriolis})^n + (\text{Pressure})^n \qquad (2.30)$$
$$+ (\text{Viscous})^{n,n+1,n-1}$$

where the DuFort-Frankel differencing is expressed as

$$\frac{\partial^2 u}{\partial \alpha^2} = \frac{u^n(I+1,J,K) + u^n(I-1,J,K) - u^{n+1}(I,K,K) - u^{n-1}(I,J,K)}{(\Delta \alpha)^2} \qquad (2.31)$$

The effect of modified DuFort-Frankel differencing is to relax
somewhat the diffusive stability criterion, Sengupta (1974).

The surface pressure equation (2.17) may be solved by
iteration, at each time step, by using successive over-
relaxation or by the modified SOR technique (Liebmann Method).

Fig.2.4 shows the flow chart for the steps involved
in propagating the numerical solution of the system of govern-
ing equations for the rigid-lid model. These steps may be
elaborated as follows:

1. The problem is set up as an initial value problem.
The values of u, v, ρ, p, Ω and T are specified initially for
time level n.

2. Using the known values of the system variables at
time level n the forcing function, $\pi(\alpha, \beta)$ is evaluated at
all half-grid nodes.

3. Surface pressure, P_s, at the "rigid lid" is eval-
uated by iteration (Liebmann method) at all half-grid nodes
using the Poisson equation.

4. Pressure gradients computed from the Poisson equation are used to compute u and v by the horizontal momentum equations for the current time level n + 1. The hydrostatic equation (2.12) is used in the process to obtain the three-dimensional pressure field.

5. The continuity equation is then used to compute equivalent vertical velocity, Ω , at time level n + 1 from the known values of u and v at time level n + 1. The values of Ω are obtained by integrating the continuity equation from $\gamma=0$ to $\gamma=1$.

6. The actual vertical velocity, w, is then computed at time level n + 1 by using equation (2.16).

7. The energy equation is then used to compute the values of T at time level n + 1 from the known values of u,v and Ω at time level n + 1 and T at time level n.

8. The solution domain is then checked for static stability. If there is cooler water on top of the lower warmer water, i.e., if

$$T_{K+1}\big|_{I+\frac{1}{2},J+\frac{1}{2}} > T_k\big|_{I+\frac{1}{2}, J+\frac{1}{2}} \text{ for unstable} \qquad (2.32)$$

conditions infinite mixing is invoked.

9. The density, ρ , is then computed from the equation of state knowing T at time level n + 1.

These nine steps are then repeated to propagate the numerical solution to time levels n + 2, n + 3, etc.

2.6.5 Stability Criteria

Since it is not possible to make a strict stability analysis for the system of governing equations under consideration, the one-dimensional Burgers equation is used for stability analysis. This is relevant since the Burgers equation contains an unsteady term, a convective term and a diffusion term. The stability criteria for Burgers equation

$$\frac{\partial u}{\partial t} + C_x \frac{\partial u}{\partial x} = D_x \frac{\partial^2 u}{\partial x^2} \qquad (2.33)$$

as discussed by Roache (1972) are as follows .

CONVECTIVE: $C_x \; \dfrac{\Delta t}{\Delta x} < 1$ (2.34)

DIFFUSIVE: $D_x \; \dfrac{\Delta t}{(\Delta x)^2} < \tfrac{1}{2}$ (2.35)

The Burgers equation represents the one-dimensional form of
incompressible fluid motion. The convective stability
criterion may be interpreted to require that no fluid
particle can move the distance of one spatial grid space
in one time step. Likewise, the diffusive stability
criterion may be interpreted to require that momentum
cannot diffuse to half the distance of one spatial grid
space in one time step in forward and backward directions.
Thus, for the numerical solution to be stable, the time
step must be small enough to give sufficient time for the
physical processes to develop at each grid node.

The stability criteria may be extended to the three-
dimensional equations as follows:

CONVECTIVE: $C_x \left(\dfrac{\Delta t}{\Delta x}\right) + C_y \left(\dfrac{\Delta t}{\Delta y}\right) + C_z \left(\dfrac{\Delta t}{\Delta z}\right) < 1$ (2.36)

DIFFUSIVE: $D_x \; \dfrac{\Delta t}{(\Delta x)^2} + D_y \; \dfrac{\Delta t}{(\Delta y)^2} + D_z \dfrac{\Delta t}{(\Delta z)^2} < \tfrac{1}{2}$ (2.37)

For the application of these criteria to the present problem,
C_x, C_y, and C_z may be interpreted as the maximum values
of u, v, and w in the domain; and D_x, D_y, and D_z may be
interpreted as the kinematic eddy diffusivities in the
x, y, and z directions, respectively.

   2.6.6 Higher Order Terms

Higher order terms resulting from the transformation
of the horizontal diffusion terms (i.e. second order
derivatives in α and β), from the Cartesian coordinate
system (x, y, z) to the vertically stretched coordinate

58

system $(x \beta \gamma)$ have been neglected. This has been done since the magnitude of the vertical diffusion terms are several orders of magnitude larger than the horizontal diffusion terms, Sengupta and Lick (1974). Appendix A of this volume presents the details of this transformation.

2.7 Sample Results

In this section sample results using the rigid-lid model for near-field and far-field applications will be presented.

2.7.1 Near-Field, Cutler Ridge Site (open basin)

The region of influence of the Cutler Ridge plume has been approximated to a rectangular domain as shown in Fig. 2.4 which is open on three lateral boundaries. The grid system for the rigid-lid near-field model of the Cutler Ridge site is shown in Fig. 2.5. The rectangular domain of solution extends 425 meters in lateral extent and 525 meters in longitudinal extent. The discharge is taken as 25 meters wide. The numerical grid system has 18 and 22 nodes across and along the axis of the jet, respectively. There are 5 nodes in the vertical direction.

In order to understand the physical processes involved and to investigate the numerical behavior of the model several simplified cases were executed before the final calibration and verification run for the data bases obtained for April 15, 1975. Volume II presents the details of this computer run. Table 2-1 shows different cases studied together with important features for each case. Lee and Sengupta (1977).

The data base for the final calibration and verification run is obtained from the field experiments conducted at the Cutler Ridge site on April 15, 1975. The initial temperature conditions are taken from the morning IR data (0911-0912 EST) shown in Fig. 2.6 and ground truth data on April 15, 1975. The computations were continued for $2\frac{1}{2}$ hours. Figs. 2.7 to 2.10 show velocity distribution at the

surface and at different vertical layers. The interaction
between the wind driven current and the plume due to current
coming from the south can be seen in these figures. The
fluid is exiting through the east and western boundaries
only. The reduction of the effects of wind and current in
the lower vertical layers can also be seen due to bottom
shear. Fig. 2.11 shows isotherms predicted by the model
along with IR data (11:45 - 11:55 EST) on April 15, 1975.
As can be seen, there is reasonably good agreement between
IR data and model predicted results. Fig. 2.12 shows
temperature decay along J at I=11 (i.e. close to the center-
line) predicted by the model along with IR data. There is
good agreement between IR data and model results. The iso-
therms along I and J sections are shown in Figs. 2.13 and
                    Stratification near the discharge with
isothermal conditions away from the plume can be seen in
Fig. 2.13.

   2.7.2 <u>Far-Field, Biscayne Bay (closed basin with ocean
          efflux)</u>

Ignoring the Cutler Ridge site thermal discharge, the
rigid-lid far-field model was applied to Biscayne Bay to
investigate the naturally occuring circulation and far-field
temperature distribution.

Applying the rigid-lid far-field model to Biscayne Bay,
solutions have been obtained in three stages. First, a
closed basin approximation was made and wind driven cir-
culation was obtained. In the second stage circulation in
the Bay was obtained with an ocean efflux specified; the
simultaneous effects of wind and ocean efflux were also
investigated. The third and final stage obtained the temp-
erature field for various ambient conditions and parameters.
The results were compared with airborne thermal scanner
IR data to calibrate the model. This procedure was followed
in order to check the performance of the model for as wide
a range of environmental situations as possible. The hor-

izontal grid system for Biscayne Bay is shown in Fig.2.15
(I=11, J=34). Five vertical layers were used in the model.

Lee and Veziroglu (1975) present results for this
application for the three stages noted. Only results for
the third and final stage will be presented and discussed now.

A 10cm/sec velocity for both the incoming and outgoing
tidal phases was assumed. The program is executed with an
incoming tide, and then the ocean-bay velocity pattern is
gradually reversed to obtain a 10cm/sec outgoing velocity.
Although the details of phase relations, level change and
time dependence cannot be precisely modeled by the rigid-
lid model (c.f. section 2.1 of Volume I), the results should
give a meaningful equalitative picture of the circulation.

Fig.2.16 shows the surface velocities with an in-
coming tide. The major portion of the tidal mass influx
travels into the South Bay while the flow towards the
closed northern region is minimal. Fig.2.17 shows the
velocities at a depth of 1 meter with an incoming tide.
The flow is unidirectional at most points. The incoming
flow was gradually reversed. Fig.2.18 shows the surface
velocities at an intermediate stage. The currents have re-
versed in some places but not in others. In Fig.2.19, the
currents at a depth of two meters are almost completely
reversed.

Fig. 2.20 shows that the bulk of the outflow comes
from south bay. At Cutler Ridge the current is now from
west to east, therefore, with outgoing tide the plume is
expected to turn towards the east.

The effects of wind and tide on the general circulation
are shown in Fig.2.21. The effect of the southeast wind is
to turn the current vectors toward the northern part of
the bay. The velocities in the south bay are still essentially
southward but are of a smaller magnitude due to the south-

61

east wind.

The temperature solutions for various combinations of parameters have been obtained for comparison to the April 15, 1975 IR data base. Table 2-2 shows a list of some of the cases for which solutions were obtained. Fig. 2.22 shows good agreement between model results and the IR data base for April 15, 1975. Fig. 2.23 shows vertical section J=7 illustrating the isotherms in a transect. As can be seen vertical temperature variation is relatively small owing to the shallowness of the bay and the turbulent mixing processes.

2.7.3 Near-Field and Far-Field, Lake Belews

For ease of mathematical modelling, the total path of water circulation is divided into two regions, namely the mixing pond (near-field) and the main lake (far-field). These two regions are treated as disconnected regions. Fig. 2.24 shows the grid system for the mixing pond (I=29, J=13). Fig. 2.25 shows the grid system for the main lake (I=29, J=13). Lee and Sengupta (1977).

The mixing pond receives hot water from the power plant, mixes it with cooler water and then discharges it into the main lake through the connecting canal. The main lake receives hot discharges from the connecting canal, cools it and from there it goes into the power plant condensers.

The primary difference in the parameters in the mixing pond and the main lake is the fact that the mixing pond is well mixed while the main lake shows thermal stratification. This in turn means that the vertical eddy diffusivity in the mixing pond is constant over the entire depth whereas in the main lake vertical diffusivity decreases with depth.

Table 2-3 gives the list of computer runs for Lake Belews site. Fig. 2.26 shows the surface velocity pattern in the mixing pond for the August 23, 1974 data base; and Fig. 2.27 shows the velocity distrubtion at four meters depth in the mixing pond. It can be seen that at the

surface the current vectors are in the direction of the wind
to right of the connecting canal. Whereas at four meters
depth the circulation to the right of the canal is reversed
from that on the surface. Figs. 2.28 and 2.29 show surface
isotherms and isotherms at four meters depth in the mixing
pond for the August 23, 1974 data base. Fig. 2.30 shows
a comparison of model predicted surface isotherms and IR
data base for May 19, 1976. The general agreement is
reasonably good.

TABLE 2-1

CASE NO.	DENSITY	DEPTH	WIND	CURRENT	TOTAL TIME
1	Constant	1.2 m	None	None	Steady State 3 hrs. 20 min.
2	Constant	Variable	None	None	Steady State 2 hrs. 35 min.
3	Constant	Variable	6.71 m/sec 160°N	None	Steady State 4 hrs.
4	Variable	1.2 m	None	None	30 min.
5	Variable	1.2 m	0.13 m/sec N.W.	None	2 hrs.
6	Variable	1.2 m	6.71 m/sec 160°N	None	2 hrs. 30 min.
7	Variable	Variable	6.71 m/sec 160°N	3 cm/sec from south	30 min.
8	Verification Case for April 15, 1975 with I.R. Data Initial Conditions				2 hrs. 35 min.

The values that have been used in the above cases are:

Discharge Velocity   : 20 cm/sec   Horizontal Eddy Viscosity : 10,000 cm^2/sec
Discharge Temperature : 35.9°C   Vertical Eddy Viscosity   : 1 cm^2/sec
Initial Temperature : 28.0°C   Surface Heat Transfer
                                          Coefficient   : 100 BTU/°F-ft^2-day

Air Temperature   : 29.5°C

64

TABLE 2-2 LIST OF COMPUTER RUNS FOR LAKE BELEWS SITE

(RIGID LID MODEL)

CASE NO.	DATE	PART OF LAKE	DEPTH (METERS)	INITIAL TEMP. ($^\circ$C)	VERTICAL DIFFUSIVITY	DISCHARGE TEMP. ($^\circ$C)	TYPE OF RESULTS	TIME (HOURS)
1	8/23/74	Mixing Pond	Variable	32.0 Const.	Const.	36.4	Currents Temp.	15.5
2	5/19/76	Mixing Pond	Variable	Variable	Const.	29.5-27.9	Currents Temp.	6.0
3	5/19/76	Main Lake	Variable	28.2 Const.	Const.	28.2	Currents	0.5
4	5/19/76	Main Lake	9.14 Const.	Variable	Variable	28.2-28.6	Currents Temp.	6.0

65

Air-water interface

Surface is plane for
rigid-lid model

Floor of basin

$\bar{h}$ is constant
at any $(\bar{x}, \bar{y})$ location
for rigid-lid model

Fig. 2-1   Coordinate system used for derivation of equations.

66

Fig. 2-2   Grid System αβγ Coordinate System

67

Horizontal Plane
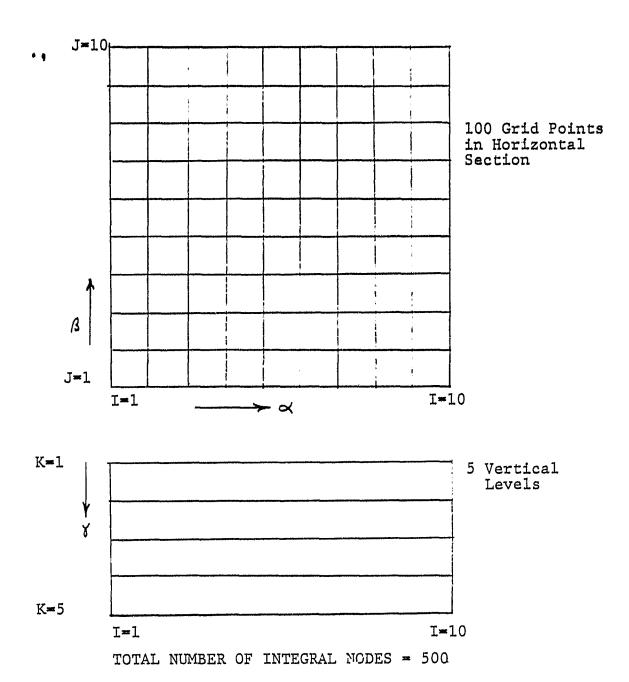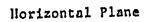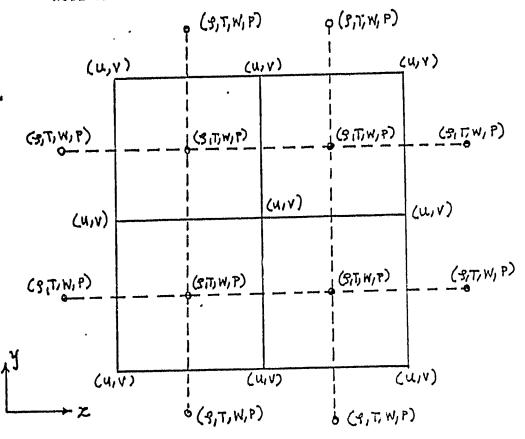
Arrangement repeated at each horizontal level.
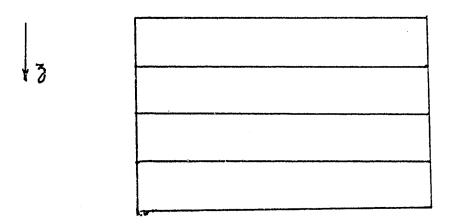
Fig. 2-3   Arrangement of staggered grid and variables.

THERMAL POLLUTION LAB
UNIVERSITY OF MIAMI

VALUES OBTAINED
BY EXTRAPOLATION

REGION OF COMPUTATION
(TOP VIEW)

NO SLIP

DISCHARGE

SHORE

AMBIENT CROSS FLOW
(CONSTANT IN TIME)

VALUES OBTAINED
BY EXTRAPOLATION

TANGENTIAL FLOW ONLY

DISCHARGE

(SIDE VIEW)

CROSS FLOW

NO SLIP

TANGENTIAL FLOW ONLY

VALUES OBTAINED
BY EXTRAPOLATION

(VIEW ALONG SECTION J-J)

VALUES OBTAINED
BY EXTRAPOLATION

NO SLIP

Fig. 2-4   Boundary Conditions for the Region
            of Computation

69
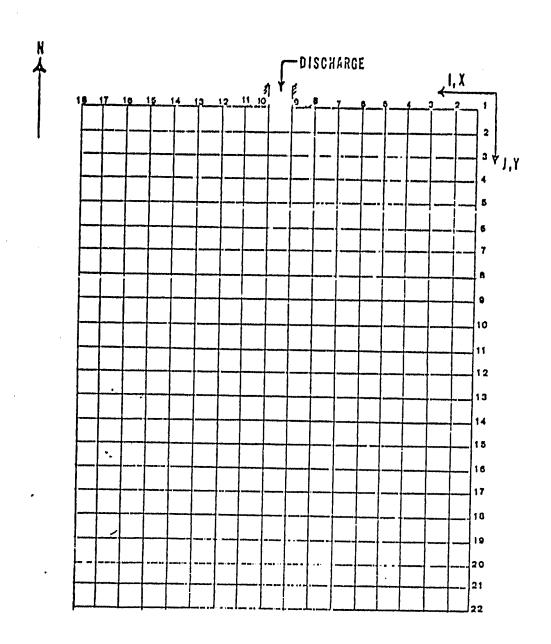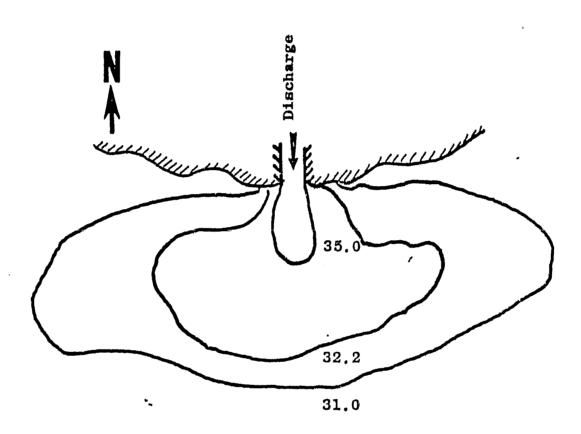
Fig. 2-5   Grid System For Rigid Lid
             Near Field Model of Cutler
             Ridge Site
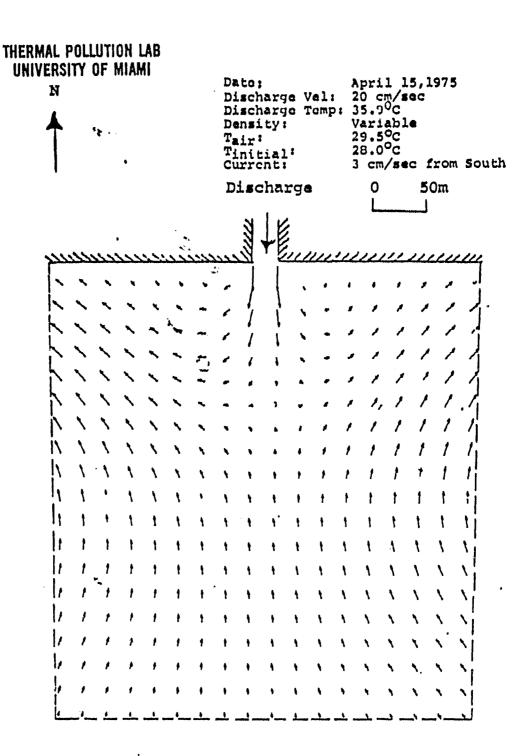
THERMAL POLLUTION LAB
UNIVERSITY OF MIAMI

Discharge Temperature : 35.9°C
Wind   : 6.71 m/sec
                        (15 mph 160°N)

Fig. 2-6   Surface Isotherms From I.R. Data For Cutler
           Ridge Power Plant, April 15, 1975
           (0911-0912 EST)

THERMAL POLLUTION LAB
UNIVERSITY OF MIAMI

N

Date: April 15,1975
Discharge Vel: 20 cm/sec
Discharge Temp: 35.9°C
Density: Variable
T_{air}:   29.5°C
$T_{initial}$:   28.0°C
Current: 3 cm/sec from South

Discharge   0   50m

·Fig. 2-7   Surface Velocity Distribution for
            April 15, 1975 at Cutler-Ridge Site
            (Case NO.8)
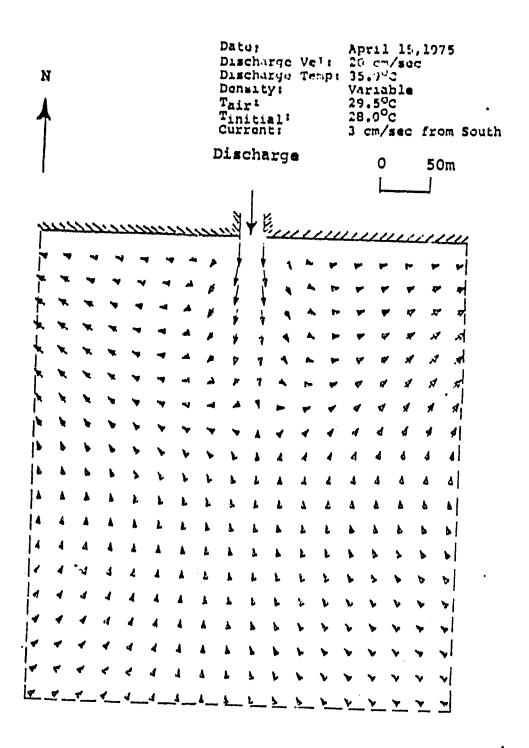
Fig. 2-8   Velocity Distribution for April 15, 1975
at K=2 for Cutler-Ridge Site (Case NO.8)

Date: April 15,1975
Discharge Vel: 20 cm/sec
Discharge Temp: 35.9°C
Density: Variable
T_{air}:   29.5°C
$T_{initial}$:   28.0°C
Current: 3 cm/sec from South

Discharge

0   50m
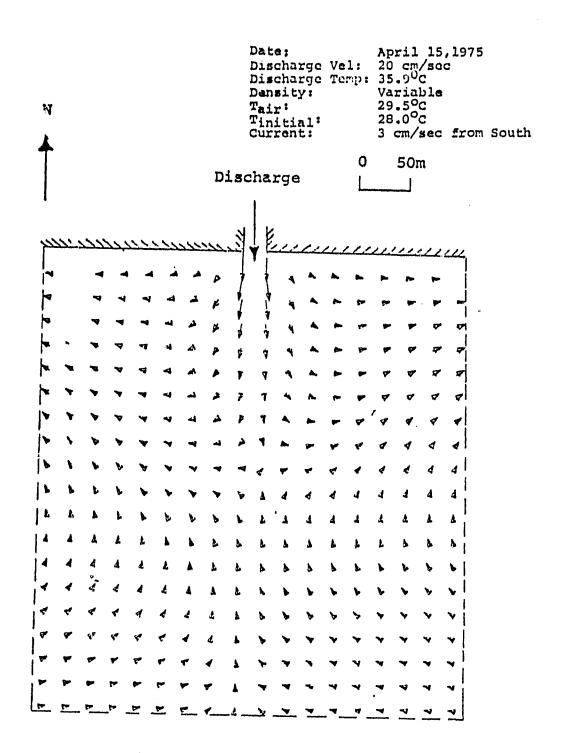
Fig. 2-9   Velocity Distribution for April 15, 1975
           at K=3 for Cutler-Ridge Site(Case NO.8)

74

Date: April 15,1975
Discharge Vel: 20 cm/sec
Discharge Temp: 35.9°C
Density: Variable
Tair: 29.5°C
Tinitial: 28.0°C
Current: 3 cm/sec from South

0   50m

Discharge
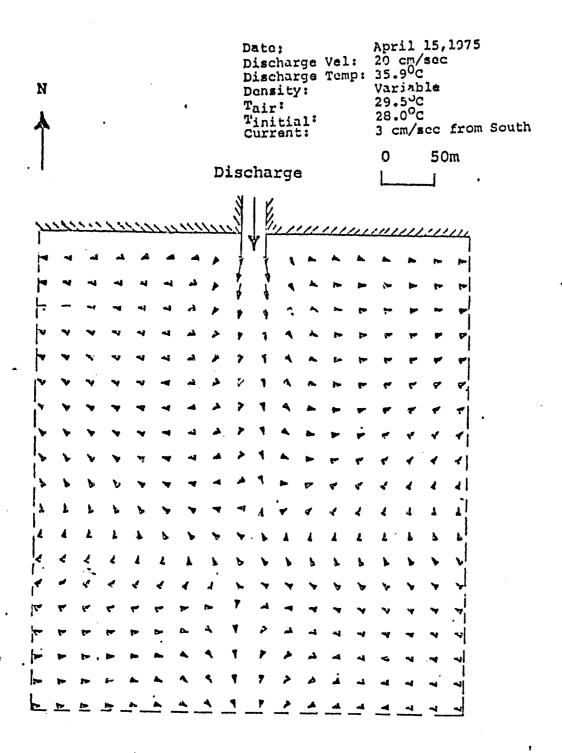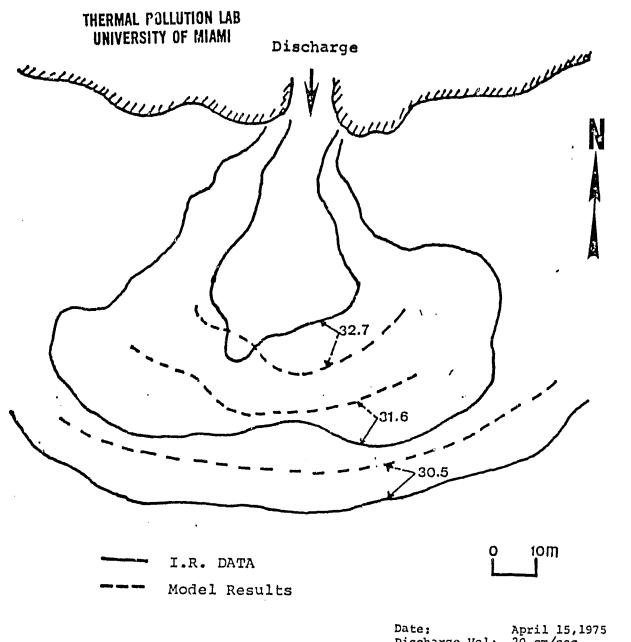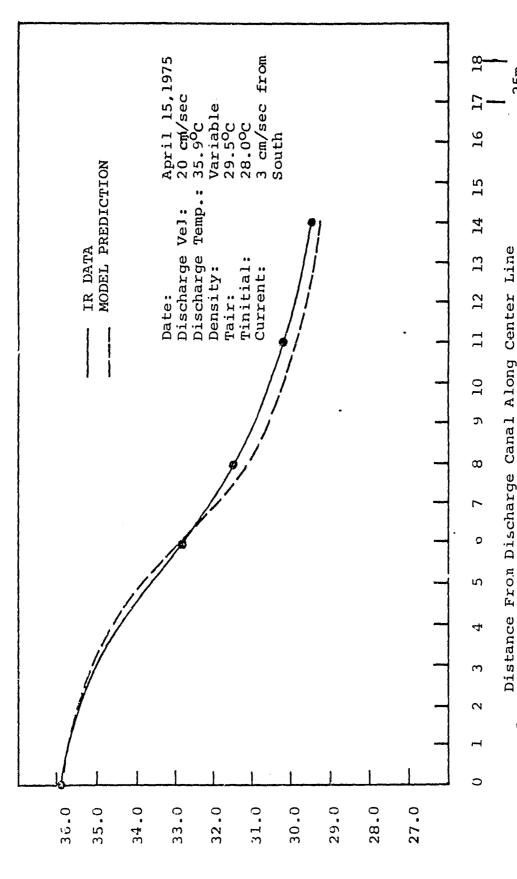
Fig. 2-10. Velocity Distribution for April 15, 1975
at K=4 for Cutler-Ridge Site (Case NO.8)

75

THERMAL POLLUTION LAB
UNIVERSITY OF MIAMI

Discharge

32.7

31.6

30.5

N

——— I.R. DATA

– – – Model Results

0   10m

Date;   April 15,1975
Discharge Vel: 20 cm/sec
Discharge Temp: 35.9°C
Density: Variable
T_{air}:   29.5°C
$T_{initial}$:   28.0°C
Current: 3 cm/sec from South

Fig. 2-11 Comparison of Isotherms for April 15, 1975
           (11:55 am) (Case NO.8)

Fig. 2-12 Comparison of Temp Decay at I=10 Along J (close to center line)
for April 15, 1975 (11:55 am) (Case NO.8)
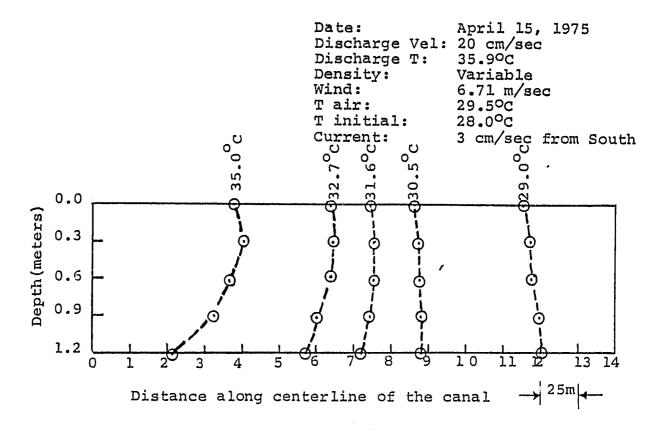
Fig. 2-13   Vertical Section Isotherms Along Canal Center
Line for April 15, 1975 at Cutler Ridge Site
(Rigid-Lid) (Case NO.8)

THERMAL POLLUTION LAB
UNIVERSITY OF MIAMI
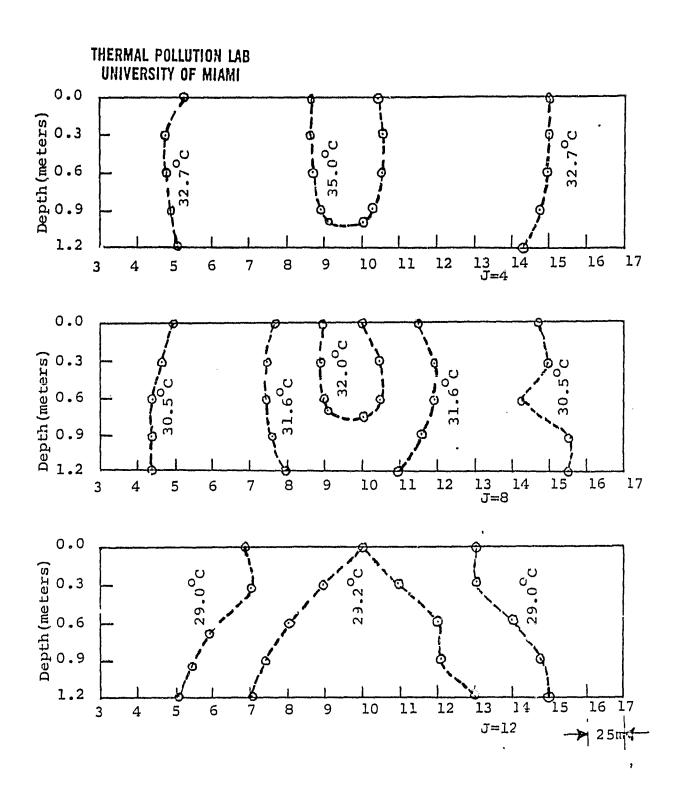
Fig. 2-14 vertical Section Isotherms at Different J
Sections for April 15, 1975 at Cutler Ridge
Site (Rigid-Lid)(Case NO.8)

79
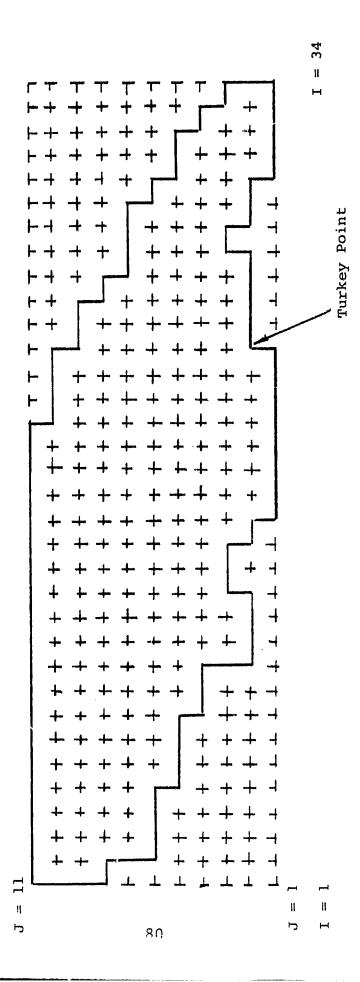
Fig. 2-15   Horizontal Grid System for Biscayne Bay

Turkey Point

I = 34

J = 11

J = 1
I = 1

80

□ .8 kilometers

2 cm/sec □
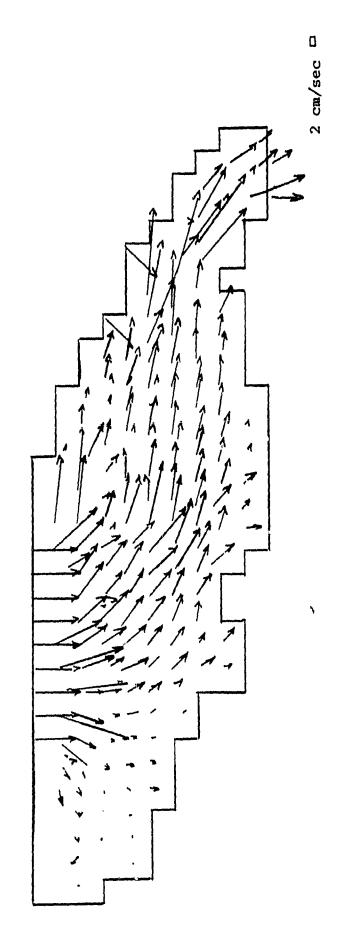
Fig. 2-16 Surface Currents with Incoming Tide
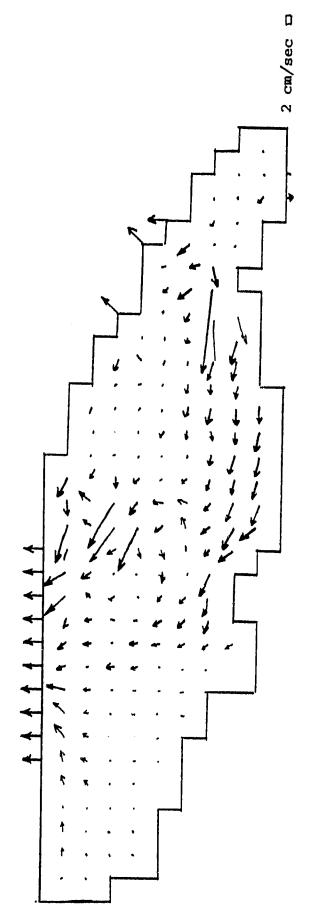
in Biscayne Bay

.8 kilometers

2 cm/sec
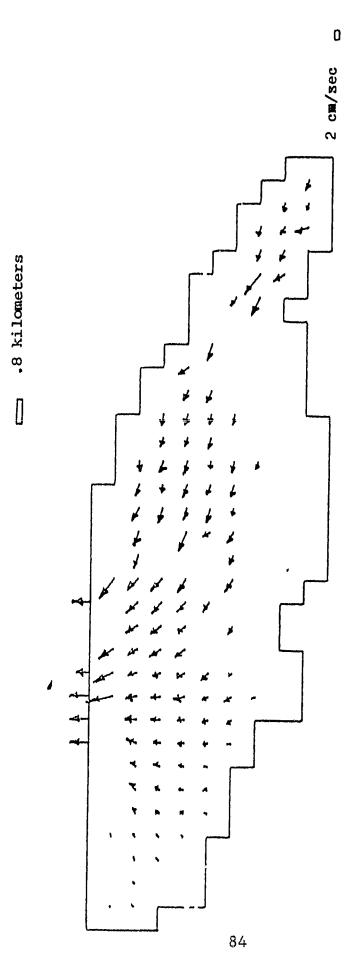
Fig. 2-17 Currents at 1 Meter Depth With Incoming Tide
into Biscayne Bay.

□ .8 kilometers

2 cm/sec □
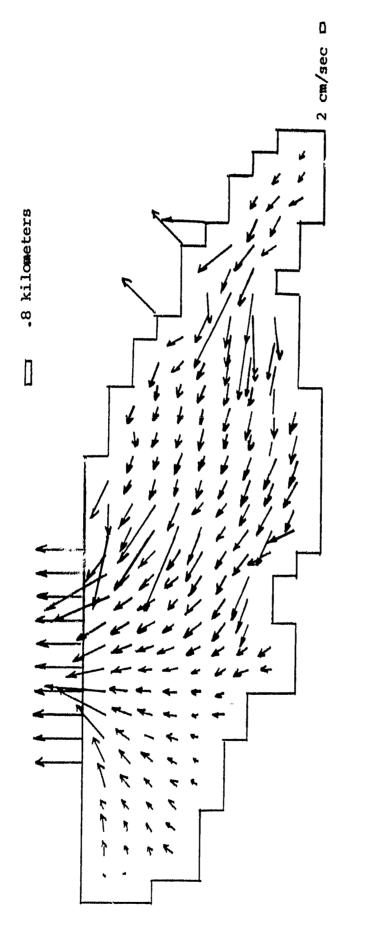
Fig. 2-18   Surface Currents During Tidal Flow Reversal in Biscayne Bay

83

.8 kilometers

2 cm/sec   0

Fig. 2-19   Currents at 2 Meters Depth During Tidal Flow Reversal in Biscayne Bay

84

Fig. 2-20   Surface Currents for Ebb Tide in   Biscayne Bay to Ocean

85

□   .8 kilometers

WIND: 10 MPH Southeast

Incoming Tide With a Velocity of 10 cm/sec.

2 cm/sec.   □
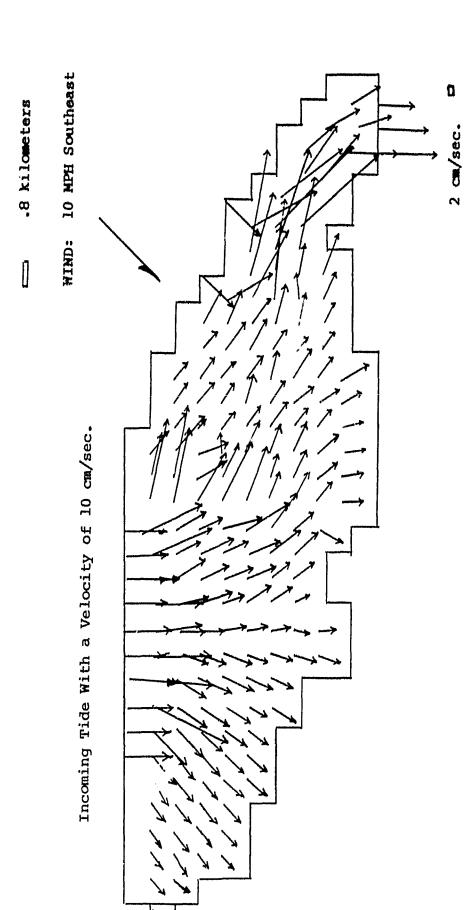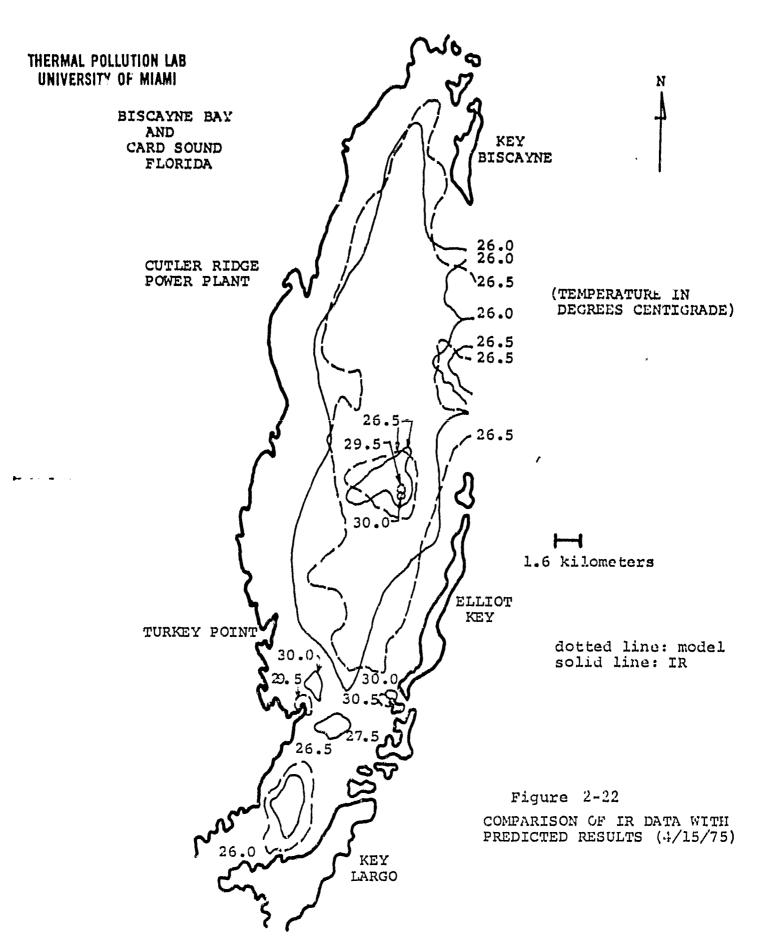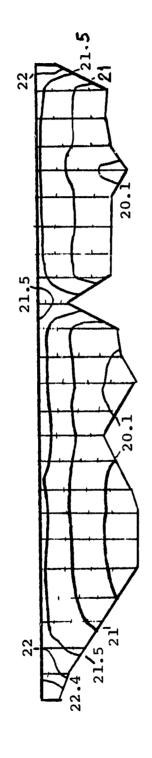
Fig. 2-21   Surface Velocities

86

THERMAL POLLUTION LAB
UNIVERSITY OF MIAMI

BISCAYNE BAY
AND
CARD SOUND
FLORIDA

CUTLER RIDGE
POWER PLANT

KEY
BISCAYNE

N

26.0
26.0
26.5

26.0

(TEMPERATURE IN
DEGREES CENTIGRADE)

26.5
26.5

26.5

26.5

29.5

30.0

1.6 kilometers

ELLIOT
KEY

TURKEY POINT

30.0

29.5

30.0

30.5

27.5

26.5

26.0

KEY
LARGO

dotted line: model
solid line: IR

Figure 2-22

COMPARISON OF IR DATA WITH
PREDICTED RESULTS (4/15/75)

WIND: 10 MPH Southeast

AIR TEMP: $29^{\circ}C$

INITIAL TEMP: $20^{\circ}C$

HEAT TRANSFER
COEFFICIENT: 1000 BTU/DAY-$^{\circ}$F-FT^2

TIME ELAPSED: 1 HR.

☐ .8 kilometers horizontal scale

▭ 3 ft. vertical scale

Isotherms For Vertical Section J=7

Fig. 2-23

C-2

THERMAL POLLUTION LAB
UNIVERSITY OF MIAMI
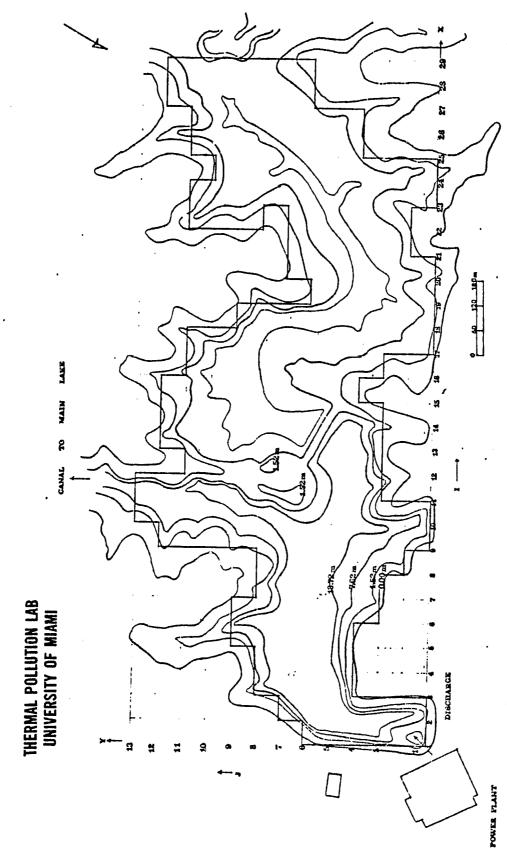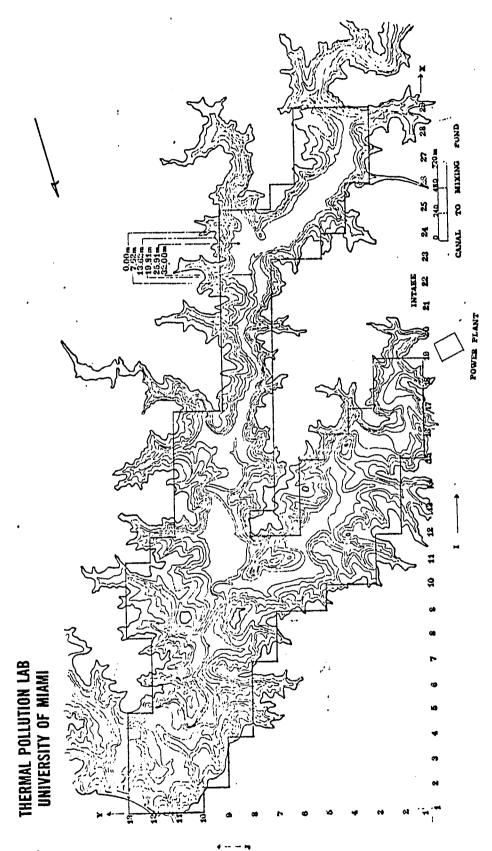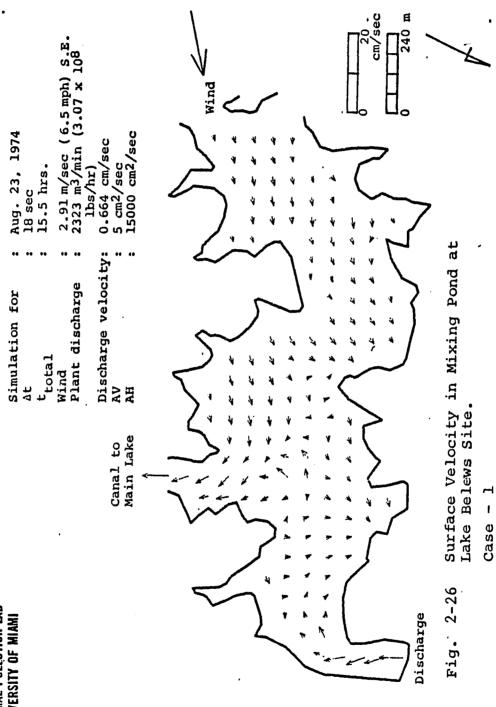
Fig. 2-24 COMPUTATIONAL GRID FOR MIXING POND AT LAKE BELEWS SITE

89
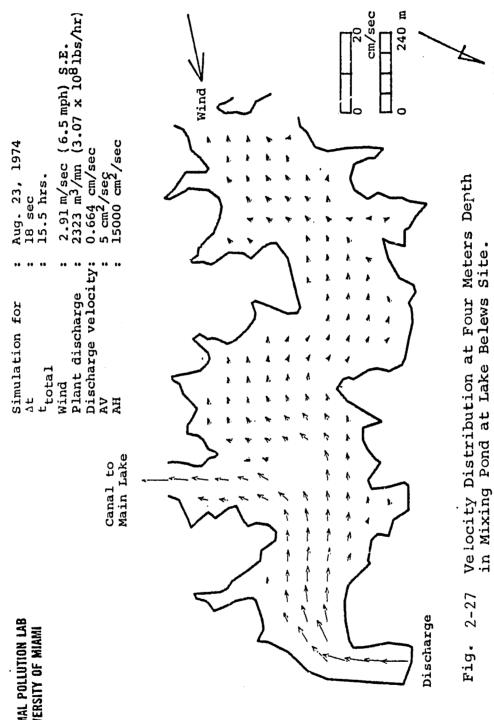
Fig. 2-25   COMPUTATIONAL GRID FOR MAIN LAKE AT BELEWS LAKE SITE

THERMAL POLLUTION LAB
UNIVERSITY OF MIAMI

Simulation for	:	Aug. 23, 1974
Δt	:	18 sec
t_{total}	:	15.5 hrs.
Wind	:	2.91 m/sec (6.5 mph) S.E.
Plant discharge	:	2323 m3/min (3.07 x 108 lbs/hr)
Discharge velocity:		0.664 cm/sec
AV	:	5 cm2/sec
AH	:	15000 cm2/sec

Canal to
Main Lake

Wind

Discharge

Fig. 2-26   Surface Velocity in Mixing Pond at
Lake Belews Site.

Case - 1

91

THERMAL POLLUTION LAB
UNIVERSITY OF MIAMI

Simulation for : Aug. 23, 1974
Δt : 18 sec
t_{total} : 15.5 hrs.
Wind : 2.91 m/sec (6.5 mph) S.E.
Plant discharge : 2323 m³/mn (3.07 × 10⁸ lbs/hr)
Discharge velocity: 0.664 cm/sec
AV : 5 cm²/sec
AH : 15000 cm²/sec

Wind

20
cm/sec
0

240 m
0

N

Canal to
Main Lake

Discharge

Fig. 2-27   Velocity Distribution at Four Meters Depth
in Mixing Pond at Lake Belews Site.

Case - 1

92

THERMAL POLLUTION LAB
UNIVERSITY OF MIAMI

Simulation for	:	Aug. 23, 1974
Δt	:	18 sec
t_{total}	:	15.5 hrs
Wind	:	2.91 m/sec (6.5 mph) S.E.
Plant discharge	:	2323 m^3/mn (3.07 x 10^8 lbs/hr)
Air temp	:	29.28°C
Discharge temp	:	36.39°C
Initial temp	:	32.0°C
Te	:	33.89°C
K	:	5.33 cal (262 BTU/ft^2°F/day
		cm^2 °C hr
Ti	:	32°C

Canal to
Main Lake

32.5C

33.0C

33.5C

GT 34.5C

34.0C

34.5
35.0
35.5
36.0

Discharge

0   240 m

N

Fig. 2-28   Surface Isotherms in Mixing Pond at Lake
Belews Site.

Case - 1

93

THERMAL POLLUTION LAB
UNIVERSITY OF MIAMI

Simulation for : Aug. 23, 1974
Δt : 18 sec
t_{total} : 15.5 hrs
Wind : 2.91 m/sec (6.5 mph) S.E.
Plant discharge : 2323 m^3/mn (3.07 x 10^8 lbs/hr)
Air temp : 29.28°C
Discharge temp : 36.39°C
Initial temp : 32.0°C
T_e : 33.89°C
K : 5.33 cal (262 BTU/ft^2/°F/day
       cm^2 °C hr
T_i : 32°C

Fig. 2-29   Isotherms at Four Meters Depth in Mixing
             Pond at Lake Belews Site.

Case - 1

94

THERMAL POLLUTION LAB
UNIVERSITY OF MIAMI

AIR TEMP : 20.00°C
DISCHARGE TEMP : 27.88°C

——— I.R. Data
- - - - Math Model

Wind

240 m

N

Canal to
Main Lake

27.13

27.68

28.24

28.79

28.24

27.68

Discharge

Fig. 2-30 Comparison of surface isotherms as obtained by mathe-
matical model for mixing pond of those obtained by
Infra-red remote sensing on May 19, 1976 at 15:30
at Lake Belews site.

Case - 2

III. The Free-Surface Model

   3.1 Brief Description of Past Experience with Free-
       Surface Formulations, Relevant Advantages and
       Disadvantages

   One of the first three-dimensional models was by Freeman
et al (1972). This model was essentially a free surface
formulation. Haq and Lick (1974) used a free surface
model to study the time-dependent flow in large lakes with
application to Lake Erie. They used a vertical stretching
to convert a variable depth basin to constant depth, thereby
permitting a constant vertical grid size to be applied
everywhere in the domain. Irregular shorelines could be
easily included without modification of the computer
program. Modified versions of the free-surface model have
been used, by the Thermal Pollution research team at the
University of Miami, at a number of sites with satisfactory
results. Lee and Sengupta (1976).

   The major advantage associated with the free-surface
model is its ability to predict surface heights everywhere
in the domain. Thus, for example, real tidal conditions
can be accounted for by this model, and, hence, verification
of the model can be made with regard to comparison with
existing tide data bases.

   The major disadvantage associated with the free-sur-
face model is its inherently small time step as determined
by the Courant-Freidrichs-Lewy Condition, Roache (1972),
Richtmyer and Morton (1967), which is based upon external
gravity waves (or so - called surface gravity waves).
However, for water bodies for which vertical diffusion
determines the maximum allowable time step, as would be
the case for shallow water basins, there is no real time
step disadvantage in using the free-surface model.

   3.2 Assumptions and Approximations

   The system of governing equations (see next section 3.3)
for the fluid flow invoke several simplifying assumptions and

approximations in the interest of saving computational time without losing significant accuracy. The following assumptions and approximations have been employed.

3.2.1 The Boussinesq Approximation

The effect of density variations on the inertial and diffusion terms in the governing conservation equations is neglected. Density variation is retained in the bouyancy terms in the equations of motion. The effect of bouyancy is thereby accounted for by allowing density variations which produce horizontal pressure gradients which influence the fluid motion through the horizontal momentum equations.

3.2.2 The Hydrostatic Approximation

The hydrostatic approximation involves neglecting the vertical convection and diffusion terms in the vertical momentum equation. This approximation implies that the vertical fluid acceleration, $\frac{Dw}{Dt}$, is negligible.

3.2.3 Constant Eddy Transport Coefficients

Turbulence modeling is very complex and has an extensive body of literature of its own. Turbulent closure has been obtained in this model by using constant eddy transport coefficients, although the horizontal eddy transport coefficient is orders of magnitude larger than the vertical eddy transport coefficient, being due to the much larger horizontal scale length, L, in comparison with the vertical scale length, H.

3.2.4 Variation of Surface Wind Stresses

The variation of the wind produced surface shear stresses with respect to x and y, $\frac{\partial \tau xz}{\partial x}$ and $\frac{\partial \tau yz}{\partial y}$, are considered negligible for the horizontal length scales of the water bodies studied. However, if the physical dimensions of the water body are so large as to require including variation of the wind stresses with respect to x and y, then the computer programs can be quite easily modified by replacing τ_{xz} and τ_{yz} with matrices $\tau_{xz}(I,J)$ and $\tau_{yz}(I,J)$ Where the indices I and J refer to the location of a grid

97

point with respect to the x, y plane.

3.2.5 Velocity Slip Conditions

The free-surface, far-field model uses velocity slip conditons at the lateral solid boundaries, although no-slip is used at the bottom boundary. The assumption of slip conditions is necessary for the free-surface model to allow for surface height variations at the solid boundaries, Freeman et al (1972), Lee et al (1976) Numerically it has been seen that lateral boundary layers are smaller than the relatively large grid spacing used, specifically for the Biscayn Bay site. Estimates by Sengupta and Lick (1974) have indicated that the sidewall boundary layers are thin for similar situations, and do not extend as far as the nearest interior node. Note, that the free-surface, far-field model uses the same velocity slip conditions used by Freeman et al (1972).

[1] Specifically, at x-boundaries $\frac{\partial (Hv)}{\partial \alpha} = o$, and at y-boundaries $\frac{\partial (Hu)}{\partial \beta} = 0$.

3.3 Governing Equations

The set of equations governing the behavior of the fluid flow are those expressing the conservation of mass, momentum, and energy in turbulent flow, and an equation of state.

3.3.1 Cartesian Coordinate Representation (x,y,z)

The Cartesian coordinate system is used with the z-coordinate in the downward vertical direction as shown in Fig. 3.1, i.e. a so-called "left-handed" coordinate system. In order to keep the generalized nature of the model, all the significant terms in the respective conservation equations are retained. Included are the effects of bouyancy, inertia, coriolis, density and turbulent mixing. Wind shear and heat flux at the surface are also considered.

[1] Note: $\frac{\partial v}{\partial \alpha} = o$ and $\frac{\partial u}{\partial \beta} = o$ yields very close results.

The following system of non-linear partial differential equations, written in Cartesian coordinates, describes the three-dimensional, unsteady fluid flow where the variables are in dimensional form.

Continuity Equation

$$\frac{\partial u}{\partial x} + \frac{\partial v}{\partial z} + \frac{\partial w}{\partial z} = 0 \tag{3.1}$$

Momentum Equation

$$\frac{\partial u}{\partial t} + u\frac{\partial u}{\partial x} + v\frac{\partial u}{\partial y} + w\frac{\partial u}{\partial z} = -\frac{1}{\rho}\frac{\partial P}{\partial x} + fv + K_H \frac{\partial^2 u}{\partial x^2}$$

$$+ K_H \frac{\partial^2 u}{\partial y^2} + K_v \frac{\partial^2 u}{\partial z^2} \tag{3.2}$$

$$\frac{\partial v}{\partial t} + u\frac{\partial v}{\partial x} + v\frac{\partial v}{\partial y} + w\frac{\partial v}{\partial z} = -\frac{1}{\rho}\frac{\partial P}{\partial y} - fu + K_H \frac{\partial^2 v}{\partial x^2}$$

$$+ K_H \frac{\partial^2 v}{\partial y^2} + K_v \frac{\partial^2 v}{\partial y^2} \tag{3.3}$$

$$\frac{\partial w}{\partial t} + u\frac{\partial w}{\partial x} + v\frac{\partial w}{\partial y} + w\frac{\partial w}{\partial z} = -\frac{1}{\rho}\frac{\partial P}{\partial z} + K_H \frac{\partial^2 w}{\partial x^2} + K_H \frac{\partial^2 w}{\partial y^2}$$

$$+ K_v \frac{\partial^2 w}{\partial z^2} - g \tag{3.4}$$

Energy Equation

$$\frac{\partial T}{\partial t} + u\frac{\partial T}{\partial x} + v\frac{\partial T}{\partial y} + w\frac{\partial T}{\partial z} = B_H \frac{\partial^2 T}{\partial x^2} + B_H \frac{\partial^2 T}{\partial y^2} + B_v \frac{\partial^2 T}{\partial z^2} \tag{3.5}$$

Equation of State

$$\rho = \rho(T) \tag{3.6}$$

Continuity Equation

$$\frac{\partial H}{\partial t} + \frac{\partial (Hu)}{\partial \alpha} + \frac{\partial (Hv)}{\partial \beta} + H \frac{\partial \Omega}{\partial \sigma} = 0 \qquad (3.9)$$

Horizontal Momentum Equations

$$\frac{\partial (Hu)}{\partial t} + \frac{\partial (Huu)}{\partial \alpha} + \frac{\partial (Huv)}{\partial \beta} + H \frac{\partial (u\Omega)}{\partial \sigma}$$

$$= H \left[- \frac{1}{\rho} \left(\frac{\partial P}{\partial \alpha} \right) + g \left(\sigma \frac{\partial H}{\partial \alpha} - \frac{\partial \eta}{\partial \alpha} \right) + fv \right]$$

$$+ K_H \left[\frac{\partial}{\partial \alpha} \left(H \frac{\partial u}{\partial \alpha} \right) + K_H \frac{\partial}{\partial \beta} \left(H \frac{\partial u}{\partial \beta} \right) + \frac{1}{\rho} \frac{\partial}{H \partial \sigma} \left(\rho K v \frac{\partial u}{\partial \sigma} \right) \right]$$

$$(3.10)$$

$$\frac{\partial (Hv)}{\partial t} + \frac{\partial (Huv)}{\partial \alpha} + \frac{\partial (Hvv)}{\partial \beta} + H \frac{\partial (v\Omega)}{\partial \sigma}$$

$$= H \left[-\frac{1}{\rho} \left(\frac{\partial P}{\partial \beta} \right) + g \left(\sigma \frac{\partial H}{\partial \beta} - \frac{\partial \eta}{\partial \beta} \right) - fu \right]$$

$$+ K_H \left[\frac{\partial}{\partial \alpha} \left(H \frac{\partial v}{\partial \alpha} \right) + K_H \frac{\partial}{\partial \beta} \left(H \frac{\partial v}{\partial \beta} \right) + \frac{1}{\rho} \frac{\partial}{H \partial \sigma} \rho K_v \frac{\partial v}{\partial \sigma} \right]$$

$$(3.11)$$

Energy Equation

$$\frac{\partial (HT)}{\partial t} + \frac{\partial (HuT)}{\partial \alpha} + \frac{\partial (HvT)}{\partial \beta} + H \frac{\partial (\Omega 1)}{\partial \sigma}$$

$$= B_H \left[\frac{\partial}{\partial \alpha} \left(H \frac{\partial T}{\partial \alpha} \right) \right] + B_H \left[\frac{\partial}{\partial \beta} \left(H \frac{\partial T}{\partial \beta} \right) \right] + \frac{1}{\rho} \left[\frac{\partial}{H \partial \sigma} \left(\rho B_v \frac{\partial T}{\partial \sigma} \right) \right]$$

$$(3.12)$$

Equation (3.4) for conservation of w-component of momentum is replaced in the free-surface model formulation by applying the hydrostatic approximation (see section 3.3.2) as follows:

100

Hydrostatic Equation

$$P(\sigma) = P\ (\sigma=0)\ +gH\ \int_{\sigma=0}^{\sigma} (\sigma)\ d\sigma \qquad (3.13)$$

Equation of State, $\rho = \rho(t)$ is given for fresh and salt water as follows:

Salt Water: $\rho(T) = 1.029431 - .000020T - .0000048T^2$:
(for a salinity of 38 parts per thousand) $\qquad (3.14)$

Fresh Water: $\rho(T) = 1.000428 - .000019T - .0000046T^2$ (3.15)

Instead of using equation (3 9), following the work by Freeman et al (1972), two integrated forms of the continuity equation are used as follows:

(1) Surface Height Equation

$$\frac{\partial H}{\partial t} = -\int_{\sigma=0}^{1} \left[\frac{\partial (Hu)}{\partial \alpha} + \frac{\partial (Hv)}{\partial \beta}\right]\ d\sigma \qquad (3.16)$$

Equivalent Vertical Velocity (in α, β, σ system)

$$\Omega = -\frac{1}{H}\int_{\sigma=0}^{\sigma} \left[\frac{\partial (Hu)}{\partial \alpha} + \frac{\partial (Hv)}{\partial \beta}\right] d\sigma$$

$$+ \frac{\sigma}{H}\int_{\sigma=0}^{1} \left[\frac{\partial (Hu)}{\partial \alpha} + \frac{\partial (Hv)}{\partial \beta}\right] d\sigma \qquad (3.17)$$

Actual Vertical Velocity (in x,y,z system)

$$w = H\Omega + \sigma \frac{dh}{dt} + (\sigma-1) \frac{dn}{dt} \qquad (3.18)$$

where, $\dfrac{dh}{dt} = \dfrac{\partial h}{\partial t} + u\dfrac{\partial h}{\partial \alpha} + v\dfrac{\partial h}{\partial \beta}$

$\dfrac{dn}{dt} = \dfrac{\partial n}{\partial t} + u\dfrac{\partial n}{\partial \alpha} + v\dfrac{\partial n}{\partial \beta}$

and, $w = \dfrac{dz}{dt}$ $\qquad \Omega = \dfrac{d\sigma}{dt}$

(1) Note: These two integrated forms of equation (3.9) consider $\Omega=0$ at $\sigma=0$, and $\Omega=0$ at $\sigma=1$. However, a special case of mass influx at the bottom boundary, where $\Omega\neq0$ at $\sigma=1$ is given in Volume III for the sample problem for Hutchinson Island site.

The symbols in equations (3.1)- (3.6) are defined in the
list of symbols for the free-surface model.

3.3.2 <u>Vertical Stretched Coordinate Representation</u> (α,β,σ)

One major difficulty in the treatment of the free-sur-
face model is at the free surface boundary. The boundary con-
ditions can be specified, but the position of the free sur-
face is irregular and time-dependent making it very diff-
icult to apply any grid system at this boundary for numerical
solution. The approach used in the model formulation is to
follow a vertical stretching transformation suggested by
Phillips (1957) and used successfully in studies by Freeman et
al (1972). Using this transformation, the free surface be-
comes a fixed flat surface and the variable depth ⊾ tom be-
comes a flat bottom boundary. This method allows easy adapt-
ation to various bottom topographies, an important require-
ment for any general model. In addition, constant vertical
grid size can be used throughout the domain.

The transformation of the vertical coordinate for the
free-surface model is obtained by letting

$$\alpha = x$$

$$\beta = y \tag{3.7}$$

$$\text{and } \sigma = \frac{Z(x,y,z,t)}{H(x,y,t)} = \frac{z + \eta(x,y,t)}{H(x,y,t)} \tag{3.8}$$

where the symbols are given in the list of symbols for the
free-surface model. Fig. 3.2 shows the (α,β,σ) coordinate
system. Note, that the value of σ ranges monotonically from
zero at the free surface to unity at the bottom boundary.

By substituting transformations (3.7) and (3.8) into
equations (3.1) - (3.6) the free-surface model governing
equations (in dimensional form) in the (α,β,σ) coordinate system
are expressed in what follows.

102

3.4 Horizontally Stretched Equations

It is desirable to obtain a more detailed description of the flow near the discharge point while larger grid size may be used in the further points to save computation time. A horizontal stretching of the coordinate system (α, β, σ) is used here to create a more efficient use of the grid points by letting

$$\alpha = a + C_1 \, \text{Sinh} \, [\, C_2 \, (X-d) \,] \qquad (3.20)$$

$$\beta = b + C_2 \, \text{Sinh} \, [\, C_4 \, (Y-e) \,]$$

where the various symbols are defined in the list of symbols for the free-surface model. Fig. 3.3 shows the X, Y, σ coordinate system, and Fig. 3.4 shows the resulting α, β, σ, coordinate system. Appendix B presents the details of this coordinate transformation and the resulting equations in the coordinate system. Also comparison of sinh stretching with tanget stretching, used by Waldrop and Farmer (1973) is given in Appendix B.

Now, after defining the following derivatives necessary for making this transformation, the horizontally stretched, free-surface model equations will be presented.

$$X' = \frac{dX}{d\alpha} \quad ; \quad Y' = \frac{dY}{d\beta} \quad ; \quad X'' = \frac{d^2X}{d\alpha^2} \quad ; \quad Y'' = \frac{d^2Y}{d\beta^2}$$

The transformed free-surface governing equations in the (X, Y, σ) coordinate system are as follows:

Continuity

$$\frac{\partial H}{\partial t} + X' \frac{\partial (Hu)}{\partial X} + Y' \frac{\partial (Hv)}{\partial Y} + H \frac{\partial \Omega}{\partial \sigma} = 0 \qquad (3.21)$$

Horizontal Momentum Equations

$$\frac{\partial (Hu)}{\partial \tau} + X' \frac{\partial (Huu)}{\partial X} + Y' \frac{\partial (Huv)}{\partial Y} + H \frac{\partial (u\Omega)}{\partial \sigma}$$

$$= H [-\frac{X'}{\rho} (\frac{\partial P}{\partial X}) + gX' (\sigma \frac{\partial H}{\partial X} - \frac{\partial \eta}{\partial X}) + fv]$$

$$+ K_H [(X')^2 \frac{\partial H}{\partial t} \frac{\partial u}{\partial t} + H (X')^2 \frac{\partial^2 u}{\partial X^2} + HX'' \frac{\partial u}{\partial X}]$$

$$+ K_H [(Y')^2 \frac{\partial H}{\partial Y} \frac{\partial u}{\partial Y} + H (Y')^2 \frac{\partial^2 u}{\partial Y^2} + HY'' \frac{\partial u}{\partial Y}]$$

$$+ \frac{1}{\rho} [\frac{1}{H} \frac{\partial}{\partial \sigma} (\rho K_v \frac{\partial u}{\partial \sigma})] \qquad (3.22)$$

$$\frac{\partial (Hv)}{\partial t} + X' \frac{\partial (Huv)}{\partial X} + Y' \frac{\partial (Hvv)}{\partial Y} + H \frac{\partial (v\Omega)}{\partial \sigma}$$

$$= H [\frac{Y'}{\rho} (\frac{\partial P}{\partial Y}) + gY' (\sigma \frac{\partial H}{\partial Y} - \frac{\partial \eta}{\partial Y}) - fu]$$

$$+ K_H [(X')^2 \frac{\partial H}{\partial X} \frac{\partial v}{\partial X} + H (X')^2 \frac{\partial^2 v}{\partial X^2} + HX'' \frac{\partial v}{\partial X}]$$

$$+ K_H [(Y')^2 \frac{\partial H}{\partial Y} \frac{\partial v}{\partial Y} + (Y')^2 \frac{\partial^2 v}{\partial Y^2} + HY'' \frac{\partial v}{\partial Y}]$$

$$+ \frac{1}{\rho} [\frac{1}{H} \frac{\partial}{\partial \sigma} (\rho K_v \frac{\partial v}{\partial \sigma})]$$

$$(3.23)$$

Energy Equation

$$\frac{\partial (HT)}{\partial t} + X' \frac{\partial (HuT)}{\partial X} + Y' \frac{\partial (HvT)}{\partial Y} + H \frac{\partial (\Omega T)}{\partial \sigma}$$

$$= B_H [(X')^2 \frac{\partial H}{\partial X} \frac{\partial T}{\partial X} + H (X')^2 \frac{\partial^2 T}{\partial X^2} + HX'' \frac{\partial T}{\partial X}]$$

$$+ B_H [(Y')^2 \frac{\partial H}{\partial Y} \frac{\partial T}{\partial Y} + H (Y')^2 \frac{\partial^2 T}{\partial Y^2} + HY'' \frac{\partial T}{\partial Y}]$$

$$+ \frac{1}{\rho} [\frac{1}{H} \frac{\partial}{\partial \sigma} (\varphi B_v \frac{\partial T}{\partial \sigma})]$$

$$(3.24)$$

104

The hydrostatic equation and the two equations of state (for salt water and fresh water, respectively) are still given by equations (3.13), (3.14) and (3.15).

Surface Height Equation[2]

$$\frac{\partial H}{\partial t} = - \int_{\sigma=0}^{1} [X' \frac{\partial (Hu)}{\partial X} + Y' \frac{\partial (Hv)}{\partial Y}] d\sigma \qquad (3.25)$$

For, the free-surface model application to the sites where the velocity on the bottom of the basin is <u>not</u> zero, such as a <u>submerged discharge</u> the vertical velocity Ω_b on the bottom no longer is zero, and then the integration of the continuity equation to get the equation for surface height can not eliminate the vertical convection term. An integration constant representing vertical velocity at the bottom, Ω_b is added to the equation. Thus, from the relationship of w and Ω we get:

$$\Omega_b = \frac{1}{H} (W_b - u_b X \frac{\partial h}{\partial X} - v_b Y' \frac{\partial h}{\partial Y}) \qquad (3.26)$$

where subscript b denotes the fluid property at the bottom of the basin. By integrating the continuity equation (3.21) with respect to σ from the free surface ($\sigma=0$) to the bottom ($\sigma=1$) we get:

$$\frac{\partial H}{\partial t} = - \int_{\sigma=0}^{1} [X' \frac{\partial (Hu)}{\partial X} + Y' \frac{\partial (Hv)}{\partial Y}] d\sigma$$

$$- (W_b - u_b X' \frac{\partial h}{\partial X} - v_b Y' \frac{\partial h}{\partial Y}) \qquad (3.27)$$

[2]NOTE: This is for the case $\Omega = 0$ at $\sigma=1$.

105

Equivalent Vertical Velocity

(3)
$$\Omega = -\frac{1}{H} \int_{\sigma=0}^{\sigma} [X'' \frac{\partial (Hu)}{\partial X} + Y' \frac{\partial (Hv)}{\partial Y}] \, d\sigma$$

$$+ \frac{\sigma}{H} \int_{\sigma=0}^{1} [X' \frac{\partial (Hu)}{\partial X} + Y' \frac{\partial (Hv)}{\partial Y}] \, d\sigma \qquad (3.28)$$

For a __submerged discharge__ at the bottom, substituting equation (3.27) into the continuity equation (3.21), and then integrating from the free-surface to $\sigma=\sigma$ we get for the equivalent vertical velocity:

$$\Omega = -\frac{1}{H} \int_{\sigma=0}^{\sigma} [X' \frac{\partial (Hu)}{\partial X} + Y' \frac{\partial (Hv)}{\partial Y}] \, d\sigma$$

$$+ \frac{\sigma}{H} \int_{=0}^{1} [X' \frac{\partial (Hu)}{\partial X} + Y' \frac{\partial (Hv)}{\partial Y}] \, d\sigma$$

$$+ \frac{\sigma}{H} (W_b - u_b X' \frac{\partial h}{\partial X} - v_b Y' \frac{\partial h}{\partial Y})$$

$$(3.29)$$

3.5 __Boundary Conditions__ (closed basins and open basins)

The nature of the system of governing equations requires initial and boundary conditions to be specified. The boundary conditions for both near-field (open basin) and far-field (closed basin) versions of the free-surface model are presented in this section. The initial conditions will be presented in the next section.

3.5.1 __Combined Near-Field and Far-Field__ (open basin)

The free-surface model with horizontal stretching has been applied to a submerged thermal discharge into the ocean at a coastal site (open basin). Tsai (1977). The boundary conditions are in summary:

[3] NOTE: Again this is for the case $\Omega= 0$ at $\sigma= 1$.

106

At the Surface, $\sigma = 0$

$\Omega = 0$

$(4)\quad \dfrac{\partial u}{\partial \sigma} = -\left(\dfrac{H}{\rho K_v}\right)\tau_{zx}$

$\dfrac{\partial v}{\partial \sigma} = -\left(\dfrac{H}{\rho K_v}\right)\tau_{zy}$

$\dfrac{\partial T}{\partial \sigma} = -\left(\dfrac{Hk_s}{\rho C_p\, B_v}\right)(T_e - T_s)$

At lateral solid boundaries
on x-boundaries

$\Omega \neq 0$

$u = 0$

$v = 0$

$\dfrac{\partial T}{\partial X} = X'\,\dfrac{\partial T}{\partial X} + \dfrac{X'}{H}\,\dfrac{\partial \eta}{\partial X}\,\dfrac{\partial T}{\partial \sigma}$

$\qquad -X'\,\dfrac{\sigma}{H}\,\dfrac{\partial H}{\partial X}\,\dfrac{\partial T}{\partial \sigma} = 0$

At the bottom, $\sigma = 1$

$\Omega = 0$ (except at submerged discharge)

$u = 0$ (except at submerged discharge)

$v = 0$ (except at submerged discharge)

$\dfrac{\partial T}{\partial \sigma} = 0$ (except at submerged discharge)

on y-boundaries

$\Omega \neq 0$

$u = 0$

$v = 0$

$\dfrac{\partial T}{\partial Y} = Y'\,\dfrac{\partial T}{\partial Y} + \dfrac{Y'}{H}\,\dfrac{\partial \eta}{\partial Y}\,\dfrac{\partial T}{\partial \sigma}$

$\qquad -Y'\,\dfrac{\sigma}{H}\,\dfrac{\partial H}{\partial Y}\,\dfrac{\partial T}{\partial \sigma} = 0$

At lateral open boundaries
on x-boundaries

$\Omega \neq 0$

$\dfrac{\partial u}{\partial X} = X'\,\dfrac{\partial u}{\partial X} + \dfrac{X'}{H}\,\dfrac{\partial \eta}{\partial X}\,\dfrac{\partial u}{\partial \sigma}$

$\qquad - X'\,\dfrac{\sigma}{H}\,\dfrac{\partial H}{\partial X}\,\dfrac{\partial u}{\partial \sigma} = 0$

on y-boundaries

$\Omega \neq 0$

$\dfrac{\partial u}{\partial Y} = Y'\,\dfrac{\partial u}{\partial Y} + \dfrac{Y'}{H}\,\dfrac{\partial \eta}{\partial Y}\,\dfrac{\partial u}{\partial \sigma}$

$\qquad - Y'\,\dfrac{\sigma}{H}\,\dfrac{\partial H}{\partial Y}\,\dfrac{\partial u}{\partial \sigma} = 0$

(4) NOTE: H is depth contour for free-surface model.

$$\frac{\partial v}{\partial X} = X' \frac{\partial v}{\partial X} + \frac{X'}{H} \frac{\partial \eta}{\partial X} \frac{\partial v}{\partial \sigma}$$

$$\frac{\partial v}{\partial Y} = Y' \frac{\partial v}{\partial Y} + \frac{Y'}{H} \frac{\partial \eta}{\partial Y} \frac{\partial v}{\partial \sigma}$$

$$- X' \frac{\sigma}{H} \frac{\partial H}{\partial X} \frac{\partial v}{\partial \sigma} = 0$$

$$-Y' \frac{\sigma}{H} \frac{\partial H}{\partial Y} \frac{\partial v}{\partial \sigma} = 0$$

$$\frac{\partial^2 T}{\partial X^2} = [(X')^2 \frac{\partial H}{\partial X} \frac{\partial T}{\partial X} + H (X')^2 \frac{\partial^2 T}{\partial X2}$$

$$\frac{\partial^2 T}{\partial Y2} = [(Y')^2 \frac{\partial H}{\partial Y} \frac{\partial T}{\partial Y} + H (Y')^2 \frac{\partial^2 T}{\partial Y2}$$

$$+ HX'' \frac{\partial T}{\partial X}] = 0$$

$$+ HY' \frac{\partial T}{\partial Y}] = 0$$

<u>at Discharge</u>

Velocity ⎫
Temperature ⎬ Specified
Density ⎭

3.5.2 <u>Far-Field</u> (closed basin)

The free-surface, far-field has been applied to the Biscayne Bay, Lee et al (1976). The boundary conditions are in summary:

<u>At the surface, $\sigma= 0$</u>

$\Omega = 0$

$$\frac{\partial u}{\partial \sigma} = - (\frac{H}{\rho K_v}) \tau_{xz}$$

$$\frac{\partial v}{\partial \sigma} = - (\frac{H}{\rho K_v}) \tau_{zy}$$

$$\frac{\partial T}{\partial \sigma} = - (\frac{HKs}{\rho C_p B_v}) (T_e - T_s)$$

<u>At the bottom, $\sigma = 1$</u>

$\Omega = 0$

$u = 0$

$v = 0$

$\frac{\partial T}{\partial \sigma} = 0$

(5) <u>At lateral solid boundaries</u>

<u>on x-boundaries</u>

$\Omega \neq 0$

$u = 0$

$$\frac{\partial (Hv)}{\partial \alpha} = 0$$

$$\frac{\partial T}{\partial \alpha} = 0$$

<u>on y-boundaries</u>

$\Omega \neq 0$

$$\frac{\partial (Hu)}{\partial \beta} = 0$$

$v = 0$

$$\frac{\partial T}{\partial \beta} = 0$$

108

[5] At lateral open boundaries (current velocity specified at inlet)

<u>on x-boundaries</u>   <u>on y-boundaries</u>

$\Omega \neq 0$ $\Omega \neq 0$

[6] $u = u(t)$ or $\frac{\partial u}{\partial \alpha} = 0$ $u = 0$

$v = 0$ $v = v(t)$ or $\frac{\partial v}{\partial \beta} = 0$

$\frac{\partial T}{\partial \alpha} = 0$ $\frac{\partial T}{\partial \beta} = 0$

At lateral open boundaries (tide height specified at inlet)

<u>on x-boundaries</u>   <u>on y-boundaries</u>

$\Omega \neq 0$ or [7]$\Omega \neq 0$ $\Omega \neq 0$ or [7]$\Omega \neq 0$

[8] $\eta = \eta(t)$ $u = 0$ $u = 0$

$\frac{\partial u}{\partial \alpha} = 0$ $\frac{\partial u}{\partial \alpha} = 0$ [8]$\eta = \eta(t)$

$v = 0$ $v = 0$ $\frac{\partial v}{\partial \beta} = 0$ $\frac{\partial v}{\partial \beta} = 0$

$\frac{\partial T}{\partial \alpha} = 0$ $\frac{\partial T}{\partial \alpha} = 0$ $\frac{\partial T}{\partial \beta} = 0$ $\frac{\partial T}{\partial \beta} = 0$

3.6 <u>Initial Conditions</u>

The initial conditions are specified by using the corrected morning IR data base for temperature; as will be illustrated in the sample problems in Volume III and zero velocity everywhere in the domain $(u = v = \Omega = 0)$, since it is quite difficult to obtain ground truth current measurements for the entire domain for the kind of grid size resolution that would be required. Although an initial free-surface $\eta=\eta(x,y,t=o)$, can be specified

[5]NOTE: $\Omega \to 0$ is used in program to save computational time, which is a good approximation, since it has been learned that $\Omega \approx 0$.

[6]NOTE: At an inlet $u(t)$ or $v(t)$ must be specified, and at an outlet $\frac{\partial u}{\partial \alpha}$ or $\frac{\partial v}{\partial \beta}$ may be specified.

from existing tide data bases, compatibility between the sur-
face heights and the velocities requires starting the computations
with a flat surface, $\eta(x,y,t=0)=0$, initially.

[7]NOTE: $\Omega=0$ is used in program to save computational time,
which is a good approximation, since it has been learned that $\Omega \approx 0$.

[8]NOTE: At an inlet $\eta = \eta(t)$ <u>and</u> either $\frac{\partial u}{\partial \alpha}$ or $\frac{\partial v}{\partial \beta}$ are specified;
and at an outlet $\frac{\partial u}{\partial \alpha}$ or $\frac{\partial v}{\partial \beta}$ <u>may</u> be specified.

3.7 Method of Solution

3.7.1 General

It is obvious that closed-form analytical solution of the
system of governing equations (3.9) - (3.18) for the free-surface
model in the (α,β,σ) coordinate system, and for equations (3.21)-
(3.29) in the (X,Y,σ) coordinate system, is impossible to get.
The set of equations consists of coupled, unsteady, three-di-
mensional, nonlinear partial differential equations. Therefore,
the finite difference method is used to obtain numerical solutions.

A three-dimensional grid system is established with respect
to the (α,β,σ) coordinate system for the vertically stretched
free-surface model equations, and a three-dimensional grid sys-
tem is established with respect to the (X,Y,σ) coordinate system
for the vertically and horizontally stretched free-surface model
equations. The governing equations are then solved over finite
time steps which are carefully selected to obey numerical stab-
ility criteria. This will be discussed in detail in a following
subsection on stability criteria (3.7.5).

In general, several methods are available for integrating
over time the governing equations for incompressible fluid flow
as discussed by Roache (1972). The two most common techniques
for integrating time-dependent partial differential equations
are the implicit and explicit finite difference methods. The
implicit method involves the solution of a set of simultaneous
equations which are obtained by writing the spatial derivatives
in terms of the respective unknown quantities at the current
time level n + 1, knowing the values of the remaining quantities
of the set (u, v, Ω, h, P, p, T) at the two previous time levels
n and n-1. For the one-dimensional case, implicit methods are
convenient because the set of simultaneous equations is tri-
diagonal, Richtmyer. and Morton (1967), and, hence, a direct
matrix inversion method of solution is used. However, in the
case of a three-dimensional model, the implicit method becomes

111

too time consuming, since the simultaneous equations must be solved at each time step by an iterative technique. Thus, although the advantage of implicit methods is that they allow larger time steps, for the three-dimensional case the iteration time for each time step more than offsets the inherently larger time step. Furthermore, alternating direction-implicit (ADI) methods may be used to obtain tri-diagonal matrices even for multidimensional equations, however, for irregular boundaries the ADI methods are impractical.

Therefore, the explicit finite difference method is used for numerical solution of the free-surface model. The solution to a particular partial differential equation is propagated from point to point on the numerical grid system. The current time level value, $n + 1$, of a particular system variable $(u, v \Omega H, P, \rho, T)$

is computed in general from known values of the corresponding system variables at the two previous time levels n and $n-1$. Thus, this is an explicit scheme.

The mathematical model is an initial-value, boundary-value problem and, hence, requires specification of both initial conditions and boundary conditions (see sections 3.5 and 3.6).

3.7.2 Computational Grid System

The free-surface model does not use the staggered grid (or mesh) system as used in the rigid-lid model (section 2.6.2). Instead, the full grid system is used for defining the system variables $u, v, \Omega, H, P, \rho, T$ at the integral nodes $(I, J. K)$. The rigid-lid model uses the half-grid system for better meshing of the solution of the Poisson equation for surface (or lid) pressure, P_s, with the horizontal velocity components u and v. This is not considered necessary for the free-surface model, since the pressure field $P (I, J, K)$ is computed from $H (I, J)$ which is computed at integral nodes from $u (I, J, K)$ and $v (I, J, K)$.

112

3.7.3 MAR Numbering System

Since the free-surface model does not use the half-grid system, only MAR (I, J) is used for distinguishing between spatial finite differences in the interior; on the boundary, and outside the domain of solution. The MAR numbering system for both the far-field (closed basin) and for the combined far-field and near-field (horizontal stretching applied to an open basin) versions of the free-surface model will be clearly specified in the sample problems in Volume III. Note, that for the far field model MAR (I, J) =6 and MAR (I, J) = 8 boundary corners are treated as interior points (MAR(I,J)=11)

3.7.4 Finite Difference Schemes
3.7.4.1 Approximation of Spatial and Temporal Partial Derivatives; Conservative Form

The spatial derivatives are central differenced in the interior, for example:

$$\frac{\partial u}{\partial \alpha} \cong \frac{u(I+1,J,K) - u(I-1,J,K)}{2\Delta\alpha} \tag{3.30}$$

and,

$$\frac{\partial^2 u}{\partial \alpha^2} \cong \frac{u(I+1,J,K) + u(I-1,J,K) - 2u(I,J,K)}{(\Delta\alpha)^2} \tag{3.31}$$

At the boundaries, three-point single sided schemes are used by fitting a parabola through three points (the boundary point and the next two coincident interior points). Thus, for example, at the left α-boundary:

$$\frac{\partial u}{\partial \alpha} \cong \frac{4u(I+1,J,K) - 3u(I,J,K) - u(I+2,J,K)}{2\Delta\alpha} \tag{3.32}$$

and,

$$\frac{\partial^2 u}{\partial \alpha 2} \cong \frac{u(I,J,K) + u(I+2,J,K) - 2u(I+L,J,K)}{(\Delta \alpha)^2} \qquad (3.33)$$

and, at the right α-boundary

$$\frac{\partial u}{\partial \alpha} \cong \frac{3u(I,J,K) + u(I-2,J,K) - 4u(I-1,J,K)}{2\Delta \alpha} \qquad (3.34)$$

and, $\frac{\partial^2 u}{\partial \alpha 2} \cong \frac{u(I,J,K) + u(I-2,J,K) - 2u(I-1,J,K)}{(\Delta \alpha)^2}$ (3.35)

Note, that the spatial finite difference approximations (3.30)-(3.35) are on order of accuracy of $(\Delta \alpha)^2$, Crandell (1965).

The _temporal_ derivatives can be expressed in two forms, first

$$\frac{\partial u}{\partial t} \cong \frac{u(I,J,K)^{n+1} - u(I,J,K)^{n}}{\Delta t} \qquad (3.36)$$

for forward differencing in time, which is on the order of accuracy of Δt and

$$\frac{\partial u}{\partial t} \cong \frac{u(I,J,K)^{n+1} - u(I,J,K)^{n-1}}{2\Delta t} \qquad (3.37)$$

for central differencing in time, which is on the order of accuracy $(\Delta t)^2$.

The finite differences in both space and time in the model are expressed in the full conservation forms following Arakawa (1966), for example:

$$\frac{\partial(Hu)}{\partial\alpha} = \frac{(Hu)_{I+1,J,K} - (Hu)_{I-1,J,K}}{2\Delta\alpha} \qquad (3.38)$$

This is done to avoid possible "leaking" of mass, momentum, and energy for long term integration with respect to time of the governing time-dependent equations.

3.7.2.4 Finite Difference Equations

The full set of finite difference equations for the far-field and combined far-field and near-field (horizontal stretching) versions of the free-surface model will now be discussed.

3.7.4.2.1 Far-Field

The two integrated forms of the continuity equation for the surface height H, (3.16) and for the equivalent vertical velocity Ω (3.17), are integrated over depth by applying Simpson's rule. The time derivative in the surface height equation is initially replaced by a forward difference in time, and thereafter a central difference in time is used.

The numerical method used for solving the horizontal momentum equations for u and v is an explicit finite difference scheme for which a forward difference in time and central differencing in space (so-called FTCS) is used. The horizontal diffusion terms are differenced at n-1, i.e., two time steps back from the currently computed time level, n+1. The vertical diffusion terms are differenced using the DuFort-Frankel scheme, Roache (1972). The FTCS method is used througout for solving the energy equation without Du-Fort-Frankel differencing of

115

the vertical diffusion term, and has produced no numerical
instability problems.

3.7.4.2.2. Combined Far-Field and Near-Field (Horizontal Stretching)

Spatial integration of equations (3.25) and (3.28), or
of (3.27) and (3.29), have been performed by applying the Trap-
ezoidal rule. Again, FTCS is used for solving the u and v
momentum equations with the horizontal diffusion terms evalu-
ated at n-1 and the vertical diffusion terms DuFort-Frankel
differenced. The energy equation, also uses FTCS with the
same differencing of the respective diffusion terms as done
for the horizontal momentum equations.

3.7.4.2.3 Flow Chart

Now we see the flow chart for the steps involved in pro-
pagating the numerical solution of the system of governing
equations for the free-surface model. These steps may be elab-
orated as follows:

1. The problem is set up as an initial-value problem.
The values of u, v, Ω, H, P, ρ, and T are specified initially for
time level n.

2. The surface height equation is then used to compute H
at time level n+1 from the known values of u and v at time level
n. P is computed at time level n+1.

3. The horizontal momentum equations are used to compute
u and v at time level n+1 from the known values of u, v, Ω, P, ρ
at time level n.

4. The equivalent vertical velocity equation is used to
compute Ω at time level n+1 from the known values of u,v
and H at time level n+1.

116

5. The energy equation is used to compute T at time level n+1 from the known values of u, v, Ω and H at time level n+1.

6. The actual vertical velocity, w, is then computed at time level n+1 from u, v and H at time level n+1.

7. The density, ρ, is computed from the equation of state knowing T at time level n+1.

These seven steps are then repeated to propagate the numerical solution to time levels n+2, n+3, etc.

3.7.5 Stability Criteria

The one-dimensional Burgers equation is used in the stability analysis by a heuristic extension into three-dimensions. This method follows Roache (1972). A strict stability analysis for the system of governing equations under consideration is not possible. The stability criteria may be extended to the three-dimensional equations as follows:

CONVECTIVE: $C_x \left(\frac{\Delta t}{\Delta x}\right) + C_y \left(\frac{\Delta t}{\Delta y}\right) + C_z \left(\frac{\Delta t}{\Delta z}\right) < 1$ \hspace{1cm} (3.39)

DIFFUSIVE : $D_x \left(\frac{\Delta t}{\Delta x}\right)^2 + D_y \left(\frac{\Delta t}{\Delta y}\right)^2 + D_z \left(\frac{\Delta t}{\Delta z}\right)^2 < \frac{1}{2}$ \hspace{1cm} (3.40)

For the application of these criteria to the present problem, C_x, C_y, and C_z may be interpreted as the maximum values of u, v, and w in the domain and D_x, D_y, and D_z may be interpreted as the kinematic eddy diffusivities in the x, y and z directions, respectively.

Another numerical stability criterion for the free-surface model is the Courant-Friedricks -Lewy (CFL) condition, Roache (1972), and Richtmyer. and Morton (1976), which is based upon external gravity waves (or so-called surface gravity waves) and is expressed as follows:

$$\Delta t < \frac{x}{\sqrt{gH}} \hspace{1cm} \text{or} \hspace{1cm} \Delta t < \frac{y}{\sqrt{gH}} \hspace{1cm} (3.41)$$

117

whichever is smaller, $C_o = \sqrt{gH}$ is defined as the phase velocity or the celerity of these external gravity waves.

3.7.6 Numerical Modeling Approximations

3.7.6.1 Adiabatic Condtion in Far-Field Version

Following Roache (1972), the lateral temperature boundary conditions is specified as:

$$T_w = T_{w+1} \text{ on } \sigma = \text{constant planes} \qquad (3.42)$$

This condition is simply set after the interior point calculation for T_{w+1} is performed. Although

$$\frac{\partial T}{\partial x} = \frac{\partial T}{\partial \alpha} + \frac{\partial T}{\partial \sigma} \left(\frac{1}{H} \frac{\partial \eta}{\partial \alpha} - \frac{\sigma}{H} \frac{\partial H}{\partial \alpha} \right) \qquad (3.43)$$

and,

$$\frac{\partial T}{\partial y} = \frac{\partial T}{\partial \beta} + \frac{\partial T}{\partial \sigma} \left(\frac{1}{H} \frac{\partial \eta}{\partial \beta} - \frac{\sigma}{H} \frac{\partial H}{\partial \beta} \right) \qquad (3.44)$$

for a shallow body of water like the Biscayne Bay, $\frac{\partial T}{\partial \sigma}$ is quite small in comparison with the horizontal temperature variations, and, therefore, is neglected by using $T_w = T_{w+1}$ on σ constant planes.

3.7.6.2 Velocity Gradient at Inlet, Far-Field Version

The velocity gradient $\frac{\partial v}{\partial \beta}$ (or $\frac{\partial u}{\partial \alpha}$ as the case might be) has been approximated as follows (for Biscayne Bay)

$$\underset{\text{inlet}}{V(I,J,K)} = \sum_{I=7}^{16} \underset{\text{interior}}{V(I,J_o,K)}/10 \qquad (3.45)$$

118

where J_o corresponds to the value of the J index at the <u>interior</u> points adjacent to the inlet. This approximation has been used, since only <u>one</u> value of η_o (t) is known at the inlet for the Biscayne Bay. However, this would not be essential if $\eta_o(t)$ was known at all points along the inlet!

3.7.7 <u>Higher Order Terms</u>

Higher order terms resulting from the transformation of the horizontal diffusion terms (i.e. second order derivatives in α and β), from the Cartesian coordinate system (x,y,z) to the vertically stretched coordinate system (α, β, σ) have been neglected. This has been done since the magnitude of the vertical diffusion terms are several orders of magnitude larger than the horizontal diffusion terms, Sengupta and Lick (1974). Appendix A of this volume presents the details of this transformation.

3.8 <u>Sample Results</u>

In this section sample results using the free-surface model for near-field and far-field applications will be presented.

3.8.1 <u>Far-Field, Biscayne Bay (closed basin with ocean efflux)</u>

Ignoring the Cutler Ridge site thermal discharge, the free-surface far-field model was applied to Biscayne Bay to investigate the general circulation, natural temperature distribution and the surface height behavior. Lee and Sengupta (1977).

Preliminary cases and governing physical factors were first studied. Table 3-1 gives the various cases run. Model execution including all the physical factors, wind, current, tide, bottom topography for the April 15, 1975 data base was the final case run for calibration and verification.

119

Fig, 3.5 shows the model predicted surface velocity distribution at 0900 EST on April 15, 1975. This case is for incoming tide with the tidal current velocity specified sinusoidally with respect to time at the ocean-bay interface. The effect of the wind is clearly indicated to be in the direction of the wind in the northern closed part of the bay. Fig, 3.6 shows the model predicted surface velocity distribution at 1300 EST. This case is for outgoing tide and the south wind effect is clearly exhibited. In Fig, 3.7 the velocity distribution at a depth of 1 meter is shown where it can be seen that the tide effect dominates the effect of the wind.

Fig. 3.8 shows the contours of constant surface height at 1100EST as predicted by the model, and Fig, 3.9 shows the contours of constant surface height at 1400EST. Now Fig, 3.10 and Fig, 3.11 show the corresponding surface velocity distribution at 1100 EST and 1400 EST, respectively. It can be seen that comparison of Fig, 3.8 with Fig 3.10, and comparison of Fig, 3.9 with Fig, 3.11 indicate the relationship between the lines of constant surface height and the velocity field.

Fig, 3.12 shows two synoptic model isotherm plots vs IR-data for April 15, 1975. The agreement is good. Fig, 3.13 shows the surface height versus time at two tide gaging stations, observed vs calculated. The agreement is relatively close. Fig, 3.14 shows surface height versus x-direction (I-direction in grid system) for varying time during the tidal cycle along the transect J=7. It can be seen that the surface moves according to the stage of the tidal cycle, as would be expected.

3.8.2 Combined Near-Field and Far-Field by Using Horizontal Stretching for Hutchinson Island (open basin)

Fig, 3.15 shows the general location of the Hutchinson Island Power Plant site. The condenser cooling water for the power plant is provided by the intake and discharge pipes which circulate the water from the Atlantic Ocean with canals to the plant. Fig, 3.16 shows the details of the submerged discharge

pipe geometry.

Fig.3.17 shows the horizontal grid system without horizontal stretching (I=20, J=20). Fig.3.18 shows the horizontal grid system with SINH stretching. Fig.3.19 shows a distorted vertical section with σ- stretching.

The model was run using the June 2, 1976 data base. On June 2, 1976 the thermal discharge had an exit velocity of 280 cm/sec (9,1 ft/sec) at each end of the Y-type discharging pipe. The discharge temperature was about $35^{o}C$.

Fig.3.20 shows the surface height variation along the I=8 transect (one grid point before the discharge points from south to north). The surface heights are negative around the area of discharge owing to viscous entrainment. Fig.3.21 shows the surface velocities with the conditions for June 2, 1976. The imposed northerly current prevails away from the discharge. Fig. 3.22 shows the horizontal velocity on the plane of the discharge. The velocity field is dominated by the discharge conditions because the inertia of the jet is the important driving mechanism near the discharge point. The velocities decreased away from the discharge owing to entrainment as is expected. Fig.3.23 shows velocity distribution in the J=10 transect which is perpendicular to the shoreline. A small vortex can be seen near the discharge region owing to entrainment just west of the discharge.

Fig.3.24 shows the comparison of model results and IR data for June 2, 1976. Relatively good agreement is observed.

The model was verified for May 17, 1977. The free surface model was run for one hour with May 17, 1977 data base as an input. Fig.3.25 shows the surface isotherms comparison of model results and IR data (1113-1118 EDT). The isotherms of $25.4^{o}C$ and $25.9^{o}C$ from model results cover a larger area than IR data. Generally, the results predicted by the model are in agreement with the IR-Data.

The results presented are taken from Tsai (1977). This model is extremely sensitive to parameters of the problem, time step and boundary condition. Further verification is ongoing. Where high resolution at discharge point is not necessary the horizontally stretched free-surface model is recommended.

TABLE 3-1 LIST OF COMPUTER CASES RUN FOR

FREE-SURFACE FAR FIELD - BISCAYNE BAY APPLICATION
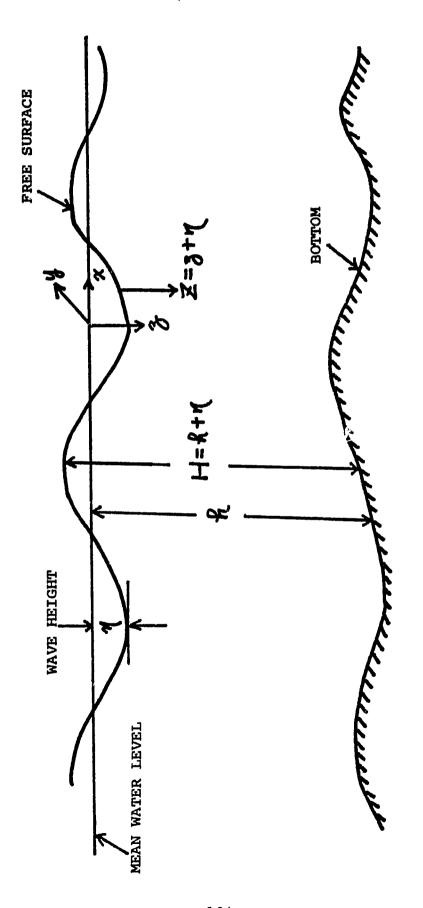
CASE NO.	DEPTH	WIND	AMBIENT TEMP.	DENSITY	TIDAL FLUX	TIME
i	Const.	None	Const.	Const.	Const.	1 hr.
ii	Const.	Const.	Const.	Const.	Const.	1 hr.
iii	Variable	Const.	Const.	Const.	Const.	1 hr.
iv*	Variable	Const.	Const.	Const.	Const.	3 hrs.
v	Variable	Const.	Const.	Const.	Const.	3,6hrs.
vi	Variable	Const.	Const.	Variable	Const.	3,6hrs.
vii**	Variable	Variable	Variable	Variable	Variable	1-7hrs.

*The model was first calibrated at this point by changing horizontal eddy kinematic viscosity, K_H, from 100,000 cm^2/sec to 10,000 cm^2/sec by comparison with rigid-lid far field results, Sengupta (1976a).

**Only results for this computer case are being presented at this time.

122
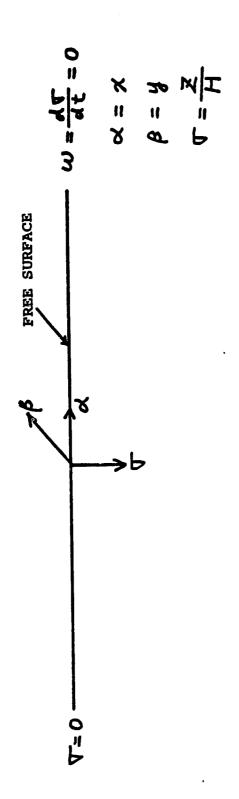
TABLE 3-2   LIST OF CASES OF THE FREE SURFACE MODEL APPLIED TO HUTCHINSON ISLAND SITE

Case No.	Density	Depth	Wind	Current	Discharge Velocity	Discharge Temp.	Air Temp.	Ocean Temp.
June 2, 1976	Varied	Varied	4.47 m/sec SE.	25 cm/sec N,	280 cm/sec	35°C	29°C	25.5°C
May 17, 1977	Varied	Varied	2.68 m/sec ESE	10 cm/sec SE	280 cm/sec	33°C	26°C	24.9°C

Figure 3-1 The xyz Coordinate System for the Free-Surface Model

Fig. 3-2 The $\alpha\beta\sigma$ Coordinate System for the Free-Surface Model

Diagram labels:

$\sigma = 0$

$\omega = \dfrac{d\sigma}{dt} = 0$

FREE SURFACE

β α σ

$\alpha = x$

$\beta = y$

$\sigma = \dfrac{z}{H}$

BOTTOM

$\sigma = 1$

$\omega = \dfrac{d\sigma}{dt} = 0$

FREE SURFACE

$$X = \frac{1}{C_1} \tan\left(\frac{\alpha}{C_2}\right)$$

$$Y = \frac{1}{C_3} \tan\left(\frac{\beta}{C_4}\right)$$

$$\sigma = \frac{Z}{H}$$

BOTTOM
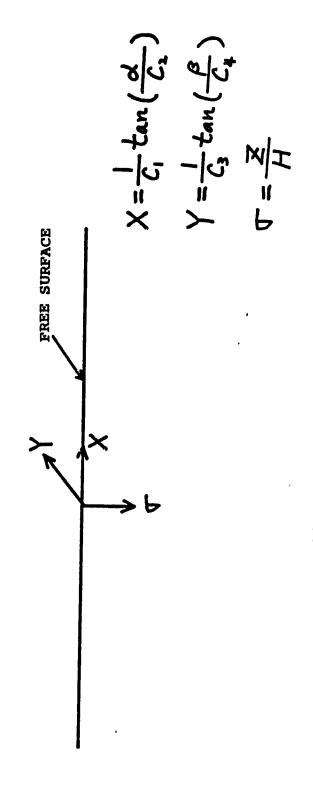
Figure 3-3   The $X|Y|\sigma$ Coordinate System for the Free-Surface Model

126

Figure 3-4   Variable Grid Size System in $\alpha - \beta$ Coordinates

127

THERMAL POLLUTION LAB
UNIVERSITY OF MIAMI

*Note: φ was selected for
$V_o(t)=0.0$ at high tide at
1010. $\omega=2\pi/12.15$ (hr^{-1})

CASE vii

Δt	:	.10 sec.
t$_{total}$	:	1 hr(900)
Wind	:	4.11 m/sec (9.2 mph) SSW
Depth	:	Variable
Tide	:	*V_o(t)=45.0 cos ω(t+φ)
		(at 0900, V_o=-25.5 cm/sec)

SSW

Wind

N

0 1.6 32 km 0 45 90cm/sec

Fig. 3-5   Surface Velocity Distribution for Biscayne Bay
at 9:00 AM, April 15, 1975 (by Free Surface Model)

128

CASE vii

Δt : 10 sec
t_{total}: 5 hrs. (1300)
Wind : 8.22m/sec(18.4 mph)S
Depth : Variable
Tide : $V_o(t) = 45.0 \cos \omega(t+\varphi)$
(at 1300, $V_o = 44.7$ cm/sec)

Fig. 3-6   Surface Velocity Distribution for Biscayne Bay at
1:00 p.m., April 15, 1975 (by Free Surface Model)

CASE vii

Δt : 10 sec
t_{total}: 5 hrs.(1300)
Wind : 8.22m/sec(18.4 mph)S
Depth : Variable
Tide : $V_-(t)=45.0 \cos w'(t+\varphi)$
(at 1300, $V_o=44.7$ cm/sec)

1300

$V_o(t)$

t

N

S

wind

0 1.6 3.2km 0 45 90 cm/sec

Fig. 3-7 Velocity Distribution at Depth of 1 Meter
For Biscayne Bay at 1:00 p.m. (Free Surface Model)

CASE vii

Δt	:	10 sec
t_{total}	:	3 hrs (1100)
Wind	:	5.60 m/sec(12.7 mph) SSW
Depth	:	Variable
Tide	:	$V_0(t) = 45.0 \cos \omega(t+\varphi)$
		(at 1100, $V_0 = 18.8$ cm/sec)

Fig. 3-8   Lines of Constant Surface Height Above Mean
Water Level for Biscayne Bay, in cm.(Free-Surface
Model)

131

THERMAL POLLUTION LAB
UNIVERSITY OF MIAMI

CASE vii

Δt : 10 sec
t_{total} : 6 hrs (1400)
Wind : 8.22m/sec(18.4mph)S
Depth : Variable
Tide : $V_o(t) = 45.0 \cos \omega (t+\varphi)$
(at 1400, V_o =41.3 cm/sec)
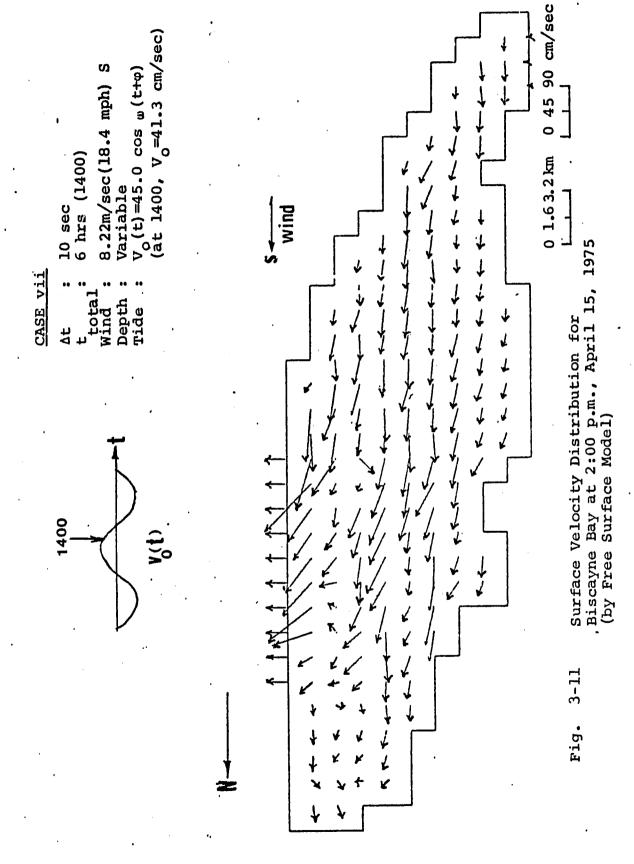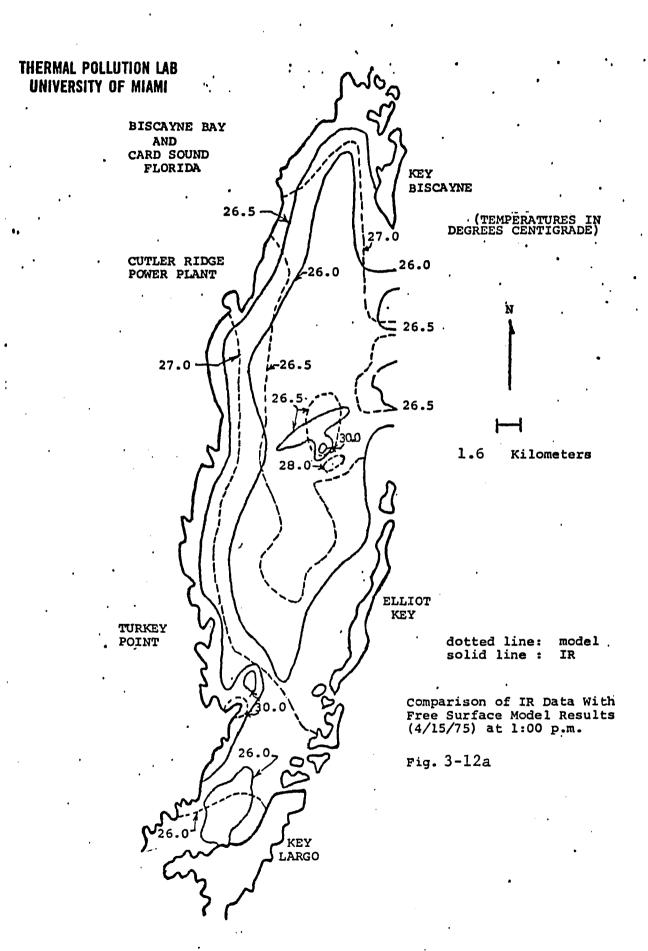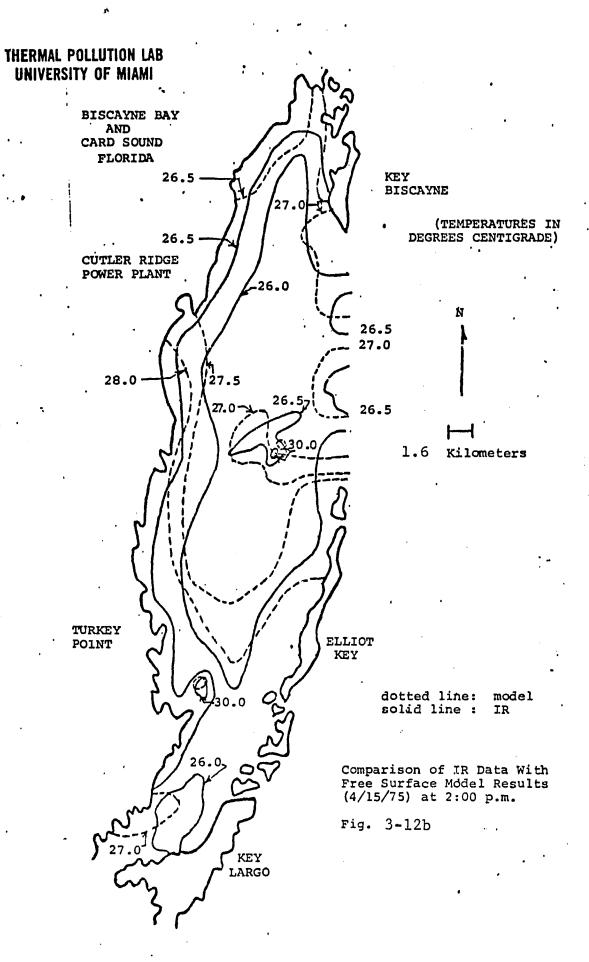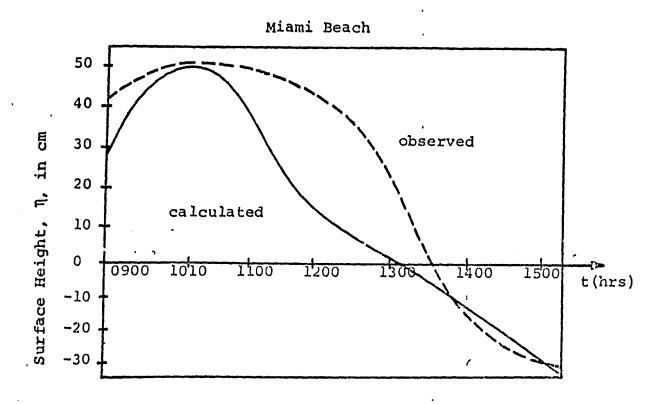
Fig. 3-9 Lines of Constant Surface Height with Respect to Mean Water Level for Biscayne Bay, in cm (Free Surface Model)

CASE vii

Δt   : 10 sec.
t_{total} : 3 hr. (1100)
Wind   : 5.68m/sec (12.7 mph)SSW
Depth   : Variable
Tide   : $V_o(t)=45.0 \cos \omega (t+\varphi)$
            (at 1100, $V_o=18.8$cm/sec)

1100

$V_o(t)$

SSW

WIND

0 16 32 km

0 45 90cm/sec

Fig. 3-10   Surface Velocity Distribution for Biscayne Bay
              at 11:00AM, April 15, 1975 (by Free Surface Model)

THERMAL POLLUTION LAB
UNIVERSITY OF MIAMI

CASE vii

Δt	:	10 sec
t_{total}	:	6 hrs (1400)
wind	:	8.22m/sec(18.4 mph) S
Depth	:	Variable
Tide	:	$V_o(t)=45.0 \cos \omega(t+\varphi)$
		(at 1400, V_o=41.3 cm/sec)

Fig. 3-11   Surface Velocity Distribution for
Biscayne Bay at 2:00 p.m., April 15, 1975
(by Free Surface Model)

0 1.6 3.2 km   0 45 90 cm/sec

THERMAL POLLUTION LAB
UNIVERSITY OF MIAMI

BISCAYNE BAY
AND
CARD SOUND
FLORIDA

KEY
BISCAYNE

(TEMPERATURES IN
DEGREES CENTIGRADE)

CUTLER RIDGE
POWER PLANT

N

1.6   Kilometers

ELLIOT
KEY

TURKEY
POINT

dotted line: model
solid line :   IR

Comparison of IR Data With
Free Surface Model Results
(4/15/75) at 1:00 p.m.

Fig. 3-12a

KEY
LARGO

THERMAL POLLUTION LAB
UNIVERSITY OF MIAMI

BISCAYNE BAY
AND
CARD SOUND
FLORIDA

26.5

KEY
BISCAYNE

27.0

26.5

(TEMPERATURES IN
DEGREES CENTIGRADE)

CUTLER RIDGE
POWER PLANT

26.0

26.5
27.0

N

28.0   27.5

27.0   26.5   26.5

1.6   Kilometers

30.0

TURKEY
POINT

ELLIOT
KEY

dotted line: model
solid line :   IR

30.0

Comparison of IR Data With
Free Surface Model Results
(4/15/75) at 2:00 p.m.

26.0

Fig. 3-12b

27.0

KEY
LARGO

Miami Beach

Coconut Grove

Fig. 3-13   Surface Height vs. Time, at
Miami Beach and Coconut Grove,
Observed versus Calculated
(Free-Surface Model)

137

CASE vii
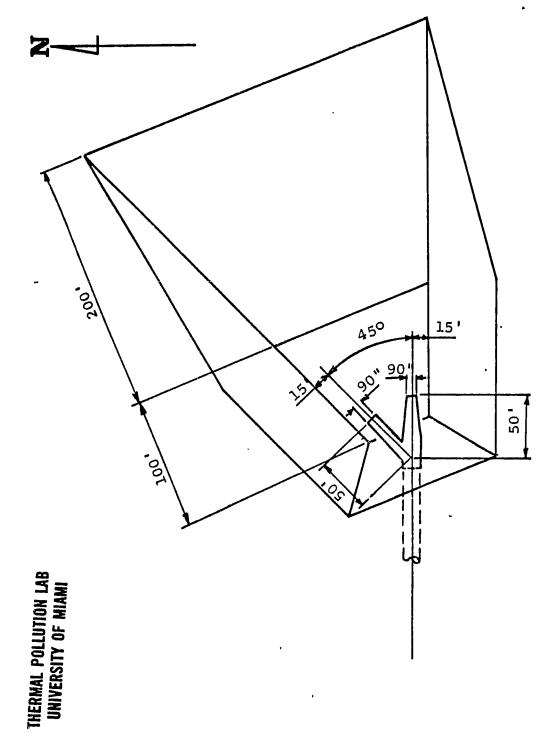
Note: April 15, 1975 Parameter
Values are Given in
Table 4.b. for this
Computer Run

Fig. 3-14 Surface Height versus I Direction, at J=7,
for Varying Time for Biscayne Bay (Free
Surface Model)

138

Atlantic
Ocean
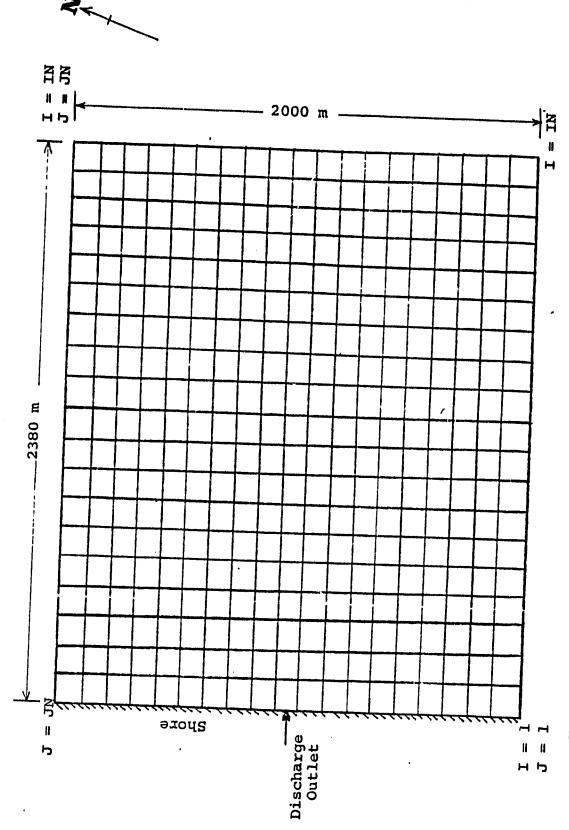
N

Shore

Hutchinson
Island

Y - type Submerge
Discharge

Power
Plant

Intake

0   400 m

Distance
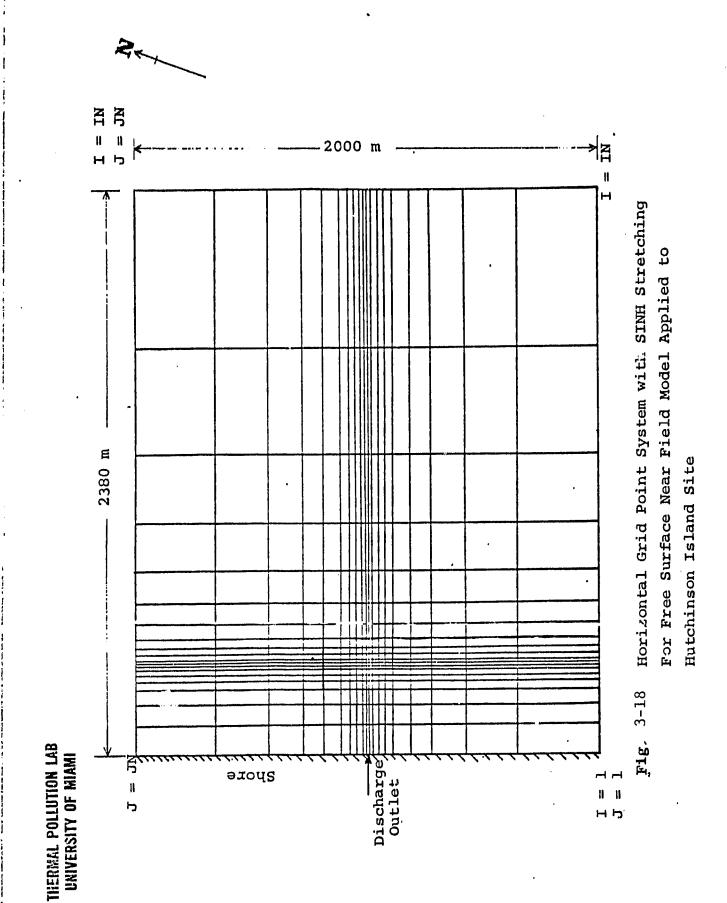
Fig. 3-15 Florida Power and Light Company's Hutchinson
Island Site Power Plant

Fig. 3-16 Submerged Y-Type Discharge at Hutchinson Island
Site (Reproduced From FPL Environmental Report)

Fig. 3-17 . Horizontal Grid Point System Without Stretching
For Free Surface Near Field Model Applied to
Hutchinson Island Site

Fig. 3-18   Horizontal Grid Point System with SINH Stretching
For Free Surface Near Field Model Applied to
Hutchinson Island Site

**THERMAL POLLUTION LAB
UNIVERSITY OF MIAMI**
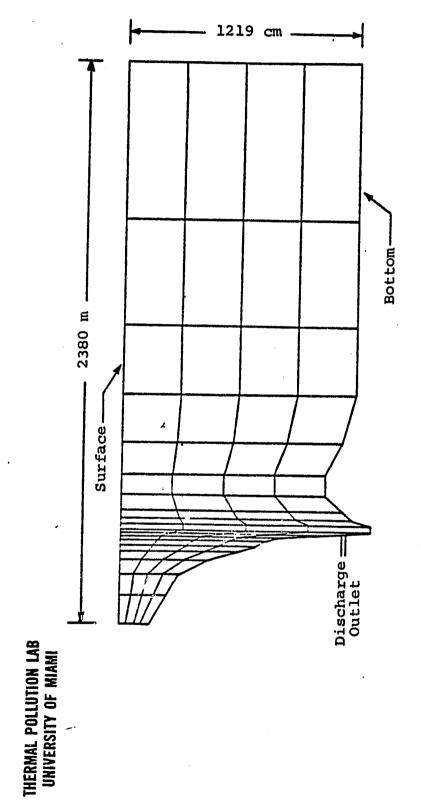
Fig. 3-19 Distorted Vertical Section With Sigma Stretching
For Free Surface Near Field Model Applied to
Hutchinson Island Site

THERMAL POLLUTION LAB
UNIVERSITY OF MIAMI

Discharge Velocity: 280 cm/sec

Wind   : 4.47 m/sec
                      (10 mph) S.E.

Current   : 25 cm/sec N.

Bottom Topography : Varied
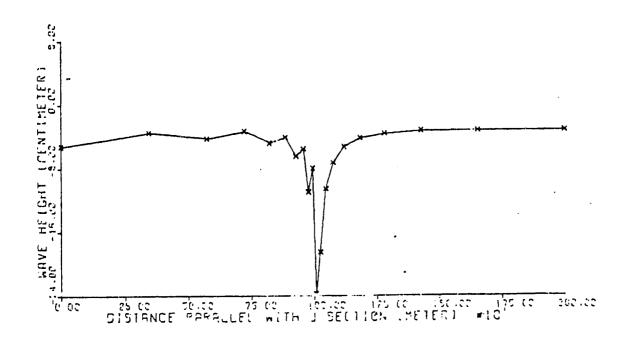
Fig. 3-20   Surface wave height along I=8 from south to
             north at Hutchinson Island Site (Free Surface
             Model)

Fig. 3-21   Surface velocity distribution with current,
             wind and bottom topography at Hutchinson
             Island Site (Free Surface Model)

145

Discharge Velocity: 280 Cm/sec
Wind   : 4.47 m/sec
                (10 mph) S. E.
Current   : 25 cm/sec N.

With Bottom Topography

Y-type
Discharge

0 _____ 280

Velocity (cm/sec)
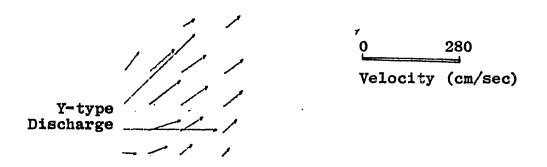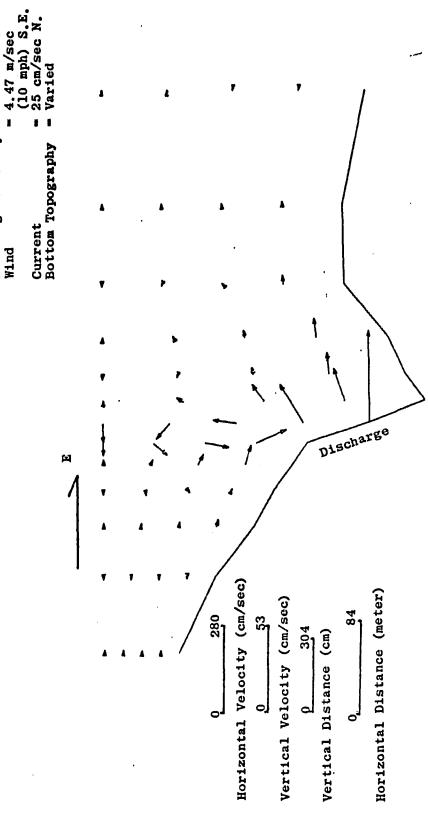
Fig. 3-22 Horizontal Velocity Distribution near the
          ocean bottom around the discharge pipe at
          Hutchinson Island Site (Free Surface Model)

146

THERMAL POLLUTION LAB
UNIVERSITY OF MIAMI

Discharge·Velocity = 280 cm/sec
Wind = 4.47 m/sec
(10 mph) S.E.
Current = 25 cm/sec N.
Bottom Topography = Varied

E

Discharge

Horizontal Velocity (cm/sec)
0 — 280

Vertical Velocity (cm/sec)
0 — 53

Vertical Distance (cm)
0 — 304

Horizontal Distance (meter)
0 — 84

Fig. 3-23   Velocity distribution at section J-11 for Hutchinson
Island Site with vertical scale exaggerated 5.25 times
(Free Surface Model).

147

THERMAL POLLUTION LAB
UNIVERSITY OF MIAMI

N

Discharge Temp	: 35°C
Air Temp	: 29°C
Ocean Temp	: 25.5°C
Current	: 25 cm/sec N.
Wind	: 4.47 m/sec (10 mph) S.E.
Bottom Topography:	Varied

shore

——— IR Data

- - - - - Model Result

0   250

Distance (meter)
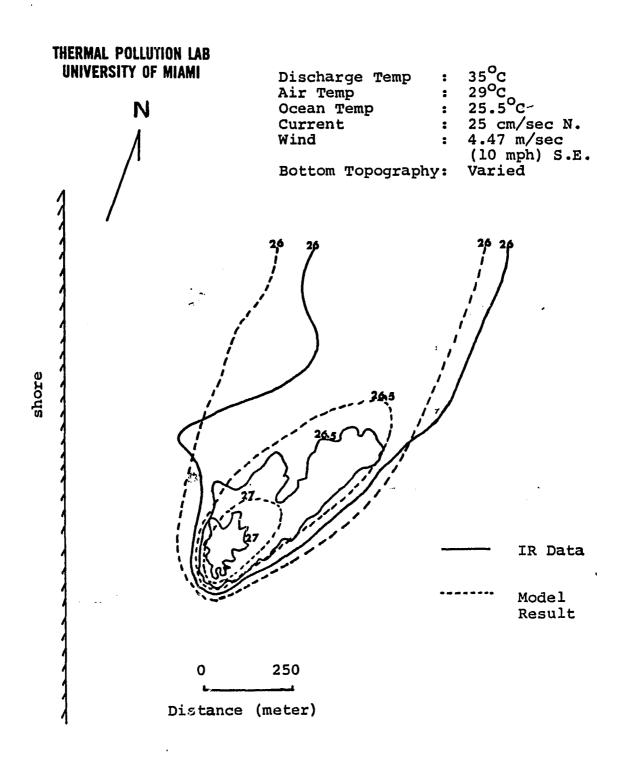
Fig. 3-24 Comparison of model results and
afternoon IR data at Hutchinson
Island Site for June 2, 1976
(Free Surface Model)

148

Discharge Temp.   : 33°C
Air Temp.   : 26°C
Ocean Temp.   : 24.9°C
Discharge Velocity : 280 cm/sec
Wind   : 2.68 m/sec
                        (6 mph) ESE.
Current   : 10 cm/sec SE

N

Discharge
Pipe

IR Data

Model Results

Shore

25.0   25.0   25.9   25.0   25.9   25.9   25.0   25.0

0   500

Distance (meter)
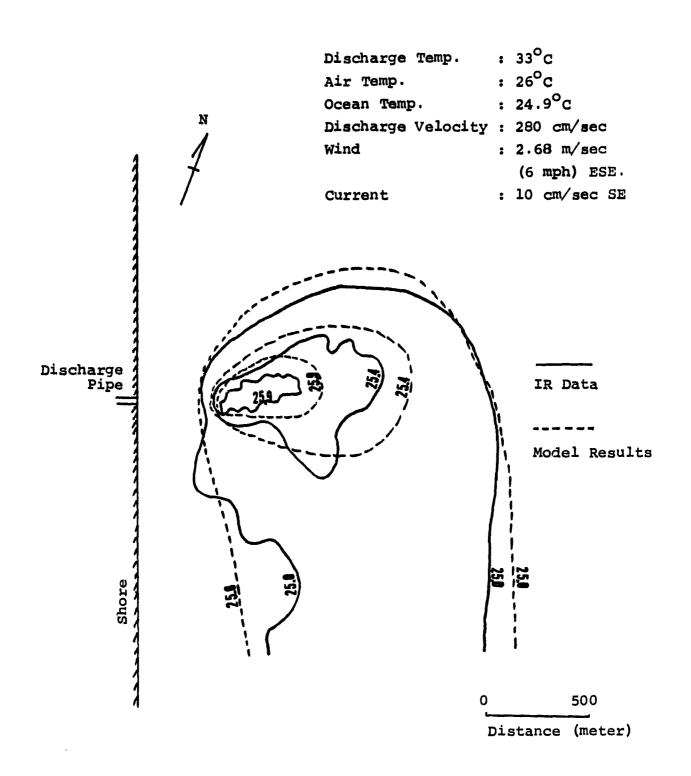
Fig. 3-25 Comparison of model results and IR
           data (1113 - 1118 EDT) at Hutchinson
           Island Site on May 17, 1977. (Free
           Surface Model)

IV. EVALUATION OF MODELS

Verification of existing models has been in general quite unsystematic. In order to provide a basis for user confidence it is essential that accuracy and versatility of models be established by repeated verification at diverse sites. While the verification procedure for the present efforts is by no means completely satisfactory, significant improvements have been made in the thoroughness of verification. A significant factor contributing to this improvement has been the integration of remote sensing and insitu data acquisition program with the model development effort. Accurate specification of initial conditions has been greatly enhanced by synoptic data bases for IR measurements. This have been a serious drawback of other efforts in thermal pollution model development to date.

Comparison of performance of different models is difficult to make. There are two reasons for this difficulty.

1. Systematic synoptic data bases which can be used as standards do not exist.

2. Performance of a given model is dependent on the validity of assumptions and approximations for a given site. Thus performance is often site specific.

An attempt at comparative evaluation was made by Dunn et al (1975). Their extensive review has been documented in a two volume report. Some models were compared using standard data bases for the Point Beach Plant. However,

confusion regarding initial and boundary conditions were still present. Since the models developed by the University of Miami team were calibrated and verified at locations where no other model has been used, detailed comparative evaluation is not possible. However, in order to present the performance of the models developed, in perspective, results presented for various models by Dunn et al (1975) are discussed briefly.

Table IV-1 shows a summary prepared by selecting the most commonly used models. These encompass phenomenological, integral and numerical models. Details of these models with critical comments are presented by Dunn et al (1975). Fig. 4-1 to 4-3 shows comparisons of results from models by Waldrop and Farmer with data at John Sevier Plant and Point Beach Plant. Surface isotherm predictions at the first site are relatively good. Errors of approximately $2^{o}C$ are present in vertical temperature distributions. Comparison of centerline trajectory is poor. Centerline temperatures show large errors after 200 meters. Area under isotherm, predictions fall approximately 7 time below measured values. No velocity comparisons were made.

The Stolzenbach-Harleman integral model was tested for results at different tide stages. Fig.4-4 to 4-6 shows surface isotherm predictions. The model consistently under predicts isotherm areas. The comparisons being poorest at low tide indicating that bottom topography effects are not adequately modelled.

Prichard's phenomenological model was compared to the same

151

data base as the Stolzenbach-Harleman model. Figs 4-7 to 4-9 shows comparisons at high tide, mid-tide and low tide. The isotherm areas are under-predicted, with error being maximum at low tide. The results are qualitatively better than the Stolzenbach-Harleman model. However, bottom topography effects make the model non-usable in practical applications.

Comparisons of results using Prych's phenomenological models are shown in Figs 4-10 and 4-11 for applications at Point Beach Power Plant and Waukegan Power Plant. Relatively good agreement is observed for the Point Beach case except very close to the discharge point. The comparison for the Waukegan Power Plant is significantly worse.

One of the models that can be used relatively easily is the one presented by Shirazi and Davis (1974). They present nomograms and sample problems in a two volume workbook. Figs 4-13 and 4-14 show comparisons of predicted values and mean data from a number of sources the agreement is good. However, this model is quite unsuitable for basins where the infinite depth assumption is not valid.

The numerical model of Till (1974) has been compared to field data obtained at Phillip Sporn Power Plant. Figs 4-15 to 4-17 show isotherms in vertical sections. Near the discharge an error of about $2^{o}C$ is observed. Comparisons become better with distance from discharge.
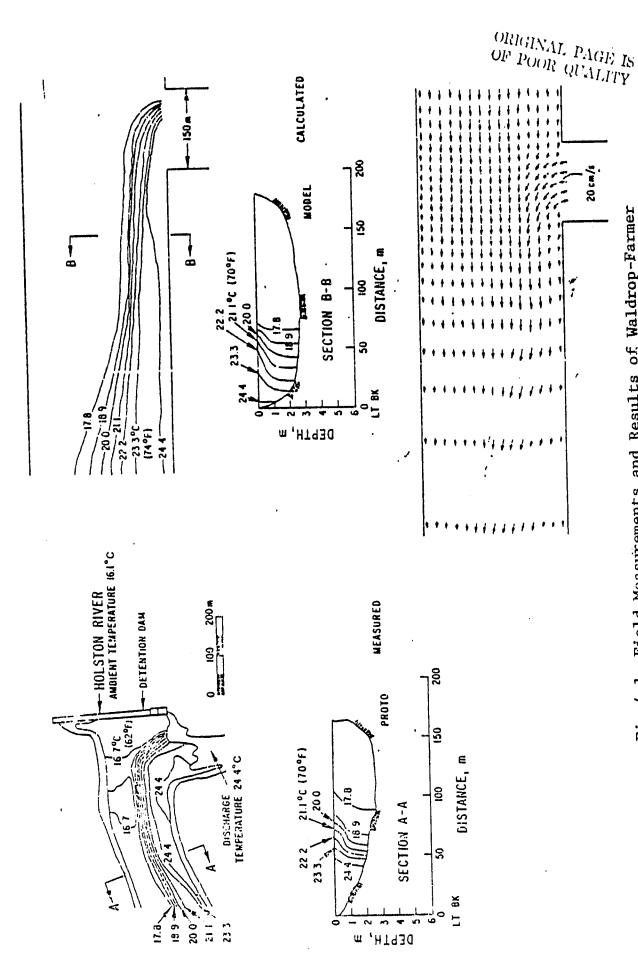
The Paul and Lick (1974) model is very similar to the rigid-lid model developed by the NASA-KSC, University of

152

Miami effort. The comparison with Point Beach field data are shown in Fig. 4-18 and 4-19. Underprediction of areas under given isotherms is observed. This could be owing to errors in choice of diffusion coefficients. Difference in plume shape may have been caused by inadequate information regarding ambient currents.

The comparisons for the present models have been presented before. The following summary statements can be made.

a). The comparisons of rigid-lid near field model for Cutler Ridge plume is in good agreement with IR data as shown in Fig 2-11. The centerline temperatures are especially well predicted as shown in Fig 2-12.

b). The predictions of rigid-lid model for Lake Belews, mixing pond is in agreement with IR data to within $0.2^{\circ}C$ as shown in Fig 2-30. The main lake predictions have shown errors of upto $3^{\circ}C$ at narrow cross sections owing to lack of spatial resolution as well as uncertainty in data regarding the thermachine location.

c). Comparisons of free surface model results with field data at Hutchinson Island show good agreement both for plume shape and temperature as shown in Fig. 3-24.

d). The far-field rigid lid model applied to Biscayne Bay shows surface isotherm predictions to be within $1^{\circ}C$ of corrected IR data, as shown in Fig 2-22.

e). The far-field free-surface model predictions for Biscayne Bay show agreement to within $1^{\circ}C$.

It is imperative at this stage to note that little or no velocity verifications exist for any of the models developed. This is true for all the models presented by Dunn et al (1975). In the present study some limited float measurements of surface velocities in Lake Belews were obtained. Qualitative agreement with model results were observed as reported by Mathavan (1977). For complete verification of models, velocity verification is essential. However, until field measurement equipment that can accurately measure velocities in the range of 0 - 10 cm/sec is developed, such verifications cannot be made.

Fig. 4-1 Field Measurements and Results of Waldrop-Farmer
Calculations for the John Sevier Steam Plant,
March 1973. (Reproduced from Dunn et al).

155
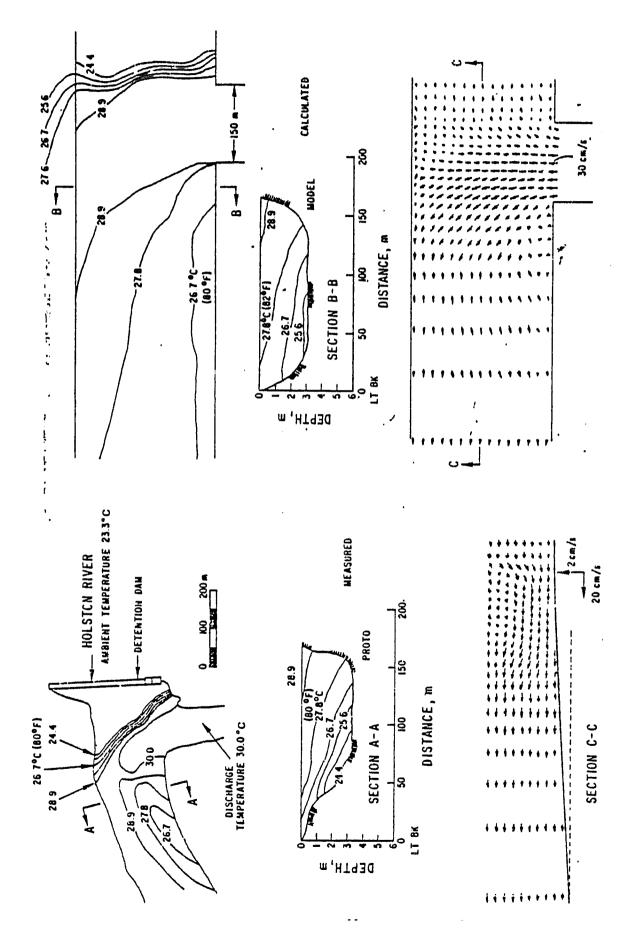
Fig. 4-2 Field Measurements and Results of Waldrop-Farmer Calculations for the John Sevier Steam Plant, July 1973. (Reproduced from Dunn et al).

156

Comparison of Waldrop-Farmer Model
Predictions for Centerline Trajectory to
Two Sets of Temperature Data Taken at
Point Beach (Unit 1) on September 1, 1971.

Surface centerline-temperature decay

Surface isotherm areas

Temperature half-width, left side
when facing offshore

Temperature half-width, right side
when facing offshore
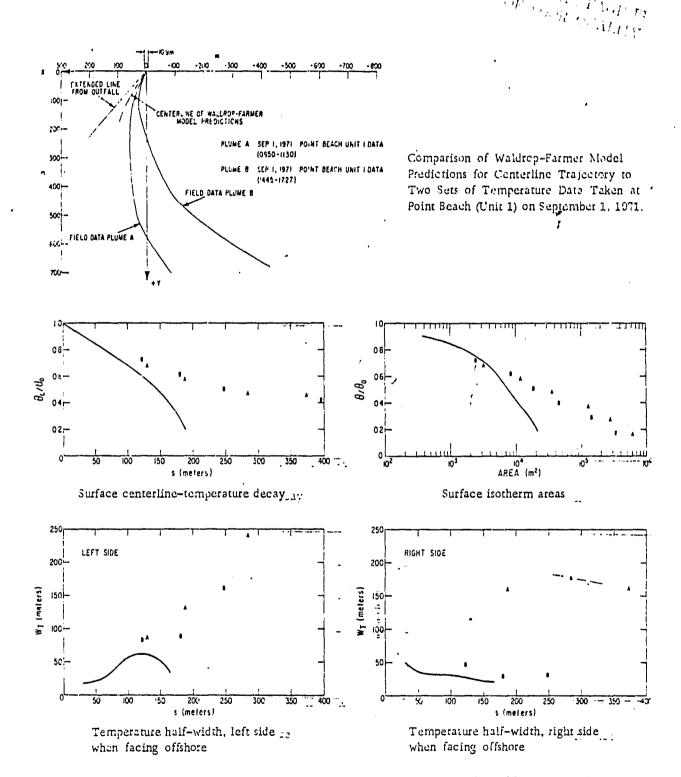
Fig. 4-3 Comparison of Waldrop-Farmer Model Predictions to Two Sets of Temperature Data
Taken at Point Beach (Unit 1) on September 1, 1971.
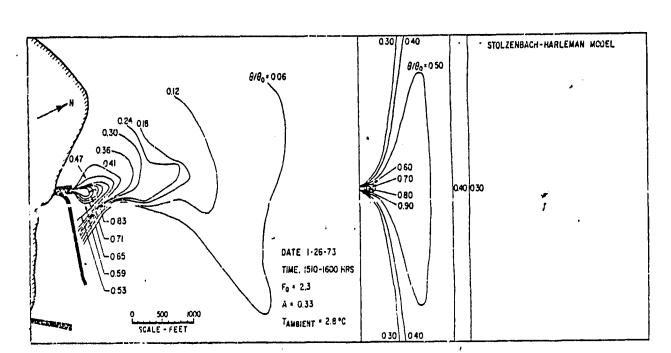
Fig. 4-4   Comparison of Measured and Stolzenbach-Harleman Surface Isotherms at High Tide
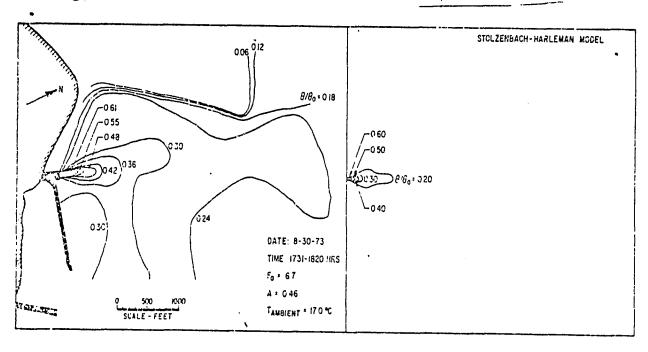
Fig. 4-5   Comparison of Measured and Stolzenbach-Harleman-predicted Surface Isotherms at Midtide

158
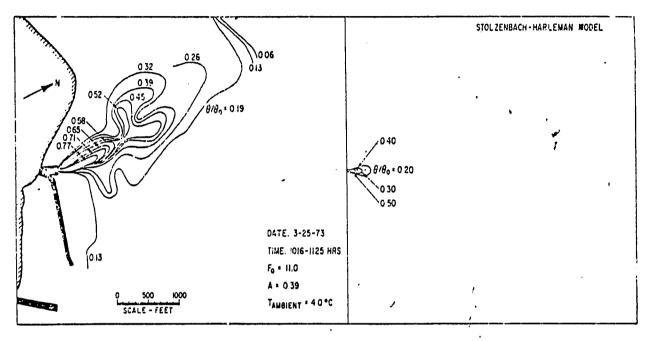
Fig. 4-6   Comparison of Measured and Stolzenbach–Harleman–predicted Surface Isotherms at Low Tide
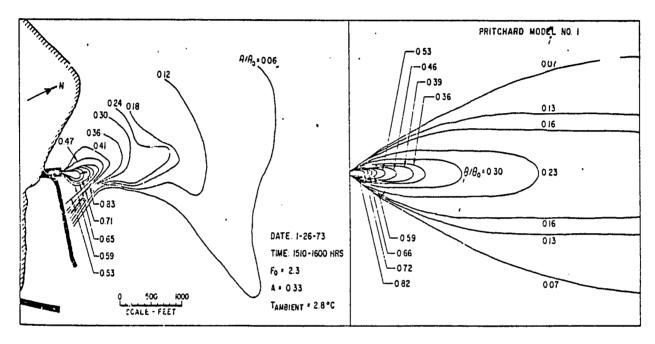
Fig. 4-7. Comparison of Measured and Pritchard-predicted Surface Isotherms at High Tide

Fig. 4-8   Comparison of Measured and Pritchard—predicted Surface Isotherms at Midtide

Fig. 4-9   Comparison of Measured and Pritchard—predicted Surface Isotherms at Low Tide

161

POINT BEACH POWER PLANT
20 JULY 1971
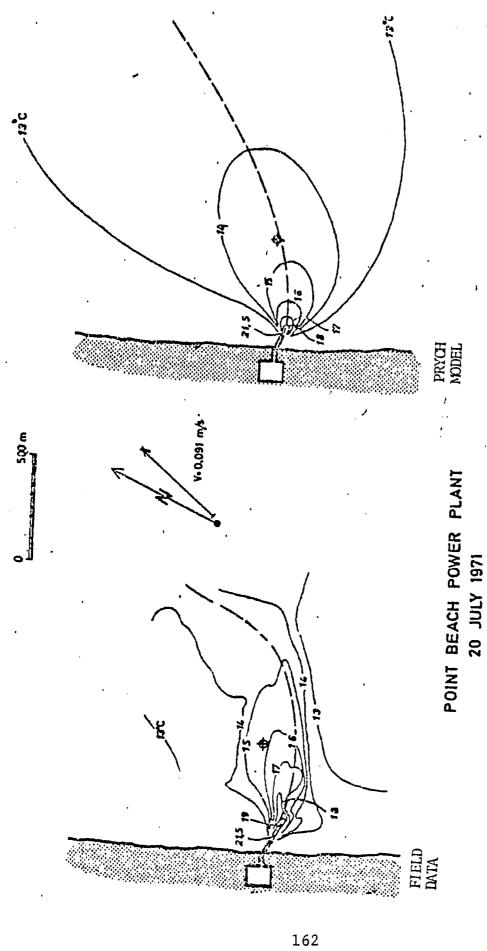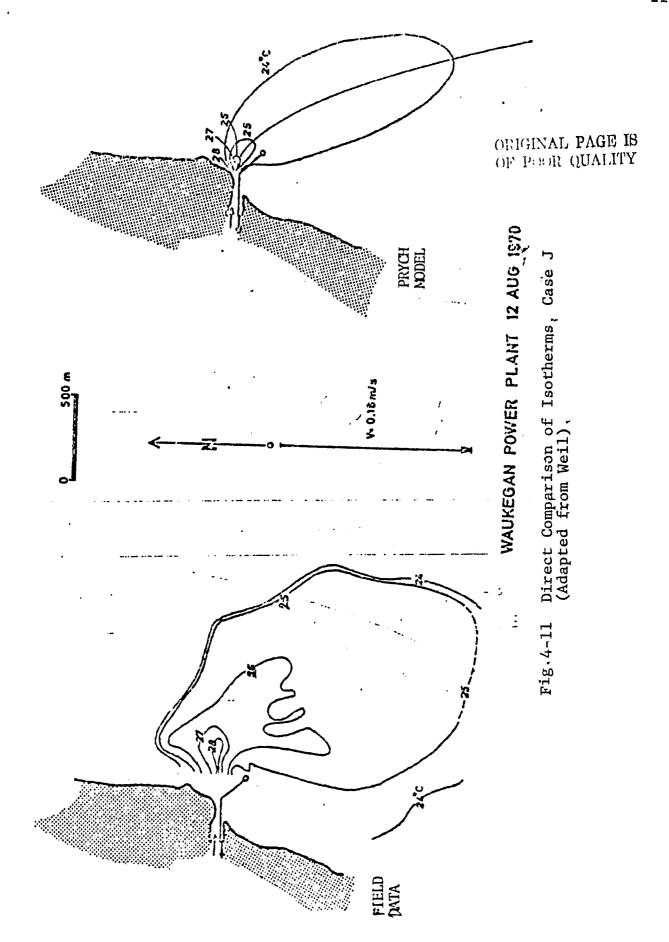
Fig 4-10 Direct Comparison of Isotherms, Case I
(Adapted from Weil).

ORIGINAL PAGE IS
OF POOR QUALITY

PRYCH
MODEL

WAUKEGAN POWER PLANT 12 AUG 1970

500 m

V. 0.18 m/s

FIELD
DATA

Fig. 4-11   Direct Comparison of Isotherms, Case J
(Adapted from Weil).
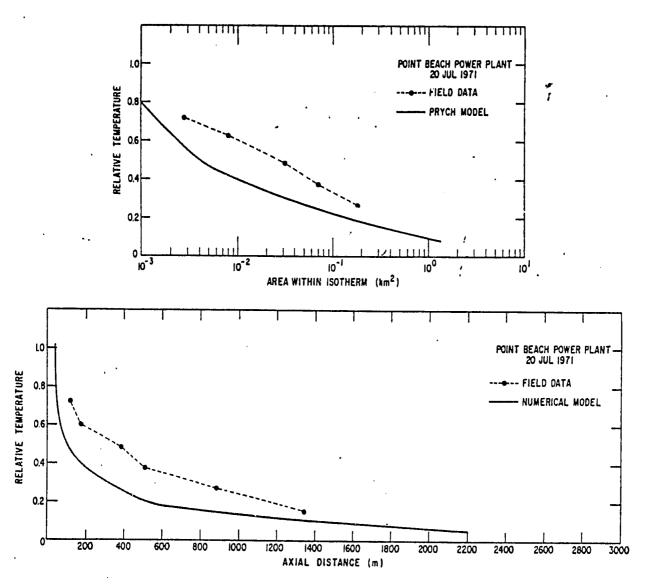
Fig. 4-12. Relative Temperature vs Enclosed Area and Distance, Case I. (Adapted from Weil.[2])
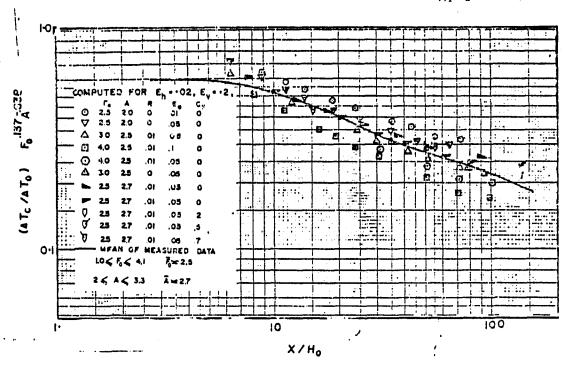
Fig.4-13 Comparison of Calculated Temperature
with Mean of Data
(Adapted from Shirazi and Davis)
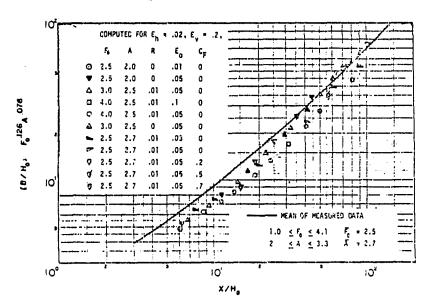
Fig.4-14 Comparison of Calculated Widths with Mean
of Data. (Adapted from Shirazi and Davis.)
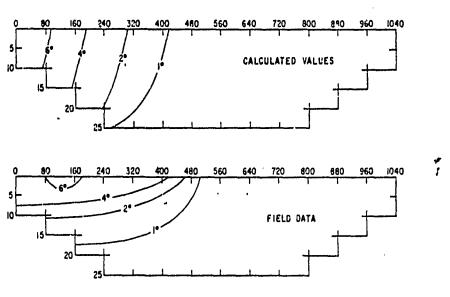
Fig.4-15   Isotherms from Field Data and Calculated Values for Philip Sporn
            Power Plant at Position C, Approximately 1000 ft Downstream
            from Discharge Point. (Adapted from Till.)
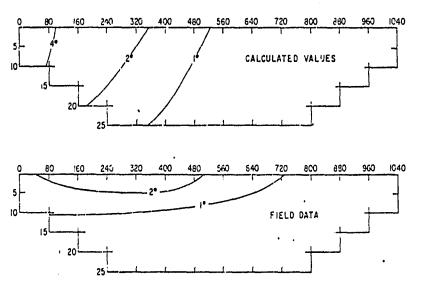
Fig.4-16.   Isotherms from Field Data and Calculated Values for Philip Sporn
            Power Plant at Position D, Approximately 3000 ft Downstream
            from Discharge Point. (Adapted from Till.)
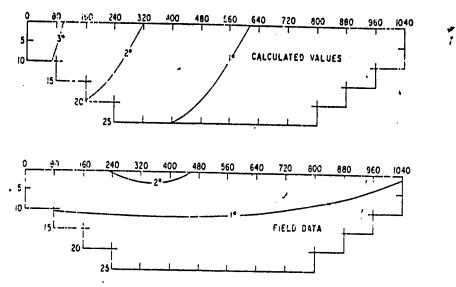
166

Fig.4-17   Isotherms from Field Data and Calculated Values for Philip Sporn
Power Plant at Position E, Approximately 4400 ft Downstream
from Discharge Point. (Adapted from Till.[1])
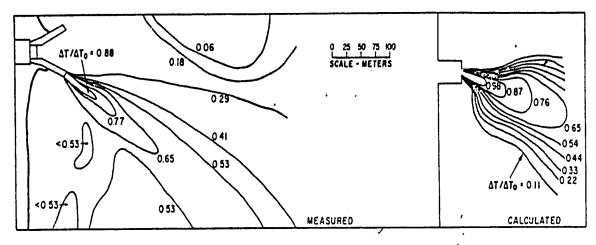
Fig. 4-18   Comparison of Surface Isotherms from Measurements and Predictions
of Paul–Lick Model: Point Beach Power Plant, May 18, 1972.
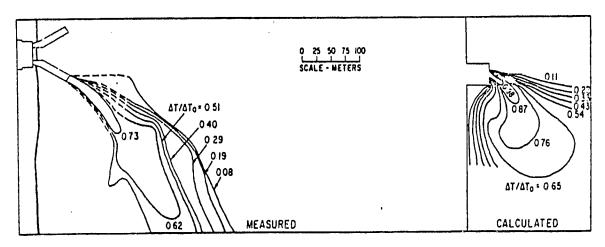
Fig. 4-19   Comparison of Surface Isotherms from Measurements and Predictions
of Paul–Lick Model: Point Beach Power Plant, May 20, 1971.

168

TABLE IV-1

	Investigators	Dimensionality	Type of Model	Application Sites	Comparison Type	Comments
1.	Waldrop and Farmer	3	Time Dependent and Numerical	a) Mississippi River b) Point Beach c) Holston River	Surface Isotherms, Vertical Section Isotherms, Centerline Temperature Decay, Isotherm Areas Fig. 4-1 - 4-3	Surface isotherm comparisons are relatively good. Vertical Section isotherms differ by about 2°C as compared with the measured data. Centerline temperature comparisons do not match at all after 200 meters distance from discharge. Area predictions fall approximately 7 times below the measured area. No velocity comparisons.
2.	Stolzenbach and Harleman	3	Steady State and Numerical	a) Pilgrim Plant b) Point Beach c) Palisades Field Data.	Surface Isotherms and Isotherm Areas Figs 4 to 4-6	Surface isotherm comparisons are very poor for high, middle and low tides (Figs 4 to 6) No velocity comparisons
3.	Pritchard	3	Steady State and Phenomenological	a) Waukengan Plant b) Point Beach c) Palisades Field Data	Surface Isotherms and Centerline Temperature Decay Figs 4-7 to 4-9 .	Though the comparison is better than the Stolzenbach and Harleman model, the comparison is still very poor (Figs 4-7 to 4-9). The surface temperatures in the near field is approximately 4°C below the measured values. No velocity comparisons.

Investigators	Dimensionality	Steady State or Time Dependent and Integral or Numerical	Application Sites	Comparison Type	Comments
4. Weil	3	Steady State and Phenomenological	a) Waukengan Plant b) Point Beach c) Oskarshamnsverket	Surface Isotherms and Centerline Temperature and Surface Area of Isotherms Figs 4-10 - 4-12	Surface isotherms comparisons are in error by 4°C in the near field. Figs 4-10 and 4-11. The centerline and area isotherms plots are 30 to 50% below the measured data. Fig.4-12. No velocity comparisons.
5. Shirazi and Davis	3	Steady State and Integral	a) Point Beach b) Palisades Field Data	Centerline Temperature with Mean of Data and Selected Data Figs 4-13 - 4-14	No surface isotherms comparisons, no velocity comparisons. Centerline values of temperature with mean of data is encouraging. It is hard to make a judgement based on the available comparisons
6. Till, J.	3	Time Dependent and Numerical	a) Philip Sporn Power Plant	Vertical Section Isotherms Figs 4-15 - 4-17	No surface isotherms comparisons, no velocity comparisons. The vertical section isotherm predictions misses from field data by 2°C near discharge.
7. Paul and Lick	3	Time Dependent and Numerical	a) Point Beach b) Cuyahoga River	Surface Isotherms, Centerline Temperature, Isotherm Areas Figs 4-18 - 4-19	The model predictions are available only for a short distance of 200 meters, whereas field data is available up to about 1600 meters. The predictions in the 200 meters distance look encouraging. No velocity comparisons.

Investigators	Dimensionality	Steady State or Time Dependent and Integral or Numerical	Application Sites	Comparison Type	Comments
8. University of Miami a) Venkata, J. Sengupta, S., et al b) Mathavan, S. Lee, S.S., et al c) Tsai, C., Lee, S.S., et al d) Lee, S.S., Sengupta, S. et al e) Lee, S. S., Sengupta, S. et al	3 3 3 3 3	Time Dependent and Numerical	a) Cutler Ridge Site, Florida, Near Field, Rigid Lid Model b) Lake Belews North Carolina; for Field Rigid Lid Model c) Hutchinson Island St. Lucie d) Biscayne Bay, Rigid-Lid Model e) Biscayne Bay Free Surface Model	Surface Isotherms, Centerline Temperature, Vertical Temperature and Comparison with Selected Experimental Data Figs 31-42	Surface isotherm comparisons are made with corrected remotely sensed data and subsurface temperatures with field data. The model comparison at Cutler Ridge for centerline temperature is very encouraging. (Fig 2-12). The surface isotherm comparisons for Lake Belew site is reasonable. In the Fig 2-20 shown, the model differs from the field by 0.2°C. There are some velocity comparisons For the free surface model at Hutchinson Island site, the model predictions are quite good as compared to remotely sensed data Fig 3-24 (This model has the disadvantage of smaller time step). The prediction of surface isotherms by free surface as well as rigid lid for far field in Biscayne Bay are good compared to remotely sensed data. Errors are less than 1°C (Figs 3-22 and 3-12)

V. CONCLUDING COMMENTS

From the experience of existing modelling efforts it can be concluded that numerical models are the only viable tools that can successfully incorporate the physical details of discharge, receiving basin and atmospheric conditions. While phenomenological and integral models are easier to use they contain generic deficiencies that cannot be solved by continued calibration and refinement. Therefore, the search for models which can be used with confidence for regulatory purposes should be directed to numerical models only.

The model package developed by the University of Miami-NASA-KSC efforts show the promise of providing a reasonably general model package. Further calibration and verification of these models should inspire user confidence.

Some comments regarding research efforts that are needed for the development of generally accepted models is appropriate to conclude this volume.

1. Formulae for eddy transport coefficients need to be developed and verified.

2. Surface heat exhcange coefficients and radiative transport of heat into aquatic domains need to be better understood.

3. Reliable anemometers sensitive at low velocity ranges need to be developed.

4. The surface "skin" temperature profile must be understood in terms of meteorological and surface turbulence

172

conditions, before extensive used of IR data can be made without ground truth measurements.

5. Most numerical models are relatively expensive to use owing to computer time costs. However, the cost of computer time is minor compared to overall cost of environmental impact statements. The situation can further improve through development of more sophisticated numerical methods as faster computers.
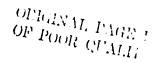
REFERENCES

Arakawa, A., "Computational Design for Long-term Numerical Integration of the Equations of Fluid Motion: two-dimensional Flow," Part I, J. Comp. Phys., Jan., 1966

Carter, H. and Regier, R., "The Three-Dimensional Heated Surface Jet in a Crossflow", Technical Report 28, Chesapeake Bay Institute, John Hopkins University, Baltimore, Md., Nov. 1974.

Crandell, S.H., Engineering Analysis, McGraw Hill, New York, 1965

Du Fort, E.C., and Frankel, S.P., "Stability Conditions in the Numerical Treatment of Parabolic Differential Equations," Math Tables and Other Aids to Computation, Vol7, pp. 135-152, 1953.

Dunn, W.E., Policastro, A.J., and Paddock, R.A., "Surface Thermal Plumes: Evaluation of Mathematical Models for the Near and Complete Field," Water Resources Research Program, Energy and Environmental Systems Division, Argonne National Laboratory, Argonne, Illinois (Part I and II), 1975.

Freeman, N.G., Hale, A.M., Danard M.B., "A Modified Sigma Equations Approach to the Numerical Modelling of Great Lakes Hydrodynamics, "J. Geo.Res., Vol.77, No. 6, 1972.

Haq, A. and Lick, W.,"The Time-Dependent Flow in Large Lakes with applications to Lake Erie,"Department of Earth Sciences, Case Western Reserve University, July 1974.

Harleman, D.R.F. and Stolzenbach, K.D., "Fluid Mechanics of Heat Disposal from Power Generation,"Annual Review of Fluid Mechanics, Vol. 4, 1972.

Krenkel, P.A., and Parker, E.L., Physical and Engineering Aspects of Thermal Pollution, The CRC Press, 1970.

Lee, S.S., Veziroglu, T.N., Weinberg, N.L., and Sengupta, S., "Application of Remote Sensing for Prediction and Detection of Thermal Pollution," NASA-CR-139182, 1974.

Lee, S.S., Veziroglu, T.N., Weinberg, N.L., and Sengupta, S., "Application of Remote Sensing for Prediction and Detection of Thermal Pollution," Phase 2, NASA-CR-139188, 1975.

Lee, S.S., and Sengupta, S., "Three-Dimensional Thermal Pollution Models," Phase III, NASA-CR-144858, 1976

Mathavan, S.K., Ph.D. dissertation, University of Miami, Coral Gables, Florida, 1977.

Motz, L. and Benedict, B., "Heated Surface Jet Discharged into a
Flowing Ambient Stream", Dept. of Environmental and Water Resources
Engineering, Vanderbilt University, Nashville, Tennessee, Report
No.4, Aug. 1972.

Phillips, N.A., "A Coordinate System Having Some Special Advantages
for Numerical Forecasting, Meteorol, J, Vol, 14, 1957.

Pritchard, D., "Design and Siting Criteria for Once-through
Cooling Systems, "American Institute of Chemical Engineers, 58th
Annual Meeting, Houston, Texas, March 2, 1971.

Pritchard, D.W., "Fate of and Effect of Excess Heat Discharged
into Lake Michigan with Specific Application to the Condenser
Cooling Water Discharge from the Zion Nuclear Power Station,
Testimony at AEC.
Pritchard, D.W., "Testimony of D.W. Pritchard for the AEC Operating
Permit of the Commonwealth Edison Zion Nuclear Electric Generating
Station", Chicago, Illinois, June 1974. Licensing Hearing for
Ion Operation Permit, Chicago, Illinois, June 1973.

Prych, E., "A Warm Water Effluent Analyzed as a Buoyant Surface
Jet," Svergis Meteorologiska Och Hydrologiska Institut, Sevie
Hydrologi, Nr. 71, Stockholm, 1972.

Prych, E., "An Analysis of a Jet into a Turbulent Ambient Fluid,"
Water Research 7, Pergamon Press, pp. 697-657, 1973.

Richtmyer, R.D. and Morton, K.W., Difference Methods for Initial
Value Problems, Interscience Publishers, New York, 1967.

Roache, J.P., Computational Fluid Dynamics, Hermosa Publishers,
1972.

Sengupta, S. and Lick W., "A Numerical Model for Wind Driven
Circulation and Temperature Fields in Lakes and Ponds, "FTAS/TR-74-99,
Case Western Reserve University, 1974 (a).

Sengupta, S., Lee, S.S., and Veziroglu, T.N., "Application of
Remote Sensing to Numerical Modelling, "Proceedings of the Symposium
on Remote Sensing Applied to Energy Related Problems, 1974 (b).
Also in Remote Sensing, John Wiley and Sons, 1975, pp.335-355.

S.S. Lee and S. Sengupta, "Three Dimensional Thermal Pollution
Models" Phase III, NASA Contract NAS10-8926

Sengupta, S., "A Three-Dimensional Model for Closed Basins," ASME
Paper 75-WA-HT21, 1976 (b).

Shirazi, M. and Davis, L., "Workbook of Thermal Plume Prediction
Volume 2: Surface Discharge", Thermal Pollution Branch, Pacific
Northwest Environmental Research Laboratory, USEPA, Cowallis,
Oregon, May 1974.

Trent, D.S., " A Numerical Model for two-dimensional Hydrodynamic . Energy Transport", Battelle Pacific Northwest Laboratories, Report BNWL-1803, VC-11, Richland, Wash, Feb. 1974.

Trent, D.S , "Mathematical Modelling of Transport Processes in Aquatic System", presented at the topical meeting on Computational Methods in Nuclear Engineering, American Nuclear Society, Charleston, South Carolina, April 15-17, 1975.

Tsai, C.F., PhD. dissertation, University of Miami, Coral Gables, Florida, 1977.

Venkata, J., Ph.D. Dissertation, University of Miami, Coral Gables, Florida, 1977.

Waldrop, W. and Farmer, R., "Three-Dimensional Flow and Sediment Transport at River Mouths," Coastal Studies Instituee, Louisiana State University, Baton Rouge, Technical Report No. 150, Sept. 1973.

Waldrop, W. and Farmer, R.C., "Three-Dimensional Computation of Bouyant Plumes," J. Geophysical Research, Vol. 79, No. 9, 1974 (a).

Waldrop, W. and Farmer, R.C., "Thermal Plumes for Industrial Cooling Water," Proceedings of the 1974 Heat Transfer and Fluid Mechanics Institute, Davis, L.R. and Wilson, R.E. (ed.) Stanford, Calif., Stanford University Press, June 1974(b).

K. Stolzenbach and D.R.F. Harleman, An Analytical and Experimental Investigation of Surface Discharges of Heated Water, Ralph M. Parsons Laboratory for Water Resources and Hydrodynamics, MIT, Cambridge, Mass., Report No. 135(Feb 1971).

J. Weil, Vertification of Heated Water Jet Numerical Model, Swedish Meteorological and Hydrological Institute, Hydrologi Och Oceanografo Iir. RHO1 (1974).

H. Till, A Computer Model for Three-Dimensional Simulation of Thermal Discharges into Rivers, doctoral dissertation, Dept. of Nuclear Eng., University of Missouri at Rolla (1973).

J. Paul, A Numerical Model for a Three-Dimensional, Variable-Density Jet, doctoral dissertation, Department of Fluid, Thermal, and Aerospace Sciences, Case Western Reserve University (Sept 1973).

J. Paul and W. Lick, Report to Argonne National Laboratory of the Application of the Point Beach Unit 1 Outfall, School of Eng., Dept. of Earth Sciences, Case Western Reserve University, Cleveland, Ohio (Nov 1974).

P. Brady and J. Geyer, Development of a General Computer Model for Simulating Thermal Discharges in Three Dimensions, Report No.7, Dept. of Geography and Environmental Eng., Johns Hopkins University, Baltimore, Md. (Feb 1972).

APPENDIX A

DERIVATION OF STRETCHED EQUATIONS

[I] Vertical Stretching Equation

To incorporate with both free surface and realistic variable bottom topography in the three-dimensional basin model is quite difficult in computer programming. A mathematical transformation of vertical coordinate is needed to convert the depth of basin to a constant non-dimensional depth one. The new coordinate system is transformed from x, y, z, to α, β, σ, where the transformation relationships are:

$$\sigma = \frac{Z\ (\sigma,\beta,z,t)}{H\ (\sigma,\beta,t)} = \frac{z + \eta\ (\sigma,\beta,t)}{H\ (\alpha,\beta) + \eta\ (\alpha,\beta,t)} \dots\dots\dots\dots (A-1)$$

$$\frac{\partial\alpha}{\partial x} = \frac{\partial\beta}{\partial y} = 1 \dots\dots\dots\dots\dots\dots\dots\dots\dots\dots\dots\dots\dots\dots\dots (A-2)$$

$$\frac{\partial\alpha}{\partial y} = \frac{\partial\alpha}{\partial z} = \frac{\partial\beta}{\partial x} = \frac{\partial\beta}{\partial z} = 0 \dots\dots\dots\dots\dots\dots\dots\dots\dots\dots\dots (A-3)$$

$$\frac{\partial Z}{\partial z} = 1 \dots\dots\dots\dots\dots\dots\dots\dots\dots\dots\dots\dots\dots\dots\dots\dots\dots (A-4)$$

$$\frac{\partial\sigma}{\partial z} = \frac{\partial\sigma}{\partial Z} = \frac{1}{H} \dots\dots\dots\dots\dots\dots\dots\dots\dots\dots\dots\dots\dots\dots (A-5)$$

$$\frac{\partial\sigma}{\partial x} = \frac{1}{H}\frac{\partial\eta}{\partial\alpha} - \frac{\sigma}{H}\frac{\partial H}{\partial\alpha} \dots\dots\dots\dots\dots\dots\dots\dots\dots\dots\dots\dots (A-6)$$

$$\frac{\partial\sigma}{\partial y} = \frac{1}{H}\frac{\partial\eta}{\partial\beta} - \frac{\sigma}{H}\frac{\partial H}{\partial\beta} \dots\dots\dots\dots\dots\dots\dots\dots\dots\dots\dots\dots (A-7)$$

By using the above relationships the first derivatives can be written as

$$\frac{\partial F}{\partial x} = \frac{\partial F}{\partial\alpha}\frac{\partial\alpha}{\partial x} + \frac{\partial F}{\partial\beta}\frac{\partial\beta}{\partial x} + \frac{\partial F}{\partial\sigma}\frac{\partial\sigma}{\partial x} = \frac{\partial F}{\partial\alpha} + \frac{\partial F}{\partial\sigma}\frac{\partial\sigma}{\partial x} = \frac{\partial F}{\partial\alpha} + \frac{\partial F}{\partial\sigma}$$

$$\left[\frac{1}{H}\frac{\partial\eta}{\partial\alpha} - \frac{\sigma}{H}\frac{\partial H}{\partial\alpha}\right] = \frac{\partial F}{\partial\alpha} + \frac{1}{H}\frac{\partial\eta}{\partial\alpha}\frac{\partial F}{\partial\sigma} - \frac{\sigma}{H}\frac{\partial H}{\partial\alpha}\frac{\partial F}{\partial\sigma} \dots\dots\dots\dots\dots (A-8)$$

$$\frac{\partial F}{\partial y} = \frac{\partial F}{\partial \beta} + \frac{1}{H} \frac{\partial \eta}{\partial \beta} \frac{\partial F}{\partial \sigma} - \frac{\sigma}{H} \frac{\partial H}{\partial \beta} \frac{\partial F}{\partial \sigma}. \dots\dots\dots\dots\dots\dots\dots\dots\dots\dots\dots\dots \text{(A-9)}$$

$$\frac{\partial F}{\partial z} = \frac{1}{H} \frac{\partial F}{\partial \sigma}. \dots\dots\dots\dots\dots\dots\dots\dots\dots\dots\dots\dots\dots\dots \text{(A-10)}$$

Where "F" is the appropriate dependent variable, the second derivatives can be written as:

$$\frac{\partial^2 F}{\partial x^2} = \frac{\partial^2 F}{\partial \alpha^2} - \frac{2}{H} \frac{\partial F}{\partial \sigma} \frac{\partial H}{\partial \alpha} \frac{\partial \sigma}{\partial x} + 2 \frac{\partial \sigma}{\partial x} \frac{\partial^2 F}{\partial \alpha \partial \sigma} + \left(\frac{\partial \sigma}{\partial x}\right)^2 \frac{\partial^2 F}{\partial \sigma^2} +$$

$$\frac{1}{H} \frac{\partial F}{\partial \sigma} \frac{\partial^2 \eta}{\partial \alpha^2} - \frac{\sigma}{H} \frac{\partial F}{\partial \sigma} \frac{\partial^2 H}{\partial \alpha^2}. \dots\dots\dots\dots\dots\dots\dots\dots\dots\dots\dots \text{(A-11)}$$

$$\frac{\partial^2 F}{\partial y^2} = \frac{\partial^2 F}{\partial \beta^2} - \frac{2}{H} \frac{\partial F}{\partial \sigma} \frac{\partial H}{\partial \beta} \frac{\partial \sigma}{\partial y} + 2 \frac{\partial \sigma}{\partial y} \frac{\partial^2 F}{\partial \beta \partial \sigma} + \left(\frac{\partial \sigma}{\partial y}\right)^2 \frac{\partial^2 F}{\partial \sigma^2}$$

$$+ \frac{1}{H} \frac{\partial F}{\partial \sigma} \frac{\partial^2 \eta}{\partial \beta^2} - \frac{\sigma}{H} \frac{\partial F}{\partial \sigma} \frac{\sigma^2 H}{\partial \beta^2}. \dots\dots\dots\dots\dots\dots\dots\dots\dots\dots\dots \text{(A-12)}$$

$$\frac{\partial^2 F}{\partial z^2} = \frac{1}{H^2} \frac{\partial^2 F}{\partial \sigma^2}. \dots\dots\dots\dots\dots\dots\dots\dots\dots\dots\dots\dots\dots\dots \text{(A-13)}$$

Define:

$$U = \frac{dx}{dt} = \frac{d\alpha}{dt}. \dots\dots\dots\dots\dots\dots\dots\dots\dots\dots\dots\dots\dots\dots \text{(A-14)}$$

$$V = \frac{dv}{dt} = \frac{d\beta}{dt}. \dots\dots\dots\dots\dots\dots\dots\dots\dots\dots\dots\dots\dots\dots \text{(A-15)}$$

$$\Omega = \frac{d\sigma}{dt}. \dots\dots\dots\dots\dots\dots\dots\dots\dots\dots\dots\dots\dots\dots\dots\dots \text{(A-16)}$$

The vertical velocity w is related to the Ω by the expression

$$w = \frac{dz}{dt} = H\Omega + (\sigma - 1) \frac{d\eta}{dt} + \sigma \frac{dh}{dt}. \dots\dots\dots\dots\dots\dots\dots \text{(A-17)}$$

Continuity Equation:

The continuity equation for three dimensional incompressible fluid flow in Cartesian coordinate may be written as:

$$H \frac{\partial u}{\partial x} + H \frac{\partial v}{\partial y} + H \frac{\partial w}{\partial z} = 0. \dots\dots\dots\dots\dots\dots\dots\dots\dots \text{(A-18)}$$

Now

$$H \frac{\partial u}{\partial x} = H \frac{\partial u}{\partial \alpha} + \frac{\partial \eta}{\partial \alpha} \frac{\partial u}{\partial \sigma} - \sigma \frac{\partial H}{\partial \alpha} \frac{\partial u}{\partial \sigma} \dots\dots\dots\dots\dots\dots\dots\dots (A-19)$$

$$H \frac{\partial v}{\partial y} = H \frac{\partial v}{\partial \beta} + \frac{\partial \eta}{\partial \beta} \frac{\partial v}{\partial \sigma} - \sigma \frac{\partial H}{\partial \beta} \frac{\partial v}{\partial \sigma} \dots\dots\dots\dots\dots\dots\dots (A-20)$$

$$H \frac{\partial w}{\partial z} = H \frac{\partial w}{\partial Z} = \frac{\partial w}{\partial \sigma} = \frac{\partial}{\partial \sigma} \left(\frac{dZ}{dt} \right) = \frac{\partial}{\partial \sigma} \left(\frac{d(Z - \eta)}{dt} \right)$$

$$= \frac{\partial}{\partial \sigma} \left(\frac{dZ}{dt} - \frac{d\eta}{dt} \right) = \frac{\partial}{\partial \sigma} \left(\frac{d(\sigma H)}{dt} - \frac{d\eta}{dt} \right)$$

$$= \frac{\partial}{\partial \sigma} \left(H \frac{d\sigma}{dt} + \sigma \frac{dH}{dt} - \frac{d\eta}{dt} \right)$$

$$= H \frac{\partial}{\partial \sigma} \left(\frac{d\sigma}{dt} \right) + \frac{dH}{dt} + \sigma \frac{\partial}{\partial \sigma} \left(\frac{dH}{dt} \right) - \frac{\partial}{\partial \sigma} \left(\frac{d\eta}{dt} \right)$$

$$= H \frac{\partial \Omega}{\partial \sigma} + \left(\frac{\partial H}{\partial t} + u \frac{\partial H}{\partial \alpha} + v \frac{\partial H}{\partial \beta} + \Omega \frac{\partial H}{\partial \sigma} \right) + \sigma \frac{\partial}{\partial \sigma} \left(\frac{\partial H}{\partial t} \right.$$

$$+ u \frac{\partial H}{\partial \alpha} + v \frac{\partial H}{\partial \beta} + \Omega \frac{\partial H}{\partial \sigma} \right) - \frac{\partial}{\partial \sigma} \left(\frac{\partial \eta}{\partial t} + u \frac{\partial \eta}{\partial \alpha} + v \frac{\partial \eta}{\partial \beta} + \Omega \frac{\partial \eta}{\partial \sigma} \right)$$

$$= H \frac{\partial \Omega}{\partial \sigma} + \frac{\partial H}{\partial t} + u \frac{\partial H}{\partial \alpha} + v \frac{\partial H}{\partial \beta} + \sigma \frac{\partial u}{\partial \sigma} \frac{\partial H}{\partial \alpha} + \sigma \frac{\partial v}{\partial \sigma} \frac{\partial H}{\partial \beta}$$

$$- \frac{\partial u}{\partial \sigma} \frac{\partial \eta}{\partial \alpha} - \frac{\partial v}{\partial \sigma} \frac{\partial \eta}{\partial \beta} \dots\dots\dots\dots\dots\dots\dots\dots\dots (A-21)$$

Substituting (A-19), (A-20), and (A-21) into (A-18) we get
the continuity equation in α β σ coordinate is:

$$\frac{\partial H}{\partial t} + \frac{\partial (Hu)}{\partial \alpha} + \frac{\partial (Hv)}{\partial \beta} + H \frac{\partial \Omega}{\partial \sigma} = 0 \dots\dots\dots\dots\dots\dots\dots (A-22)$$

Momentum Equation and Energy Equation

The inertia terms in the momentum or energy equations
in the xyz Cartesian coordinate can be written as:

$$H \frac{\partial F}{\partial t} + uH \frac{\partial F}{\partial x} + vH \frac{\partial F}{\partial y} + wH \frac{\partial F}{\partial z} \dots\dots\dots\dots\dots\dots\dots (A-23)$$

where F is the appropriate dependent variable u, v or T for
the momentum and energy equation respectively. By using the
relationships in (A-8), (A-9), (A-10), (A-17) and added F

179

times the continuity equation $[F \ (\frac{\partial H}{\partial t} + \frac{\partial (Hu)}{\partial \alpha} + \frac{\partial (Hv)}{\partial \beta} + H \frac{\partial \Omega}{\partial \sigma})]$,
then the equation (A-23) becomes:

$$\frac{\partial (HF)}{\partial t} + \frac{\partial (HFu)}{\partial \alpha} + \frac{\partial (HFv)}{\partial \beta} + H \frac{\partial (F\Omega)}{\partial \sigma} \dots\dots\dots\dots\dots\dots\dots (A-24)$$

The pressure terms can be written as:

$$\frac{1}{\rho} \frac{\partial P}{\partial x} = \frac{1}{\rho} \frac{\partial P}{\partial \alpha} + \frac{1}{\rho H} \frac{\partial \eta}{\partial \alpha} \frac{\partial P}{\partial \sigma} - \frac{\sigma}{\rho H} \frac{\partial H}{\partial \alpha} \frac{\partial P}{\partial \sigma}$$

$$= \frac{1}{\rho} \frac{\partial P}{\partial \alpha} - \frac{1}{\rho H} \frac{\partial P}{\partial \sigma} \ (\sigma \frac{\partial H}{\partial \alpha} - \frac{\partial \eta}{\partial \alpha})$$

$$= \frac{1}{\rho} \frac{\partial P}{\partial \alpha} - \frac{1}{\rho H} \frac{\partial (\rho \ g \ Z)}{\partial \sigma} \ (\sigma \frac{\partial H}{\partial \alpha} - \frac{\partial \eta}{\partial \alpha})$$

$$= \frac{1}{\rho} \frac{\partial P}{\partial \alpha} - \frac{g}{H} \frac{\partial Z}{\partial \sigma} \ (\sigma \frac{\partial H}{\partial \alpha} - \frac{\partial \eta}{\partial \alpha})$$

$$= \frac{1}{\rho} \frac{\partial P}{\partial \alpha} - g(\sigma \frac{\partial H}{\partial \alpha} - \frac{\partial \eta}{\partial \alpha}) \dots\dots\dots\dots\dots\dots\dots\dots\dots (A-25)$$

$$\frac{1}{\rho} \frac{\partial P}{\partial y} = \frac{1}{\rho} \frac{\partial P}{\partial \beta} - g(\sigma \frac{\partial H}{\partial \beta} - \frac{\partial \eta}{\partial \beta}) \dots\dots\dots\dots\dots\dots\dots\dots\dots (A-26)$$

By using the relationships of second derivatives, the
diffusion terms can be written as:

$$\frac{\partial^2 F}{\partial x^2} = \frac{\partial^2 F}{\partial \alpha^2} - \frac{2}{H} \frac{\partial \sigma}{\partial x} \frac{\partial H}{\partial \alpha} \frac{\partial F}{\partial \sigma} + 2 \frac{\partial \sigma}{\partial x} \frac{\partial^2 F}{\partial \alpha \partial \sigma} + (\frac{\partial \sigma}{\partial x})^2 \frac{\partial^2 F}{\partial \sigma^2} + \frac{1}{H}$$

$$\frac{\partial F}{\partial \sigma} \frac{\partial^2 \eta}{\partial x^2} - \frac{\sigma}{H} \frac{\partial F}{\partial \sigma} \frac{\partial^2 H}{\partial \alpha^2}$$

$$= \frac{1}{H} \ (H \frac{\partial^2 F}{\partial \alpha^2} + \frac{\partial H}{\partial \alpha} \frac{\partial F}{\partial \alpha}) - \frac{1}{H} \frac{\partial H}{\partial \alpha} \frac{\partial F}{\partial \alpha} - \frac{\sigma}{H} \frac{\partial F}{\partial \sigma} \frac{\partial^2 H}{\partial \alpha^2}$$

$$- \frac{2}{H} \frac{\partial \sigma}{\partial x} \frac{\partial H}{\partial \alpha} \frac{\partial F}{\partial \sigma} + 2 \frac{\partial \sigma}{\partial x} \frac{\partial^2 F}{\partial \alpha \partial \sigma} + (\frac{\partial \sigma}{\partial x})^2 \frac{\partial^2 F}{\partial \sigma^2} + \frac{1}{H} \frac{\partial F}{\partial \sigma} \frac{\partial^2 \eta}{\partial \alpha^2}$$

$$= \frac{1}{H} \ [\ \frac{\partial}{\partial \alpha} \ (H\frac{\partial F}{\partial \alpha})] + \text{High order terms} \dots\dots\dots\dots\dots (A-27)$$

using the same procedure as above:

$$\frac{\partial^2 F}{\partial y^2} = \frac{1}{H} \ [\frac{\partial}{\partial \beta} \ (H \frac{\partial F}{\partial \beta})] + \text{High order terms} \dots\dots\dots\dots\dots (A-28)$$

and the vertical diffusion term is:

Neglecting the high order terms in Equations (A-27) and (A-28), then

$$\frac{\partial^2 F}{\partial x^2} = \frac{1}{H} \left[\frac{\partial}{\partial \alpha} \left(H \frac{\partial F}{\partial \alpha} \right) \right] \dots\dots\dots\dots\dots\dots\dots\dots\dots\dots\dots\dots\dots (A-30)$$

$$\frac{\partial^2 F}{\partial y^2} = \frac{1}{H} \left[\frac{\partial}{\partial \beta} \left(H \frac{\partial F}{\partial \beta} \right) \right] \dots\dots\dots\dots\dots\dots\dots\dots\dots\dots\dots\dots\dots (A-31)$$

By using the relationships in Equations (A-24), (A-25), (A-26), (A-29), (A-30) and (A-31), then the momentum and energy equations become:

u-momentum:

$$\frac{\partial (Hu)}{\partial t} + \frac{\partial (Huu)}{\partial \alpha} + \frac{\partial (Huv)}{\partial \beta} + H \frac{\partial (u\Omega)}{\partial \sigma}$$

$$= H \left[- \frac{1}{\rho} \left(\frac{\partial P}{\partial \alpha} \right) + g \left(\sigma \frac{\partial H}{\partial \alpha} - \frac{\partial \eta}{\partial \alpha} \right) + fv \right] + K_H \left[\frac{\partial}{\partial \alpha} \left(H \frac{\partial u}{\partial \alpha} \right) \right]$$

$$+ K_H \left[\frac{\partial}{\partial \beta} \left(H \frac{\partial u}{\partial \beta} \right) \right] + \frac{1}{\rho} \left[\frac{\partial}{H \partial \sigma} \left(\rho K_V \frac{\partial u}{\partial \sigma} \right) \right] \dots\dots\dots\dots\dots (A-32)$$

v-momentum:

$$\frac{\partial Hv}{\partial t} + \frac{\partial (Huv)}{\partial \alpha} + \frac{\partial (Hvv)}{\partial \beta} + H \frac{\partial (v\Omega)}{\partial \sigma} = H \left[- \frac{1}{\rho} \left(\frac{\partial P}{\partial \beta} \right) \right.$$

$$+ g \left(\sigma \frac{\partial H}{\partial \beta} - \frac{\partial \eta}{\partial \beta} \right) - fu \right] + K_H \left[\frac{\partial}{\partial \alpha} \left(H \frac{\partial v}{\partial \alpha} \right) \right] + K_H \left[\frac{\partial}{\partial \beta} \left(H \frac{\partial v}{\partial \beta} \right) \right]$$

$$+ \frac{1}{\rho} \left[\frac{\partial}{H \partial \sigma} \left(\rho K_V \frac{\partial v}{\partial \sigma} \right) \right] \dots\dots\dots\dots\dots\dots\dots\dots\dots\dots\dots\dots\dots (A-33)$$

Energy Equation:

$$\frac{\partial (HT)}{\partial t} + \frac{\partial (HuT)}{\partial \alpha} + \frac{\partial (HvT)}{\partial \beta} + H \frac{\partial (\Omega T)}{\partial \sigma} = B_H \left[\frac{\partial}{\partial \alpha} \left(H \frac{\partial T}{\partial \alpha} \right) \right]$$

$$+ B_H \left[\frac{\partial}{\partial \beta} \left(H \frac{\partial T}{\partial \beta} \right) \right] + \frac{1}{\rho} \left[\frac{\partial}{H \partial \sigma} \left(\rho B_V \frac{\partial T}{\partial \sigma} \right) \right] \dots\dots\dots\dots\dots (A-34)$$

[II] Horizontal Stretching Equation

Before writing the equations in finite difference form, the horizontal stretching transformation which provided a

more efficient use of grid points within a large domain was applied in α and β direction. The hyperbolic sine stretching equation was used by letting:

$$\alpha = a + C_1 \, \text{Sinh} \, [C_2 \, (X - d)] \dots\dots\dots\dots\dots\dots (A-35)$$

$$\beta = b + C_2 \, \text{Sinh} \, [C_4 \, (Y - e)] \dots\dots\dots\dots\dots (A-36)$$

where α, β is a real coordinate, X and Y are stretched coordinate, a and b are the distance at which the minimum step size is desired. C_1, C_2, C_3, C_4, d, e are the constants to be determined by the imposed conditions.

The differential derivatives transformation relationships for the new X Y σ coordinate from α β σ coordinate are written as:

$$\frac{\partial F}{\partial \alpha} = \frac{\partial X}{\partial \alpha} \cdot \frac{\partial F}{\partial X} = X' \, \frac{\partial F}{\partial X} \dots\dots\dots\dots\dots\dots\dots\dots\dots (A-37)$$

$$\frac{\partial F}{\partial \beta} = \frac{\partial Y}{\partial \beta} \cdot \frac{\partial F}{\partial Y} = Y' \, \frac{\partial F}{\partial Y} \dots\dots\dots\dots\dots\dots\dots\dots\dots (A-38)$$

$$\frac{\partial^2 F}{\partial \alpha^2} = \frac{\partial}{\partial \alpha} \left(\frac{\partial F}{\partial \alpha}\right) = (X')^2 \, \frac{\partial^2 F}{\partial X^2} + X'' \, \frac{\partial F}{\partial X} \dots\dots\dots\dots\dots (A-39)$$

$$\frac{\partial^2 F}{\partial \beta^2} = \frac{\partial}{\partial \beta} \left(\frac{\partial F}{\partial \beta}\right) = (Y')^2 \, \frac{\partial^2 F}{\partial Y^2} + Y'' \, \frac{\partial F}{\partial Y} \dots\dots\dots\dots\dots (A-40)$$

where

$$X' = \frac{\partial X}{\partial \alpha} \; ; \quad Y' = \frac{\partial Y}{\partial \beta}$$

$$X'' = \frac{\partial^2 X}{\partial \alpha^2} \; ; \quad Y'' = \frac{\partial^2 Y}{\partial \beta^2}$$

By using the above relationships, then the set of equations in transformed X Y σ coordinate are:

Continuity Equation:

$$\frac{\partial H}{\partial t} + X' \, \frac{\partial (Hu)}{\partial X} + Y' \, \frac{\partial (Hv)}{\partial Y} + H \, \frac{\partial \Omega}{\partial \sigma} = 0 \dots\dots\dots\dots\dots (A-41)$$

Momentum Equations:

u-momentum:

$$\frac{\partial(Hu)}{\partial t} + X' \frac{\partial(Huu)}{\partial X} + Y' \frac{\partial(Huv)}{\partial Y} + H \frac{\partial(u\Omega)}{\partial \sigma} = H \left[-\frac{X'}{\rho}\left(\frac{\partial P}{\partial X}\right)\right.$$

$$+ g X' \left(\sigma \frac{\partial H}{\partial X} - \frac{\partial \eta}{\partial X}\right) + fv] + K_H \left[(X')^2 \frac{\partial H}{\partial X} \frac{\partial u}{\partial X}\right.$$

$$+ H (X')^2 \frac{\partial^2 u}{\partial X^2} + H X'' \frac{\partial u}{\partial X}] + K_H \left[(Y')^2 \frac{\partial H}{\partial Y} \frac{\partial u}{\partial Y}\right.$$

$$+ H(Y')^2 \frac{\partial^2 u}{\partial Y^2} + H Y'' \frac{\partial u}{\partial Y}] + \frac{1}{\rho} \left[\frac{\partial}{H\partial\sigma} \left(\rho K_V \frac{\partial u}{\partial \sigma}\right)\right] \dots\dots\dots (A-42)$$

v-momentum:

$$\frac{\partial(Hv)}{\partial t} + X' \frac{\partial(Huv)}{\partial X} + Y' \frac{\partial(Hvv)}{\partial Y} + H\frac{\partial(v\Omega)}{\partial \sigma}$$

$$= H\left[- \frac{Y'}{\rho} \left(\frac{\partial P}{\partial Y}\right) + g Y' \left(\sigma \frac{\partial H}{\partial Y} - \frac{\partial \eta}{\partial Y}\right) - fu\right]$$

$$+ K_H \left[(X')^2 \frac{\partial H}{\partial X} \frac{\partial v}{\partial X} + H(X')^2 \frac{\partial^2 v}{\partial X^2} + HX'' \frac{\partial v}{\partial X}\right]$$

$$+ K_H \left[(Y')^2 \frac{\partial H}{\partial Y} \frac{\partial v}{\partial Y} + H(Y')^2 \frac{\partial^2 v}{\partial Y^2} + HY'' \frac{\partial v}{\partial Y}\right]$$

$$+ \frac{1}{\rho} \left[\frac{\partial}{H\partial\sigma} \left(\rho K_V \frac{\partial v}{\partial \sigma}\right)\right] \dots\dots\dots\dots\dots\dots\dots\dots (A-43)$$

Energy Equation:

$$\frac{\partial(HT)}{\partial t} + X' \frac{\partial(HuT)}{\partial X} + Y' \frac{\partial(HvT)}{\partial Y} + H \frac{\partial(\Omega T)}{\partial \sigma}$$

$$= B_H \left[(X')^2 \frac{\partial H}{\partial X} \frac{\partial T}{\partial X} + H(X')^2 \frac{\partial^2 T}{\partial X^2} + H X'' \frac{\partial T}{\partial X}\right]$$

$$+ B_H \left[(Y')^2 \frac{\partial H}{\partial Y} \frac{\partial T}{\partial Y} + H(Y')^2 \frac{\partial T}{\partial Y^2} + H Y'' \frac{\partial T}{\partial Y}\right]$$

$$+ \frac{1}{\rho} \left[\frac{\partial}{H\partial\sigma} \left(\rho B_V \frac{\partial T}{\partial \sigma}\right)\right] \dots\dots\dots\dots\dots\dots\dots\dots (A-44)$$

APPENDIX B

Hyperbolic Sine Horizontal Stretching System

It is desirable to obtain a more detailed description
of the flow near the discharge point while large grid size
may be used in the further points to prevent the unnecess-
ary computation time. A horizontal stretching has been in-
vestigated and incorporated to allow for high resolution
near the discharge with gradually increasing grid sizes aw-
ay from the discharge. The tangent equation which was used
by Waldrop and Farmer (1974) appeared to have the most des-
irable characteristics. However, it has been noted that
when the number of grid points is small and the domain is
large, the tangent equation produces relatively little str-
etching until close to a boundary, then jumps to the bound-
ary in a relatively large steps. This behavior appears un-
desiarble and further effects to find a suitable alternative
equation. The hyperbolic sine has been investigated by C. V.
Carter (1976). It appears to have somewhat better charact-
eristics than the tangent equation.

(I) The Hyperbolic Sine Stretching Equation :

The hyperbolic sine stretching equations used for both
transverse and lateral directions are

$$x = a + C_1 \; Sinh\{C_2(X-d)\} \quad \ldots\ldots\ldots\ldots\ldots\ldots (B-1)$$

$$y = b + C_2 \; Sinh\{C_4(Y-e)\} \quad \ldots\ldots\ldots\ldots\ldots\ldots (B-2)$$

where x and y are the real horizontal coordinate; a nad b
are the distance at which the minimum step size is desired;

C_1, C_2, C_3, C_4, d, and e are the constants to be determined by the imposed conditions; X and Y are the stretched horiz-ontal coordinate.

The variables X and Y are computed as

$$X = (I-1) \Delta x_o \quad \dots\dots\dots\dots\dots\dots\dots\dots\dots\dots \text{(B-3)}$$

$$Y = (J-1) \Delta y_o \quad \dots\dots\dots\dots\dots\dots\dots\dots\dots\dots \text{(B-4)}$$

where I is the grid point number on x-axis; J is the grid point number on y-axis; Δx_o is the minimum desired step size in x-direction; Δy_o is the minimum desired step size in y-direction.

In order to determine the constants, we impose the following conditions:

(a) When x = 0 then X = 0, y = 0 then Y = 0. Form equations (B-1) and (B-2), this condition will be satisried if

$$d = \frac{1}{C_2} \text{Sinh}^{-1} \left(\frac{a}{C_1}\right) \quad \dots\dots\dots\dots\dots\dots\dots\dots \text{(B-5)}$$

$$e = \frac{1}{C_4} \text{Sinh}^{-1} \left(\frac{b}{C_3}\right) \quad \dots\dots\dots\dots\dots\dots\dots\dots \text{(B-6)}$$

(b) When it reaches to the boundary, the equations (B-1) and (B-2) have the form as

$$x_b = a + C_1 \text{Sinh}\{C_2 \ (N_x-1)\Delta x_o - d \} \quad \dots\dots\dots\dots \text{(B-7)}$$

$$y_b = b + C_3 \text{Sinh}\{C_4 \ (N_y-1)\Delta y_o - e \} \quad \dots\dots\dots\dots \text{(B-8)}$$

where x_b and y_b are the x and y reach to the boundary resp-ectively; N_x is the total number of grid points on the x-axis; N_y is the total number of grid points on the y-axis; then the

values of X and Y at the boundary are $(N_x-1)\Delta x_0$ and $(N_y-1)\Delta y_0$ respectively.

(c) Both (a) and (b) above are the required boundary conditions. The imposed conditions at $x = a$ and $y = b$ which can be anywhere in the domain. When $x = a$, it is required that the step size be minimum in x-axis. When $y = b$, it is required that the step size be minimum in y-axis. That is

$$\Delta x = \Delta x_0 \qquad \text{when} \quad x = a \quad \dots\dots\dots\dots\dots\dots(B-9)$$

$$\Delta y = \Delta y_0 \qquad \text{when} \quad y = b \quad \dots\dots\dots\dots\dots\dots(B-10)$$

one can write

$$\Delta x = \frac{dx}{dX} \Delta X \quad \dots\dots\dots\dots\dots\dots\dots\dots\dots\dots\dots(B-11)$$

$$\Delta y = \frac{dy}{dY} \Delta Y \quad \dots\dots\dots\dots\dots\dots\dots\dots\dots\dots\dots(B-12)$$

but $\Delta X = \Delta x_0$; $\Delta Y = \Delta y_0$, therefore

$$\Delta x = \frac{dx}{dX} \Delta x_0 \quad \dots\dots\dots\dots\dots\dots\dots\dots\dots\dots(B-13)$$

$$\Delta y = \frac{dy}{dY} \Delta y_0 \quad \dots\dots\dots\dots\dots\dots\dots\dots\dots\dots(B-14)$$

From (B-9), (B-10), (B-13), (B-14), we can find that

$$\frac{dx}{dX} = 1 \qquad \text{when} \quad x = a \quad \dots\dots\dots\dots\dots\dots\dots(B-15)$$

$$\frac{dy}{dY} = 1 \qquad \text{when} \quad y = b \quad \dots\dots\dots\dots\dots\dots\dots(B-16)$$

Differentiating equation (B-1) and (B-2) and setting the result equal to 1, we can find that

$$C_2 = \frac{1}{C_1} \quad \dots\dots\dots\dots\dots\dots\dots\dots\dots\dots\dots\text{(B-17)}$$

$$C_4 = \frac{1}{C_3} \quad \dots\dots\dots\dots\dots\dots\dots\dots\dots\dots\dots\text{(B-18)}$$

Substituting equation (B-17) into (B-1) and (B-18) into (B-2) and the result are

$$x = a + C_1 \text{ Sinh}\left(\frac{X - d}{C_1}\right) \quad \dots\dots\dots\dots\dots\dots\text{(B-19)}$$

$$y = b + C_3 \text{ Sinh}\left(\frac{Y - e}{C_3}\right) \quad \dots\dots\dots\dots\dots\dots\text{(B-20)}$$

By substituing equation (B-17) into (B-5) and (B-18) into (B-6), we can get

$$d = C_1 \text{Sinh}^{-1}\left(\frac{a}{C_1}\right) \quad \dots\dots\dots\dots\dots\dots\dots\dots\text{(B-21)}$$

$$e = C_3 \text{Sinh}^{-1}\left(\frac{b}{C_3}\right) \quad \dots\dots\dots\dots\dots\dots\dots\dots\text{(B-22)}$$

At the boundary, the equations (B-19) and (B-20) becomes

$$x_b = a + C_1 \text{ Sinh}\left\{\frac{(N_x-1)\Delta x_o - d}{C_1}\right\} \quad \dots\dots\dots\dots\text{(B-23)}$$

$$y_b = b + C_3 \text{ Sinh}\left\{\frac{(N_y-1)\Delta y_o - e}{C_3}\right\} \quad \dots\dots\dots\dots\text{(B-24)}$$

There is only an unknown C_1 in the equations (B-21) and (B-23), an unknown C_3 in the equations (B-22) and (B-24). The iteration method was used for solving the equations to obtain C_1 and C_3. The d and e are obtained by substituting C_1 and C_3 into equations (B-21) and (B-22) respectively.

The derivatives $\frac{dX}{dx}$; $\frac{d^2X}{dx^2}$; $\frac{dY}{dy}$; $\frac{d^2Y}{dy^2}$ are needed for the governing equations when horizontal stretching equation are used. The derivetives are obtained from differen- equation (B-19) and (B-20) and that are:

$$\frac{dX}{dx} = X' = \frac{1}{\text{Cosh } (\frac{X - d}{C_1})} \quad \dots\dots\dots\dots\dots\dots (B-25)$$

$$\frac{d^2X}{dx^2} = X'' = - \frac{1}{C_1} \frac{\text{Sinh } (\frac{X - d}{C_1})}{\text{Cosh}^3 (\frac{X - d}{C_1})} \quad \dots\dots\dots\dots (B-26)$$

$$\frac{dY}{dy} = Y' = \frac{1}{\text{Cosh } (\frac{Y - e}{C_3})} \quad \dots\dots\dots\dots\dots\dots (B-27)$$

$$\frac{d^2Y}{dy^2} = Y'' = - \frac{1}{C_3} \frac{\text{Sinh } (\frac{Y - e}{C_3})}{\text{Cosh}^3 (\frac{Y - e}{C_3})} \quad \dots\dots\dots\dots (B-28)$$

(II) <u>Numerical Results</u> :

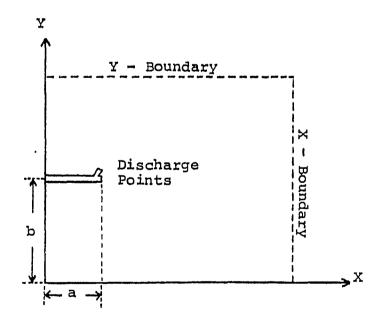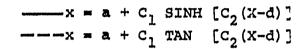The following characteristics were chosen as an init-ial domain for the Hutchinson Island Site:

TABLE B-1. Sample Of Numerical Results

	X-Axis	Y-Axis
Total number of points	20	20
Boundary distance	$x_b = 238000$cm	$y_b = 200000$cm
Discharge pipe outlet location	$a = 38000$ cm	$b = 100000$ cm
Minimum desired step size	$X = 1500$ cm	$Y = 1500$ cm
Constant	$C_1 = 3696.57$	$C_3 = 3530.03$
Constant	$d = 11184.66$	$e = 14251.88$

Fig.B-1 and Fig.B-2 are the comparison of hyperbolic sine stretching equation and tangent stretching equation. These graphs show that for the specified conditions, the tangent equation produces relatively little stretching until quite close to the boundaries. The sinh equation is somewhat better in this respect and stretching occurs more gradually as x and y vary between their limits.
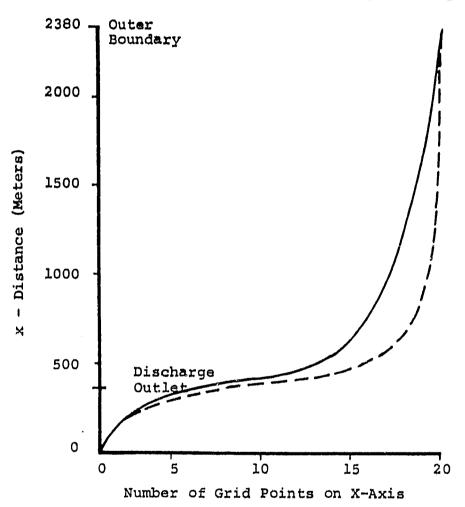
189

Fig. (B-1) Comparison of TAN and SINH Horizontal
Stretching on X-Axis with 20 Points and
Boundary at 2380 m.

$$y = a + C_1 \text{ SINH } [C_2(Y-d)]$$
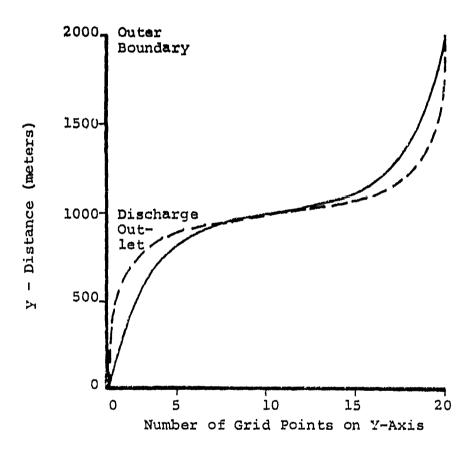$$y = a + C_1 \text{ TAN } [C_2(Y-d)]$$

Fig. (B-2) Comparison of TAN and SINH Horizontal
Stretching on Y-Axis With 20 Points
And Boundary at 2000 m.

191